

Stability of open granular filters under wave loading

W. Hollander

Delft University of Technology

Master of Science Thesis

Stability of open granular filters under wave loading

by

W. Hollander

in partial fulfilment of the requirements for the degree of

Master of Science

in Civil Engineering

at the Delft University of Technology and the National University of Singapore.

to be presented publicly on Thursday February 12, 2015 at 11:00 AM (CEST).

An electronic version of this thesis is available at <http://repository.tudelft.nl/>.

Rotterdam, February 2015

Report type: MSc Thesis

Report name: Stability of open granular filters under wave loading

Contact Author: wesselhollander@gmail.com

Author: W. Hollander (CITG, DUT)

Graduation Committee:

Prof. dr. ir. W.S.J. Uijtewaal	(CITG, DUT)
ir. J.P. van den Bos	(CITG, DUT)
ir. H.J. Verhagen	(CITG, DUT)
ir. H.J. Verheij	(CITG, DUT)
dr. Jing Yuan	(NUS)
ir. J.S. Reedijk	(DMC)



Delft University of Technology (DUT)
Faculty of Civil Engineering and Geosciences
Section Hydraulic Engineering
Stevinweg 1
P.O. Box 5048
2600 GA Delft
The Netherlands



The National University of Singapore (NUS)
Department of Civil & Environmental Engineering
Block E1A, #07-03
No.1 Engineering Drive 2
Singapore 117576



Delta marine Consultants (DMC)
Tradename of BAM Infraconsult bv.
H.J. Nederhorststraat 1
2800 GA Gouda
The Netherlands

Summary

A filter can be applied to protect a bed against scour. Normally, these filters are geometrically closed, to prevent winnowing of the base material through the filter. However, geometrically closed filters are expensive and difficult to realize in the field. Geometrically open filters can serve as an alternative. Within an open filter, the pores of the filter material are large enough for the base material to move through. The philosophy behind this concept is to reduce the hydraulic loading within the filter, in order to avoid initiation of the base material.

This research focusses on open filters. A design formula for open filters was established by Hoffmans (2012). This formula is recently validated for uniform flow (Van de Sande, 2012) and for flow with additional turbulence by a sill and a pier (Joustra, 2013). The applicability for wave loading - although suggested by Hoffmans- is not yet confirmed. No validation study was carried out in which Hoffmans formula was validated for wave loading. In this research, the main question is defined as follows:

“Is the design formula of Hoffmans (2012) valid for wave loading on horizontal filters?”

In the original formula by Hoffmans (2012), it is considered that the penetration of turbulence energy dominates the instability of the base material. Two different hypotheses are stated for the application of the Hoffmans formula under wave loading. Both hypotheses give a relation between the load damping length and the wave period. The load damping length is a parameter which determines the efficiency of the load damping of the turbulence energy inside the filter.

Laboratory experiments are carried out in a wave flume, with the purpose to obtain values for the load damping length. These experimentally obtained values are tested against the hypotheses. For the model tests, a horizontal filter structure was built and loaded by waves. Multiple configurations of the horizontal filter were tested, in which different layer thicknesses and different filter materials were used. For each configuration, the critical wave height was determined for a wave period of 2.0s, 2.5s and 3.0s. The critical wave height is defined as the height for which incipient motion of the base material occurs. The filter material was stable during all tests. The depth above the filter was held constant for the tests.

To express the loading on the base and filter material, Hoffmans uses the critical shear stresses in his formula. In the physical experiments, it was not possible to generate filter instability due to the dimensions of the flume, so the generated shear stress on the filter material was lower than the critical value of this parameter. Under the assumption that besides the critical shear stress on the filter material, also the generated shear stress can be used in Hoffmans formula, the load damping lengths are obtained. The obtained load damping length (L_d') is assumed to be similar to the load damping length in Hoffmans' original formula (L_d). The hypothetical values for the load damping parameter do not match with the values obtained from the experiments.

The experimentally obtained results indicate that the value for the load damping length depends on the layer thickness. This finding is counterintuitive and indicates that besides the penetration of turbulence energy, another type of loading influences the stability of the base-filter interface. Hoffmans neglected a term in his formula (called the “source term”, which is related to the hydraulic gradient). Under uniform flow it is acceptable that this source term was negligible (because the hydraulic gradients under uniform flow are relatively small), It is speculated that this source term was not negligible under wave loading. The following conclusion is drawn:

Under the assumption that $L_d' = L_d$, it is concluded that original formula as proposed by Hoffmans (2012) cannot be validated under wave loading.

The hydraulic gradient under waves is large compared with uniform flow. The hydraulic gradient generates a pore velocity in the filter and influences the stability of the base material. The experiments did show an increased critical wave loading when the filter thickness was enlarged. This implies that the penetration of turbulence energy does still play a role on the stability of the filter interface. It might be possible that the interface stability is influenced by a combination of the penetration of turbulence energy and the hydraulic gradient. Further research is necessary to investigate the influence of the turbulence energy compared with the influence of the hydraulic gradients on the stability of the filter interface. Hoffmans suggests that the influence of the hydraulic gradient can be incorporated by the use of a source term in his formula. It is not known yet how this source term is exactly related to the hydraulic gradient, it is proposed to carry out further research to the use of the source term in Hoffmans formula.

The following recommendations are made:

- Validate the assumption that the load damping length in Hoffmans formula can also be found without the critical load on the filter material.
- Carry out test where the hydraulic gradients on the interface are measured, and the filter thickness is increased step by step. Above a certain thickness, it expected that only the hydraulic gradient will affect the interface stability, and the penetration of turbulence energy will be negligible. Insight in the source term may be gained in this research.
- Hoffmans claims that the source term depends on the hydraulic gradient. However, it is not known how these two are exactly related. It is recommended to carry out research to the relation between the source term and the hydraulic gradients.
- It is also recommended to evaluate the influence of the gradient under uniform flow. It is recommended to measure the hydraulic gradients on the interface, and carry out tests where the hydraulic gradient is varied. If it turns out that the hydraulic gradient also plays a role under uniform flow, the load damp coefficients under uniform flow can be evaluated again. This might lead to new insights.
- The influence of the wave period is still unknown. It is assumed that for very long waves, the loading conditions will be similar to uniform flow. It is suggested to investigate the effect of the wave period on the stability of an open filter in more detail. It is suggested to use a wider range of wave periods than applied in this research.

Preface

This report is written as the final fulfillment for the completion of the Double Degree program at the Delft University of Technology and the National University of Singapore. This thesis was partially conducted in the fluid mechanics laboratory at the Delft University of Technology and commissioned by Delta Marine Consultants.

The completion of my research would not be possible without the support of the following people. First of all, I am grateful to all members of my graduation committee. During the meetings with the members of my committee, I was provided with new insights, criticisms and thorough discussions which provided the guidance for my research.

Furthermore, I would like to thank my colleagues at Delta Marine Consultants. Besides Bas Reedijk, who took part in my graduation committee, I'm also very thankful to Markus Muttray. His enthusiasm for scientific research and knowledge of physical experimental was very inspiring.

A very import role in my research was taken by Gijs Hoffmans. In my thesis, I did an attempt to continue on his work. I'm very grateful for our talks and his feedback on my work.

Last but not least I would thank Sander de Vree and Jaap van Duin. Their advice, guidance and assistance in the lab was crucial for the success of the experiments.

Rotterdam, February 2015

Wessel Hollander

Table of Contents

Summary.....	IV
Preface.....	VI
Table of Contents.....	VII
List of symbols.....	X
List of figures.....	XII
List of tables.....	XIV
1 Introduction.....	1
1.1 General introduction.....	1
1.2 Problem definition.....	2
1.3 Research question.....	2
1.4 Research method.....	2
1.5 Outline of the report.....	3
2 Theoretical background.....	5
2.1 Failure mechanisms of open filters.....	5
2.2 Wave theory.....	6
2.2.1 Linear waves.....	6
2.2.2 Non linear waves.....	7
2.2.3 Breaker criterion.....	9
2.3 Stability of the bed material.....	9
2.3.1 Forces on a single grain.....	9
2.3.2 Stability relations.....	11
2.3.3 Classification of instability.....	15
2.4 Design approaches for open filters.....	16
2.4.1 Two types of open filters.....	16
2.4.2 Base-filter interface stability.....	16
2.4.3 Design methods open filters.....	17
2.5 Previous experimental research to open filters under wave loading.....	19
2.5.1 Halter (1999).....	19
2.5.2 Jansens (2000).....	20
2.5.3 Wolters & Van Gent (2012).....	20
2.6 Chapter review.....	21
3 Hoffmans' design formula for open filters.....	23
3.1 Background of Hoffmans' formula.....	23
3.1.1 Derivation.....	23
3.1.2 The load damping.....	25
3.2 validation of Hoffmans formula.....	27
3.2.1 Hoffmans' validation.....	27

3.2.2	Van de Sande (2012)	28
3.2.3	Joustra (2013)	30
3.2.4	Overview of the load damp coefficients	31
3.3	Validation method of Hoffmans formula under wave loading	31
3.3.1	Approach for experiments	32
3.3.2	Other datasets which can be used for the validation of Hoffmans' formula	34
3.4	Discussion and necessity for further experimental research.....	34
3.5	Chapter review	35
4	Physical model	37
4.1	Model layout	37
4.2	Instrumentation.....	40
4.2.1	Wave generator	40
4.2.2	Wave gauges.....	40
4.2.3	Velocity meter (EMS)	41
4.2.4	Camera set up.....	41
4.3	Material properties.....	41
4.3.1	Filter material	42
4.3.2	Base material	42
4.4	Test program	43
4.5	Wave behavior and side effects in the flume	44
4.5.1	Wave linearity.....	44
4.5.2	Shoaling & reflection in the flume	45
4.5.3	Mass flux and return currents.....	46
4.5.4	Wall friction	46
4.6	Model scaling.....	46
5	Results.....	49
5.1	Overview of the results.....	49
5.2	Classification of instability	50
5.3	Unexpected phenomena	51
5.4	Bacteria in the flume	52
5.5	Inaccuracies in the experiments.....	53
5.5.1	Qualification of instability.....	53
5.5.2	Thickness of the filter layer.....	53
5.6	Chapter review	53
6	Analysis	55
6.1	Classical validation approach.....	55
6.2	New approach (using the assumption that $Ld'=Ld$).....	56
6.2.1	Overview of the results.....	56
6.2.2	Sensitivity analysis	57
6.2.3	Validity of the original Hoffmans formula under wave loading	59
6.2.4	Validity of the van de Sande formula under wave loading	59
6.2.5	Testing of the hypotheses of Hoffmans and Verheij (2013)	60
6.3	Chapter review	63
7	Discussion	65

7.1	Assumption $Ld' = Ld$	65
7.2	Source term in Hoffmans formula	66
7.3	Feedback on the validity of Hoffmans formula under wave loading and the hypotheses (feedback on Bezuijen and Kohler)	67
7.4	Comparison of the data with Jansens (2000)	68
7.5	Comparison of the data with Wolters & Van Gent (2012).....	69
8	Conclusions & recommendations	73
8.1	Conclusions.....	73
8.2	Recommendations.....	75
9	Bibliography	77
Appendices		
80		
A	- Background information of previous experimental research	81
A1	Halter (1999).....	81
A2	Jansens (2000)	82
A3	Wolters & van Gent (2012)	83
B	- Material properties.....	85
B1.	Filter materials	85
B2.	Base material.....	87
C	- Experimental results	89
C1	Overview	89
Test 1	91
Test 2	93
Test 3	95
Test 4	96
Test 4 (repeated)	98
Test 5	99
Test 6	100
Test 7	101
Test 8 (no filter layer)	103
D	- Sensitivity analysis.....	105
D1	Base parameters and uncertainty.....	105
D2	Propagation of uncertainty.....	107
D3	Influence of the individual parameters.....	108
D4	Critical note to the reflection analysis	108
E	- Addition to analysis; graphs including uncertainties of the data	111
E1	Graph with error bars for hypothesis 1	112
E2	Graphs with error bars for hypothesis II	113

List of symbols

Symbol	Definition	Unit
a	Wave amplitude	m
a_b	Wave amplitude at bottom	m
A_D	Surface exposed to the drag force	m^2
A_L	Surface exposed to the lift force	m^2
C	Dimensionless parameter	-
c_f	Friction coefficient	-
c_{fw}	Friction coefficient under waves	-
c_v	Consolidation coefficient	m^2/s
C	Chezy coefficient	$m^{1/2}/s$
C_b	The bulk coefficient that accounts for drag and lift forces	-
C_D	Drag coefficient	-
C_L	Lift coefficient	-
C_m	The bulk coefficient that accounts for the effect of the acceleration	-
$C_{m:b}$	The added mass over the bulk coefficient	-
d	Grain diameter	m
d_x	Grain diameter where x % of the grain mass has a smaller diameter	m
e	Ratio between the shear velocity and pore velocity at interface	-
D_f	Thickness of the filter layer	m
F_A	Acceleration force	$kg.m/s^2$
F_D	Drag force	$kg.m/s^2$
F_L	Lift force	$kg.m/s^2$
F_u	Velocity force	$kg.m/s^2$
g	Acceleration of gravity	m/s^2
h	Water depth	m
H	Wave height	m
i	Hydraulic gradient	-
i_c	Critical gradient in filter	-
I	Slope	-
k	Wave number	1/m
k_b	Turbulence energy near the bed	m^2/s^2
k_f	Local turbulence energy in the filter layer	m^2/s^2
$k_{f,s}$	Turbulence energy resulting from the hydraulic gradient	m^2/s^2
k_r	(equivalent) roughness of bottom	m
k_t	Turbulent kinetic energy	m^2/s^2
K	Shape coefficient in Izbash formula	-
L	Wave length	m
L_d	Load damping length	m
L_m	Mixing length	m
m	Dimensionless parameter	-
n_f	Porosity of filter material	-
p	Pressure	N/m^2
R	Hydraulic radius	m
Re	Particle Reynolds number	-
s	Wave steepness	-

T	Wave period	s	
T_p	Peak wave period	s	
u	Velocity in x-direction	m/s	
\bar{u}	Velocity averaged in time or space	m/s	
u_b	Bottom velocity	m/s	
u_c	Critical velocity	m/s	
u_*	Shear velocity	m/s	
u_{c*}	Critical shear velocity	m/s	
V	Volume	m ³	
V_c	$= \frac{\tau_{RMS,c}}{\tau_c} \approx 1 - d_{15}/d_{50}$	Variation coefficient that represents the influence of the non-uniformity of heterogeneity of the soil	-
v_p	Velocity of the particle	m/s	
x	Horizontal direction	m	
y	Transversal direction	m	
z	Vertical direction	m	

Greek Symbols

α_d	Load damp coefficient	-
$\alpha_{d,H}$	Load damp coefficient according to the Hoffmans formula $\alpha_{d,H} = L_d/d_{f15}$	-
$\alpha_{d,S}$	Load damp coefficient according to Van de Sande formula $\alpha_{d,S} = L_d/d_{f50}$	-
γ	Loading coefficient	-
δ	Thickness of the boundary layer	m
Δ	Relative density	-
κ	Von Kármán constant	-
ν	Kinematic viscosity	m ² /s
ρ	Density	kg/m ³
ρ_s	Density of sediment	kg/m ³
ρ_w	Density of water	kg/m ³
η_c	Relative strength	-
τ	Shear stress	N/m ²
τ_c	Critical shear stress	N/m ²
$\tau_{RMS,c}$	Root mean square value of the fluctuating critical bed shear stress	N/m ²
$\hat{\tau}_w$	Shear stress under waves	N/m ²
ω	Radian frequency	1/s
Ψ_c	Critical shields stability parameter	-

List of figures

Figure 2-1 Failure mechanisms (Verheij <i>et al.</i> , 2012)	6
Figure 2-2 The orbital motion in deep water, intermediate-depth and very shallow water (Holthuijsen, 2007).....	7
Figure 2-3 The ranges of applicability of the various wave theories (Holthuijsen, 2007) (in this graph, d is the water depth)	8
Figure 2-4 The surface profile a second-order Stokes wave (Holthuijsen, 2007).....	8
Figure 2-5 forces on a grain in flow (Schierreck & Verhagen, Introduction to bed, bank and shore protection, 2012).....	9
Figure 2-6 pressure differences due to acceleration Dessens (2004)	10
Figure 2-7 Values of C_b and C_m found by Dean and Dalrymple (1991), Dessens (2004) and Tromp (2004) (From Steenstra (2014))	10
Figure 2-8 changes of integrated forces on a stone. The vectors represent the resulting forces (Hofland 2005).....	11
Figure 2-9 critical shear stress according to Shields - van Rijn (1984).....	12
Figure 2-10 Modified shields curve for unsteady flow (Sleath, 1978).....	13
Figure 2-11 different transport stages (CUR, 2010)	15
Figure 2-12 critical hydraulic gradient with steady flow parallel to interface (de Graauw, van der Meulen, & van der Does de Bye, 1984)	16
Figure 3-1 experimental data of Klar (Wenka and Köhler 2007)	25
Figure 3-2 DF/df_{50} versus the critical df_{50}/db_{50} . (Verheij, Hoffmans, Dorst, & van de Sande, 2012)..	28
Figure 3-3 movement of filter material and base material (Verheij, Hoffmans, Dorst, & van de Sande, 2012).....	29
Figure 3-4 Experimental data to validate Hoffmans' load damp coefficient (Van de Sande (2012))	29
Figure 3-5 visualization of the load damping through the filter	33
Figure 4-1 the wave flume.....	37
Figure 4-2 fabricated filter slab.	40
Figure 4-3 wave gauge.....	41
Figure 4-4 grain size distribution of the filter materials	42
Figure 4-5 Sievedistribution of the base material	43
Figure 4-6 Overview of the tests	44
Figure 4-7 red area indicates the work area of this research	44
Figure 4-8 Two measured wave profiles in the flume. The red profile shows more nonlinearity than the black profile.....	45
Figure 4-9 analysis of the orbital wave velocity in the flume near the bed	45
Figure 4-10 wave profiles before and above the filter-setup.....	46
Figure 5-1 Erosion after a long duration test (test 2 $T=2.0s$ $H=0.12m$)	51
Figure 5-2 winnowing trough the filter (test 6 $T=2.5s$ $H=0.08m$)	51
Figure 5-3 Dirt from the filter clouding the water (test 4)	51
Figure 5-4 scour hole next to the tray (test 1, after a long duration test of 20 hour).....	52
Figure 5-5 bacteria in the flume (test 4).....	52
Figure 5-6 distribution of the deviations in the measured filter layer thickness compared with the average value.....	53

Figure 6-1 Classical validation approach (for shown data points are classified as “only base erosion”). The following assumptions are made for the data of Wolters & Van Gent (2012): $\Delta f \Delta b \approx 1$, and $\gamma V_c, f \gamma V_c, b \approx 1$	55
Figure 6-2 Influence of the individual uncertainties on the obtained value for the load damping length (based on test 4).....	59
Figure 6-3 Hypothetical values (obtained by hypothesis I) for Ld and the Ld values obtained in the experiments.....	61
Figure 6-4 Hypothetical values (obtained by hypothesis II) for Ld and the Ld values obtained in the experiments.....	62

List of tables

Table 2-1 parameters in formula for critical filter velocity (Klein Breteler, den Adel, & Koenders, 1992)	17
Table 3-1 proposed load damp parameters by Van de Sande (2012)	30
Table 3-2 classification of base stability in Joustra's research	31
Table 3-3 classification of filter stability	31
Table 3-4 Suggested values for the load damp coefficients	31
Table 3-5 used parameters to find the load damp parameter	34
Table 4-1 Left: setup of the camera. Right: a camera shot of the transparent tray.	41
Table 4-2 Overview filter properties	42
Table 4-3 overview base material properties	42
Table 4-4 Test program	43
Table 5-1 Overview of the test results	50
Table 6-1 overview of the calculated values for the load damping length and the load damp coefficients per test	57
Table 6-2 Uncertainty of the parameters	57
Table 6-3 standard deviation of Ld'	58
Table 7-1 estimated pore velocities for the critical hydraulic conditions. The pore velocity is estimated with equation 73	69
Table 7-2 Transport rates using Wolters and Van Gent's (2012) formula (with the use of the relation between KCf and $i2\%$	70
Table 7-3 Transport rates using Wolters and Van Gent's (2012) formula (where $imax$ is calculated using the linear wave theorem)	71

Chapter 1

Introduction

1.1 General introduction

Granular filters are structures to protect a bed or construction against scour and erosion. Filters are constructed of rock material and can be applied in single or multiple layers. The different types of filters are categorized in “geometrically closed” and “geometrically open” filters.

In a geometrically closed filter the base material cannot move through the filter. These filters are built up with multiple layers. The upper layer of the filter is designed such that it is stable under the hydraulic loading. Due to the accuracy of the filter construction in practice, every individual layer has a minimum thickness of about 30 cm, this makes a closed filter relatively thick in practice. Thereby these closed filters are expensive difficult to realize in wet conditions.

Geometrically open filters can serve as an alternative. Within an open filter, the pores of the filter material are large enough for the base material to move through. The philosophy behind this concept is to reduce the hydraulic loading within the filter, so that movement of the base material is not initiated. Thus the filter is *geometrically open*, but *hydraulically closed*. Sometimes limited amounts of erosion can be accepted, in this scenario an unstable open filter can be applied. For these unstable open filters reference is made to Wolters and van Gent (2012), who carried out physical tests with base material transport for open filters loaded by waves and currents.

In contrast with closed filters, open filters do not necessarily consist out of multiple layers. For this reason open filters are easier to realize in the field and may lead to a more economical design. Open filters may be used for bed-, toe- and slope protections.

Several design approaches exist for open filters. The most recent method is founded by Hoffmans (2012). Hoffmans' formula is validated by Van de Sande (2012) for uniform flow conditions. Van de Sande made suggestions for a modification in Hoffmans' formula, i.e. the load damp coefficient. Van de Sande also observed an increased bed mobility for flows with additional turbulence. Joustra (2013) extended the validation research and performed experiments with additional turbulence. Joustra validated the formula for flows with sill-induced additional turbulence and for flows with a cylindrical

pier. This research resulted in suggestions for alternative load damp coefficients in Hoffmans' formula for these specific situations with additional turbulence.

1.2 Problem definition

Hoffmans suggests that his recently founded relation is applicable for uniform and non-uniform flow. However, the validity of the formula under wave loading is never proven. The oscillatory flow near the bed has another turbulence intensity than uniform flow. Therefore, it might be necessary to use other values of the load damp coefficients in the formula than suggested by Van de Sande and Joustra. Bezuijen & Köhler (1996) stated that the damping length of a porous medium depends on the pressure period (and thereby the wave period). This implies that the load damp coefficient in Hoffmans formula also depends on the wave period.

At this moment the load damp coefficients are validated for uniform flow, flow with additional turbulence by a sill and flow with additional turbulence by a cylindrical pier. For wave loading, no validation study is conducted yet. Although, based on literature it is expected that the period of the oscillating flow has an effect on the load damping in the filter. Furthermore, it is discussed whether the values for the load damp coefficient should be lower or higher than for uniform flow.

1.3 Research question

The aim of this research is to validate Hoffmans formula for wave loading. It will be attempted to find the load damp coefficient for oscillatory flow. Because it is supposed that the wave period has an influence on the load damp parameter, the influence of the wave period will be investigated. The research question is stated as follows:

“Is the design formula of Hoffmans (2012) valid for wave loading on horizontal filters?”

The sub questions are formulated as follows:

- “What can be said about the value for the load damp coefficient under wave loading?”
- “Is it possible to verify or falsify the hypotheses for the load damping length?”
- “What is the difference between an oscillating flow and an uniform flow regarding the stability of an open filter?”

1.4 Research method

Similar to previous validation experiments, physical model tests are carried out. The wave flume of the TU Delft Laboratory is used. Experiments are configured with different filter thicknesses and different base- and filter material properties. Since it is questioned how the wave period influences the load damp coefficient in a filter, the experiments are carried out with regular waves. Hence, it is attempted to investigate the effect between different wave periods.

The validation procedure will be carried out in a similar way as previous validation research (referred to as “the classical approach”). To do an accurate suggestion for the load damp coefficient, this approach requires experimental data with simultaneous erosion of the filter and base layer. Due to practical limitations and the limited dimensions of the flume, no tests are performed where the filter material became unstable. For this reason no accurate suggestion can be done for the load damp coefficient under wave loading when the classical approach is used. For this reason, a new approach for the validation procedure is introduced. The major difference with the classical approach is that the generated shear stress upon the base and filter material is used, instead the critical shear stress.

The classification of base material instability is determined with visual observations. Camera recordings of each test are made. Thereby recordings with a wave gauge and a EMS are made. These test results are used for the validation procedure.

1.5 Outline of the report

Chapter 2 gives a theoretical framework for this research. First, the hydraulic loading is discussed, where the difference between uniform and oscillating flow is pointed out. Subsequently the hydraulic loading is related to the stability of granular material. Finally, attention is being paid to open filters, for which different stability relations and design approaches are presented.

Chapter 3 gives a comprehensive background on Hoffmans formula. This formula is a fundamental part of this research. The derivation of the formula is discussed, and more background is given about the load damp coefficients. Thereby, the new validation approach is introduced.

In chapter 4 the model setup is explained. Also, the material properties and hydraulic conditions in the flume are analyzed. The test program is shown and the model scale is discussed.

In chapter 5 the test results are explained. For every test, a background is given. This section shows numerous pictures of the tests.

Then, in chapter 6 the data is analyzed and the hypotheses are tested.

In Chapter 7, the results of the analysis and the assumptions made in this research are discussed.

Finally, the conclusions and recommendations are given in chapter 8.

Chapter 2

Theoretical background

This section gives a brief background on the hydraulic loading, stability of granular material and existing theories on open filters. For more detailed information is referred to the original publications. In particular the book “Introduction to bed, bank and shore protection” written by Schiereck & Verhagen (2012) gives a comprehensive background on this field of study.

This chapter is started with an explanation of the failure mechanisms for granular bed protections. Consequently the processes behind the failure are explained. The physics will be described starting from the water surface, where the wave theory is explained. Next, the hydraulic conditions above the filter bed and the stability relations of granular material are presented.. Subsequently the processes within the granular filter are explained.

The existing design approaches for open filters are discussed in paragraph 2.4. The Hoffmans formula is explained separately in chapter 3, where an extensive background on this relation is given.

2.1 Failure mechanisms of open filters

Filters are used to protect a bed against scour. The filter is placed over the original bed. The main principle is that the larger grains of the filter material are stable under the hydraulic loading. There are different failure mechanisms for filters, as can be seen in Figure 2-1. The filter material itself may be unstable or the base material may be transported through the filter. For both mechanisms, the failure occurs when the hydraulic loading exceeds the strength of the material. To prevent shear failure, a more stable filter should be selected (e.g. a larger grain diameter or a higher density). To prevent winnowing, the hydraulic loading at the bed-filter interface should be decreased (e.g. by increasing the thickness of the filter, or selecting a smaller filter diameter).

Conventional filters are geometrically closed. This means that the underlying material is too coarse to move through the overlying layer. These closed filters mostly consist out of multiple layers which are carefully selected based on their grading. Bed material movement within these layers is not possible. Therefore the failure mechanism on the right hand side in Figure 2-1 (winnowing) does not apply for geometrically closed filter.

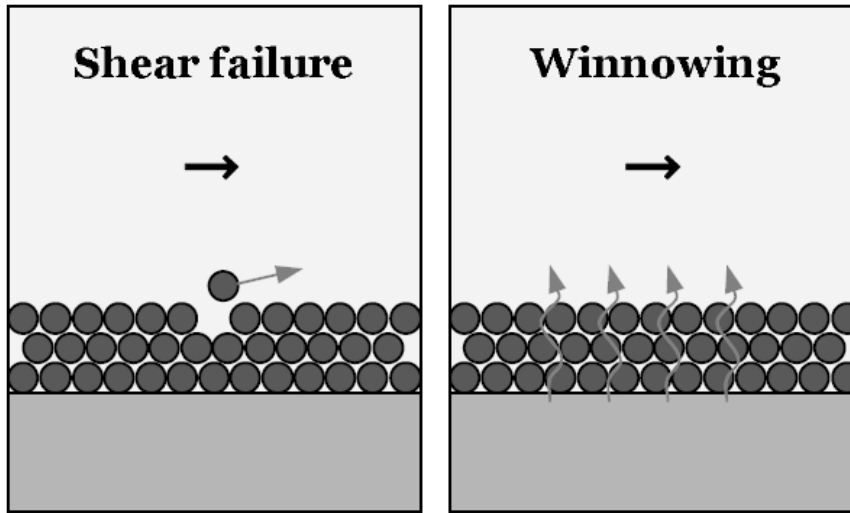


Figure 2-1 Failure mechanisms (Verheij *et al.*, 2012)

Another type of filter is the geometrically open filter. Geometrically open filters are based on the philosophy that the hydraulic loading is reduced within the filter, such that the base material is stable. In contrast to geometrically closed filters, geometrically open filters are not constructed using multiple different layers, in practice these filters have the advantage that only one gradation of filter material needs to be applied, which significantly reduces the costs. This research is focused on open filters. Both failure mechanisms depicted in Figure 2-1 may apply for geometrically open filters.

2.2 Wave theory

This paragraph presents a concise review of the linear wave theory. For an extensive background of the wave theory is referred to Holthuijsen (2007).

2.2.1 Linear waves

In general the waves can be described according to the linear wave theory. For an ideal fluid, the density is constant and the fluid is incompressible. The linear wave theory can be applied if the amplitude of the waves is small relative to the wave length and the water depth. This small amplitude approximation is important for the behavior of the waves (otherwise the waves become nonlinear).

The basis of the linear wave theory are the mass balance and continuity equations. With the use of some boundary conditions the wave equation is found:

$$\eta(x, t) = a \cdot \sin(\omega t - kx) \text{ or } \eta(x, t) = a \cdot \sin\left(\frac{2\pi}{T}t - \frac{2\pi}{L}x\right) \quad (1)$$

The radiation frequency and wave number can also be expressed in respectively the wave period and wave length. A (water depth dependent) relation exists between these 2 parameters; the dispersion relation:

$$\omega^2 = gk \cdot \tanh(kh) \quad (2)$$

From the dispersion relation the wave speed for deep and shallow water can be derived. The wave speed is depth dependent. In deep water the wave speed is independent from the water depth, and only depends on the wave period. In shallow water, it works the other way around, and the wave speed is only dependent from the water depth.

$$c = \frac{\omega}{k} \rightarrow \text{Deep water } c = \frac{g}{\omega} \quad \text{shallow water } c = \sqrt{gh} \quad (3)$$

The water particles move in orbital motions below the waves. The magnitude of these motions is smaller deeper in the water column. In deep water, these motions are unaffected by the bottom. In shallow water, the motions are affected.

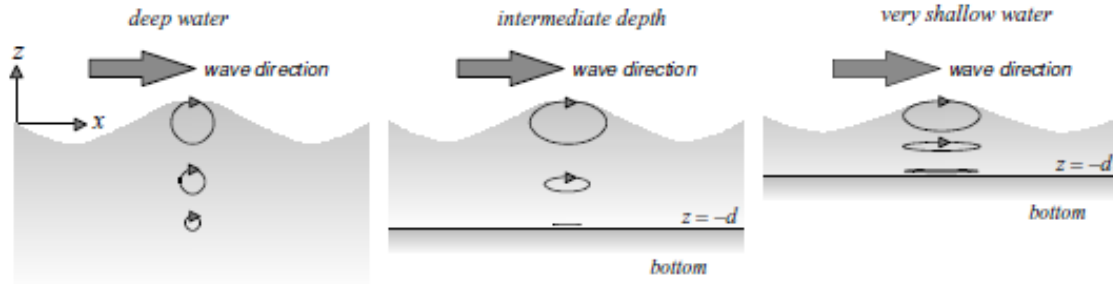


Figure 2-2 The orbital motion in deep water, intermediate-depth and very shallow water (Holthuijsen, 2007)

The linear wave theory gives the definition for the velocity of the water particles:

$$u_x = \hat{u}_x \sin(\omega t - kx) \quad \text{with} \quad \hat{u}_x = \omega a \frac{\cosh[k(h+z)]}{\sinh(kh)} \quad (4)$$

$$u_z = \hat{u}_z \cos(\omega t - kx) \quad \text{with} \quad \hat{u}_z = \omega a \frac{\sinh[k(h+z)]}{\sinh(kh)} \quad (5)$$

The pressure under waves is described by the following relation;

$$p = -\rho g z + \hat{p}_w \sin(\omega t - kx) \quad \text{with} \quad \hat{p}_w = \rho g a \frac{\cosh[k(h+z)]}{\cosh(kh)} \quad (6)$$

Thus the pressure gradient is under waves described as:

$$i = ka \frac{\cosh[k(h+z)]}{\cosh(kh)} \cos(\omega t - kx) \quad (7)$$

2.2.2 Non linear waves

In the previous section the wave components were considered to be harmonic and independent, and could be described as linear harmonic waves. However, when the waves become too steep, or when the water depth becomes too shallow, the linear wave theory cannot be applied any more. The degree of nonlinearity of waves is often quantified with the Ursell number, which incorporates the wave steepness and water depth. The linear wave theory is applicable when the Ursell number is smaller than 10. When the Ursell number is larger than 26, the cnoidal wave theory describes the wave more accurately. Figure 2-3 gives the ranges of applicability of various wave theories.

$$N_{Ursell} = \frac{\text{steepness}}{(\text{relative depth})^3} = \frac{\frac{H}{L}}{\left(\frac{h}{L}\right)^3} = \frac{HL^2}{h^3} \quad (8)$$

The description of nonlinear waves can be approximated by adding corrections to the (linear) harmonic wave profile. This means, that extra harmonics are added to the basic harmonic (see Figure

2-4). When waves become more non-linear, more harmonics can be added to approximate the wave conditions. It should be noticed that nonlinear waves have steeper crests and longer troughs, the waves are more peaked. The steepness of the crests is therefore larger than that of the basic harmonic (the steepness of the basic harmonic can easily be approximated with the linear wave theory).

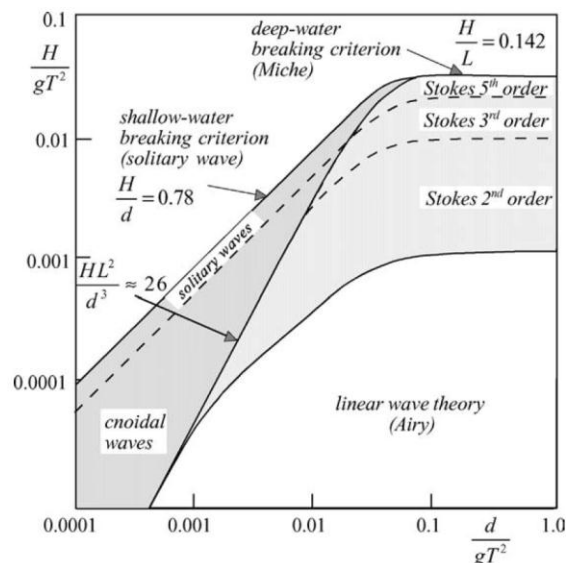


Figure 2-3 The ranges of applicability of the various wave theories (Holthuijsen, 2007) (in this graph, d is the water depth)

The description of nonlinear waves can be approximated by adding corrections to the (linear) harmonic wave profile. This means, that extra harmonics are added to the basic harmonic (see Figure 2-4). When waves become more non-linear, more harmonics can be added to approximate the wave conditions. It should be noticed that nonlinear waves have steeper crests and longer troughs, the waves are more peaked. The steepness of the crests is therefore larger than that of the basic harmonic (the steepness of the basic harmonic can easily be approximated with the linear wave theory).

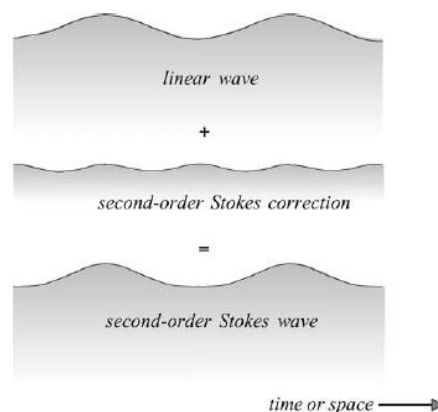


Figure 2-4 The surface profile a second-order Stokes wave (Holthuijsen, 2007)

Although the linear wave theory is not perfectly applicable it is still prominently used in the field of shore protections. Compared to the nonlinear theories, the linear wave theory is far more easy to use. Thereby the linear theory gives most of the time an accurate approximation. LeMéhauté (1968) showed that the linear wave theory predicts the orbital velocities quite well, even far outside the validity limits of the linear wave theory.

2.2.3 Breaker criterion

The maximum wave height is limited by two factors; the wave steepness and the water depth. When waves become too steep, they break. The maximum value for the steepness ($s=H/L$) is approximately 5%. As mentioned in the previous section, nonlinear waves are more peaked than linear waves, and therefore quite steep.

In shallow water the water depth influences the maximum wave height, this water depth can be found with the breaker index ($\gamma=H/h$). The values for this index have a range between 0.6 and 1.6 (found by Kaminsky and Kraus (1993)). An average value of 0.78 is often used.

2.3 Stability of the bed material

2.3.1 Forces on a single grain

To understand the phenomena of instability of bed material, the force scheme of a single grain is discussed. The forces which influence the stability of individual stones are discussed in this paragraph. First, the forces resulting from an uniform flow are discussed. Then, the acceleration term is taken into account. Subsequently, the influence of turbulent eddies and the influence of gravity is discussed.

Uniform flow

When a flow passes a single stone, the fluid particles have to pass a larger distance to pass the stone than the fluid particles under the stone. This causes a velocity difference between the top and the bottom of the stone. This velocity difference results in a *lift force*.

$$F_l = \frac{1}{2} C_l A_l \rho_w u |u| \quad (9)$$

The surface of a stone has a certain roughness. When a flow passes a stone, a shear force results. Besides this shear force, a small wake occurs behind the stone. The shear force and the influence of this wake are represented by the *drag force*. The relative importance of the shear force and the small wake can be determined using the particle Reynolds number (see equation 11). For small particle Reynolds numbers (<3.5) the viscous stresses are large and so is the shear force. For large particle Reynolds numbers (>500) the viscous stresses are small and the shear stress on the stone becomes negligible, so the influence of the small wake dominated the drag force.

$$F_D = \frac{1}{2} C_D \rho_w u |u| \quad (10)$$

$$Re_* = \frac{u_* c d}{\nu} \quad (11)$$

The resistant forces of the stone are its own weight and also a friction force. The force scheme is presented in Figure 2-5.

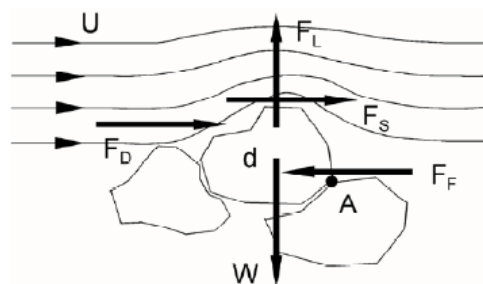


Figure 2-5 forces on a grain in flow (Schierck & Verhagen, Introduction to bed, bank and shore protection, 2012)

Acceleration

The acceleration in a flow creates a pressure difference on a stone. This pressure difference results in a net force. For accelerating flows the net force is in the same direction as the flow. For decelerating flows the opposite happens, the net force due to the acceleration is in the opposite direction of the flow. The magnitude of the acceleration force can be found with equation 12. In this equation, the added mass of the particle is also taken in to account. This added mass represents a force which occurs when a particle is accelerating through a flow.

$$F_a = \rho V \frac{D\bar{U}}{Dt} + \rho V C_m \left(\frac{D\bar{U}}{Dt} - \frac{dv_p}{dt} \right) \quad (12)$$

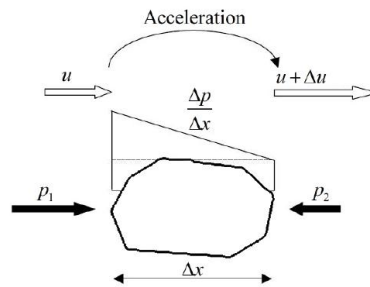


Figure 2-6 pressure differences due to acceleration Dessens (2004)

The total force on a stone can be found with the Morison approach (Morison et al (1950)). In this approach, the sum of the acceleration and velocity force is used to calculate the total force.

$$F_{tot} = F_u + F_a = \frac{1}{2} C_b A \rho u_x |u_x| + C_m \rho V \frac{Du_x}{Dx} \quad (13)$$

Parameters C_b and C_m give the relative importance of the flow and acceleration respectively. The effect of the accelerations is investigated by Dessens and Tromp. Dessens carried out research to flows with a constant acceleration. Dessens states that the values of C_b and C_m depend on the pivoting angle (the angle in which the stone particle is expected to move when the stone becomes unstable). Tromp did research to the stability of stones under wave loading. It has to be noticed that the relative influence of the acceleration term is smaller under wave loading than for flows with a constant acceleration.

Pivoting angle	C_b	C_m	C_m / C_b
Dean and Dalrymple [1991]			
-	-	0.3 - 3.0	-
Dessens [2004]			
30°	0.10	3.92	39.2
45°	0.14	5.55	39.6
Tromp [2004]			
-	0.40 - 0.55	2.67 - 3.75	4.85 - 9.375

Figure 2-7 Values of C_b and C_m found by Dean and Dalrymple (1991), Dessens (2004) and Tromp (2004) (From Steenstra (2014))

If only the fluid velocity and acceleration are considered, one would say that an accelerating flow leads to a decreasing stability of the bed material, and a decelerating flow leads to a more stable bed. This is, because under accelerating flow the net force that results from the pressure difference is in the same direction as the flow, which leads to an increased resulting force on the stone. For a decelerating flow, the opposite occurs. However, it is very important to bear in mind that the acceleration interacts with the turbulence near the bed. The turbulence does also influence the

stability of the bed. Huijsmans (2006) has found in his research that the turbulence intensity decreases for accelerating flows, and increases for decelerating flows. Huijsmans even made observations where the stability increased for an increased acceleration.

Turbulence

Turbulence can be found as a fluctuation in the velocity of the flow. The resulting force on a stone will also fluctuate due to these velocity fluctuations. The intensity of the turbulent fluctuations varies for different situations (e.g. the turbulence intensity behind a cylindrical pier is much more intense than the turbulence intensity over a horizontal bed loaded by uniform flow).

Turbulent wall pressures

The turbulent wall pressures are induced by the turbulent flow. The pressures result in a net force on the stone. Hofland (2005) states that the turbulent wall pressures merely lead to an up or downward movement of the stone, but are important since it can give the initial lift to the stone which result in further instability.

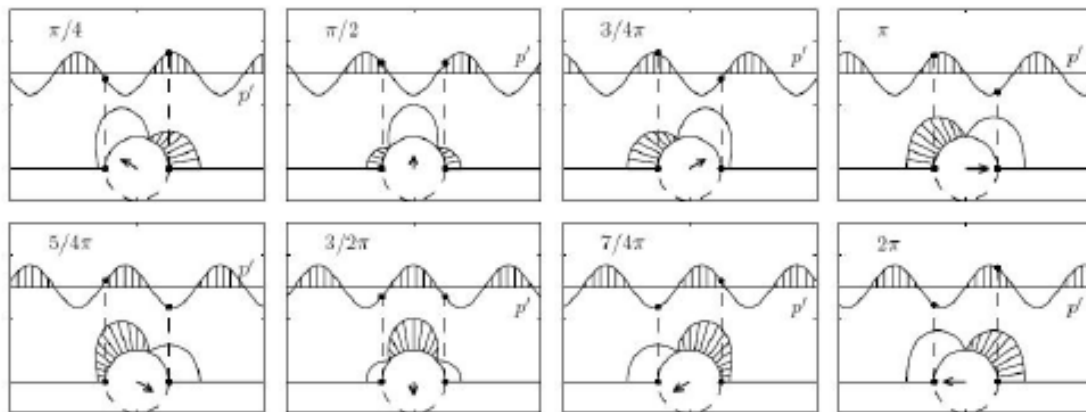


Figure 2-8 changes of integrated forces on a stone. The vectors represent the resulting forces (Hofland 2005)

Gravity

For the stability of a single stone its own weight is of importance, this force stabilizes the stone. Thereby the weight has an effect on the friction between the individual stones. When stone material is placed on a slope, gravity can be a force that contributes to the instability.

2.3.2 Stability relations

2.3.2.1 General form

A single stone becomes unstable when the load on this stone exceeds its strength. Basically, this is also the definition of the stability parameter. This dimensionless parameter gives the ratio between the strength and load. Hofland (2005) proposes a general form for this parameter (see equation 14). This form of the equation includes the velocity, the acceleration and the turbulence (the fluctuations in the velocity and acceleration).

$$\psi_{tot} = \frac{(C_b(\bar{u} + \tilde{u}') + C_m(\bar{a} + \tilde{a}')d)}{\Delta g d} \quad (14)$$

Multiple variants for the stability relation are derived in the last decennia. Some of them focus on the incorporation of the effect of the turbulence (Jongeling et al. (2003), Hofland (2005), Hoan (2008)), while other authors focused on the effect of the acceleration on stability (Dessens (2004), Tromp (2004), Huijsmans (2006)). In this report a few of these parameters will be discussed. The most well-

known stability relations of Izbash and Shields (1936) are further explained. Subsequently some relations are discussed to determine stability under wave loading (Sleath, Rance & Warren and Tromp). Finally the relation of Steenstra is presented, which is the most recent parameter and incorporates the effects of both turbulence and accelerating flows. Reference is made to Steenstra for a comprehensive background on the different stability formulas.

2.3.2.2 Izbash

Izbash considers the forces on an individual grain. For this reason, the velocity near the grain must be known. The forces on a single grain are depicted in Figure 2-5. Balancing the drag force, the shear force and the lift force gives an expression for the critical velocity, see equation 15. Values for coefficient K in the equation are found empirically for different turbulence situations (e.g. behind a groin, a pier etc.) Notice that this stability relation is based on the flow near the stone, and does not incorporate accelerations.

$$u_c^2 \propto \left(\frac{\rho_s - \rho_w}{\rho_w} \right) gd = \Delta gd \quad \rightarrow \quad u_c^2 = K \Delta gd \quad (15)$$

2.3.2.3 Shields

In contrary to the latter, where the stability of granular material is based on the forces on a single stone, Shields (1936) considers an average shear stress over a bed surface. A relation is given between the particle shear stress and the Reynolds number, see equation 16. This relation is found for uniform flow. The stability curve is showed in Figure 2-9. Van Rijn (1984) replaced the particle Reynolds number on the x-axis by a dimensionless particle diameter. It can be seen that for grains larger than 7 mm the stability parameter has a constant value of $\Psi_c = 0.056$. Notice that Shields stability relation is based on uniform flow and uses only the bed shear stress, it does not incorporate accelerations or additional turbulence.

$$\Psi_c = \frac{\text{load}}{\text{strength}} = \frac{\tau_c}{(\rho_s - \rho_w)gd} = \frac{u_{*c}^2}{\Delta gd} = f(Re_*) = f\left(\frac{u_{*c}d}{\nu}\right) \quad (16)$$

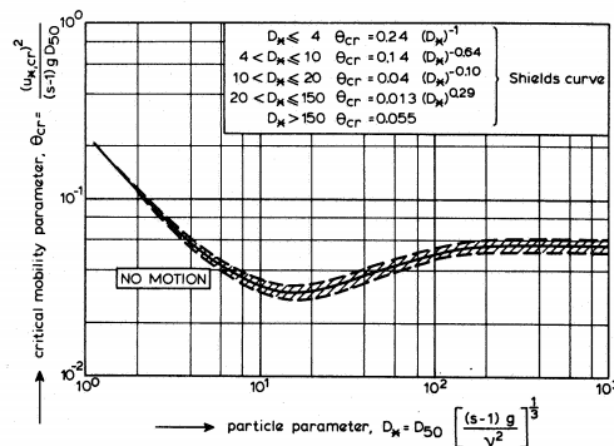


Figure 2-9 critical shear stress according to Shields - van Rijn (1984)

2.3.2.4 Sleath

The stability of granular material under waves differs from the stability under uniform flow. However, a similar approach is used as in Shields' approach. The Shields curve is adapted for oscillatory flows by Sleath (1978) (see Figure 2-10). For the smaller grain diameters a smaller Shields value is found. The difference between Sleath's modified curve and Shields' original curve originates from the difference in the turbulence intensity which is generated under waves.

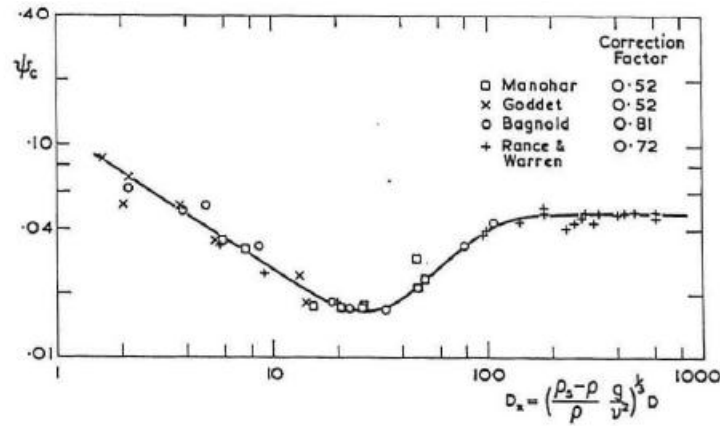


Figure 2-10 Modified shields curve for unsteady flow (Sleath, 1978)

Similar to uniform flow, oscillatory flow also generates friction near the bed. In contrast with uniform flow, the equilibrium cannot be found using the Chezy equation, because no constant hydraulic gradient can be considered. However, the waves that generate the oscillatory flow can be described using the linear wave theory. From this theory the near bed velocity of the fluid particles can be derived. Subsequently, this near bed velocity can be expressed in the shear stress analogous with equation 22.

First the movement of the water particles under waves is described with the linear wave theory. The oscillatory fluid particle velocity at the bed can be found with equation 17.

$$\hat{u}_b = \omega a_b = \frac{\omega a}{\sinh kh} \quad (17)$$

$$u = \hat{u}_b \sin \omega t \quad (18)$$

Similar to uniform flow, the oscillatory flow generates a shear stress near the bottom. This shear stress can be expressed as:

$$\hat{\tau}_w = \frac{1}{2} \rho c_{fw} \hat{u}_b^2 \quad (19)$$

Equation 19 shows similarities with equation 22, for oscillatory flow the average value for the shear stress is half the amount of the maximum shear stress (because the oscillatory shear stress is sinusoidal). The friction factor c_f under wave loading is not obtained in the same ways as for uniform flow. The direction of the flow constantly changes, so the boundary layer cannot fully develop over the water depth as is possible for uniform flow. This results in higher friction factors near the bed. The expression for the friction factor under waves is as follows (Jonsson, 1966):

$$c_{fw} = \frac{0.0604}{\log^2 \frac{2.2\delta}{k}} \quad (20)$$

Based on Jonsson (1966), an expression by Swart is given in which the friction factor is given as a function of the orbital stroke a_b at the bed and the bottom roughness (CUR 2010).

$$c_{fw} = 0.237 \left(\frac{a_b}{k_r} \right)^{-0.52} \quad \text{for } a_b > 0.636k_r \quad [\text{or } c_{fw,max} = 0.3] \quad (21)$$

For the larger grain diameters a value a stability parameter of $\Psi = 0.056$ is found, the same value as for uniform flow. The modified Shields curve found by Sleath (1978) is partly based on data by Rance & Warren (1968).

Intermezzo: shear stress under uniform flow

If a fluid flows over a bed, it will result in a friction between the bed and the fluid. This bed resistance is expressed as the shear stress. For laminar flow, this resistance is linear related to the flow velocity. In the field of study of this research is mostly dealt with turbulent flows. For turbulent flows, the relation between the shear stress and velocity becomes quadratic:

$$\tau = c_f \rho u^2 \quad (22)$$

For uniform flow on a slope, an equilibrium exists between the bottom shear stress and the fluid pressure on the slope. These two components can be coupled as follows:

$$\tau = \rho ghI = c_f \rho \bar{u}^2 \rightarrow \bar{u} = \frac{1}{\sqrt{c_f}} \sqrt{\rho ghI} \quad (23)$$

Now we can rewrite this into the Chezy equation:

$$\bar{u} = C\sqrt{RI} \quad \text{with: } C = \sqrt{\frac{g}{c_f}} \quad (24)$$

Where the Chezy coefficient depends on the dimensionless friction coefficient. The Chezy value can be determined with the help of the equivalent sand roughness relation of Nikuradse-Colebrook:

$$C = \frac{\sqrt{g}}{\kappa} \ln \frac{12R}{k_r} \approx 18 \log \frac{12R}{k_r} \quad (25)$$

In the field of this research the shear velocity is often used. In this parameter the shear stress is expressed in the dimensions of a velocity. This is not a velocity which really exists. It can be expressed as follows:

$$u_* = \sqrt{\frac{\tau}{\rho}} = \bar{u} \frac{\sqrt{g}}{C} \quad (26)$$

To summarize; the velocity of a fluid over a bed can be expressed in a shear stress. Using the Chezy equation, an equilibrium can be found between the shear stress and the hydraulic gradient for uniform flows. Finally the shear velocity is introduced, a shear stress expressed in the dimensions of a velocity.

2.3.2.5 Rance and Warren

Rance and Warren (1968) carried out research to the stability of bed material under oscillatory flow. The relation found in their experiments can be rewritten as follows (Schrierek & Fontijn, 1996):

$$d_{50} = \frac{2.56 \cdot \hat{u}_b^{2.5}}{\sqrt{T_p} \cdot (\Delta g)^{1.5}} \quad (27)$$

In contrast to the stability approach according to Sleath (1978), the approach based on the experiments of Rance & Warren (1968) does not include a friction factor. For smaller stone diameters in relatively deep water the difference between the two approaches is small. The difference increases when the stone diameters are larger. Larger stone diameters give a larger friction coefficient, this effect is not included in Rance and Warren's approach.

For the experiments conducted by Schiereck *et al* (1994) small differences are computed between Sleath (1978) and Rance & Warren (1968) for the smaller stone diameters. The agreement for regular waves is quite good for a certain range of wave periods, but can deviate significantly outside that range. Thus the two approaches are not always in agreement. For the larger grain diameters Rance & Warren (1968) seem to underestimate the stone size for incipient motion.

2.3.2.6 Other stability relations

Several other stability relations can be found in literature. Mostly, these relations are based on the same philosophy as equation 14. For more background of the stability of granular material under wave loading, reference is made to Tromp (2004).

A sophisticated formula which incorporates the effects of the fluid velocity, acceleration and turbulence is found by Steenstra (2014).

2.3.3 Classification of instability

For larger stone diameters a critical shields parameter of $\Psi_c = 0.056$ is found. This implies that there is a critical threshold value for transport; but this does not exist in reality. The grain material on the bed is irregular and smaller grains may move below the critical value. Breusers (1968) conducted an experiment to incipient motion and found 7 stages of transport; from “occasional movement at some locations” to “general transport of the grains”. A value of $\Psi_c = 0.03$ is considered safe for the threshold of motion.

Under oscillatory flow it is harder to classify instability; the particles brought in motion during the first half of the wave period are subsequently placed back during the second half of the wave period. Therefore the particles will bounce back and forth, and structural erosion is less likely. However, when the waves become irregular or non-linear (e.g. second order stokes waves), a net transport can be observed (Wolters, Rudolph, Hofland, & Verheij, 2010).

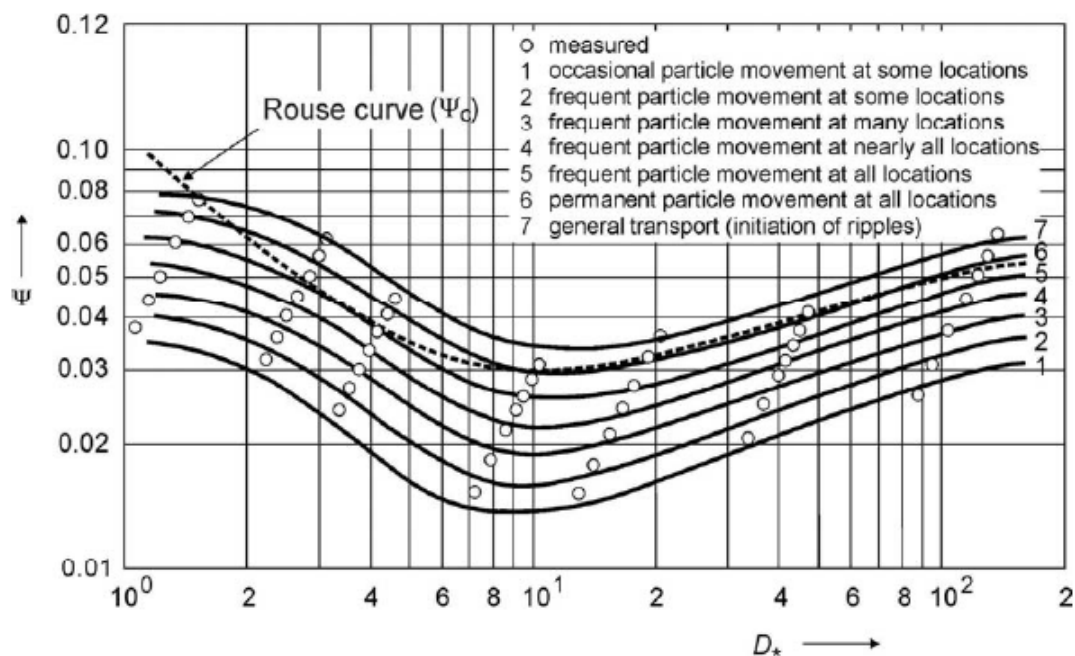


Figure 2-11 different transport stages (CUR, 2010)

2.4 Design approaches for open filters

2.4.1 Two types of open filters

Two types of open filters can be distinguished; stable geometrically open filters and unstable geometrically open filters. The difference between these two types is that the hydraulic loading is different at the base-filter interface. For stable open filters, the hydraulic loading at the interface is reduced so that initiation of motion is not possible. For unstable open filters the hydraulic loading at the interface is above the critical value of the base material. Thus transport of base material is enabled under unstable open filters. The research described in this report focusses on stable geometrically open filters. For unstable open filters under wave loading is referred to Wolters and van Gent (2012).

2.4.2 Base-filter interface stability

During the 1980s and 1990s much research is carried out to determine criteria for initiation of motion in open filters. Two different flow directions can be distinguished; perpendicular flow through the filter and parallel flow through the filter. The stability is mostly expressed in a critical hydraulic gradient in relation to the filter material diameter. In the research discussed in this report is focused on the stability under parallel flow.

2.4.2.1 (de Graauw, van der Meulen, & van der Does de Bye, 1984)

De Graauw *et al.* (1984) used an extensive experimental dataset to find the design criteria for the interface in open filters. In Figure 2-12 the results are presented. Interesting to see, is that for constant ratios between the filter and base diameter, the critical hydraulic gradient decreases as the diameter of the filter material increases. This phenomenon results from the lower pore velocities in the finer filter material. In the pores of larger filter material the pore velocities are higher, and therefore the critical hydraulic gradient has a lower value. From the data in this research also an empirical relation for the critical hydraulic gradient is found, see equation 28. The critical shear velocity can be found with the Shields approach, see section 2.3.2.3. It is interesting to note that for cyclic flow the same critical hydraulic gradients were found. However, the thickness of a filter layer is not taken into consideration in this research, which makes it inapplicable for practical purposes.

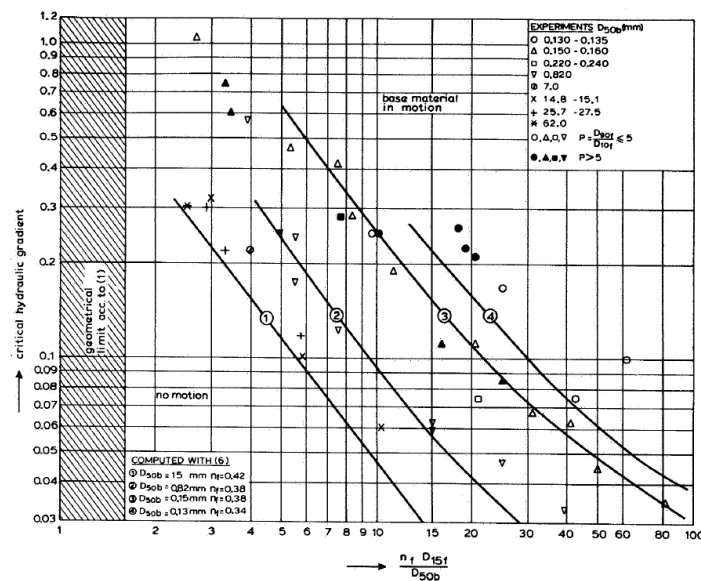


Figure 2-12 critical hydraulic gradient with steady flow parallel to interface (de Graauw, van der Meulen, & van der Does de Bye, 1984)

$$i_{cr} = \left[\frac{0.06}{n_f^3 d_{15,f}^{4/3}} + \frac{n_f^{5/3} d_{15,f}^{1/3}}{1000 d_{50,b}^{5/3}} \right] u_{*cr}^2 \quad (28)$$

where

$$u_{*cr} = 1.3 d_{b50}^{0.57} + 8.3 \cdot 10^{-8} d_{b50}^{-1.2}$$

It should be taken in mind that this formula is not derived under free surface waves. Studies (e.g. Van Os, 1998) have shown that erosion may occur for gradients which are lower than critical gradient calculated with de Graauw's formula.

2.4.2.2 (Klein Breteler, den Adel, & Koenders, 1992)

This research was carried out to find the critical velocity for the base material inside the filter. The critical filter velocity is defined as: "the maximum velocity in the filter at which the sediment motion is such that the stability of the total structure is not yet in danger" (Bezuijen, Klein Breteler, & Bakker, 1987). A dry sand transport of 0.2 gr/s/m was considered to be critical. For the initiation of motion of the base material, the following relation for the critical hydraulic gradient was derived for base material diameters between 0.1 and 1 mm, see equation 29 :

$$u_{f,cr} = \left(\frac{n_f}{c} \left(\frac{D_{f15}}{v_w} \right)^m (\Psi \cdot \Delta_b \cdot d_{b50} \cdot g)^{0.5} \right)^{\frac{1}{(1-m)}} \quad (29)$$

In equation 29, the parameters c and m are dimensionless parameters which are dependent of the size of the base material. See Table 2-1 for the values that should be used.

Table 2-1 parameters in formula for critical filter velocity (Klein Breteler, den Adel, & Koenders, 1992)

d_{b50} [mm]	c [-]	m [-]
0.1	1.18	0.25
0.15	0.78	0.20
0.2	0.71	0.18
0.3	0.56	0.15
0.4	0.45	0.11
0.5	0.35	0.07
0.6	0.29	0.04
0.7	0.22	0
0.8	0.22	0
1.0	0.22	0

Additionally experiments were carried out for non-uniform flows parallel to the interface (Bezuijen, Klein Breteler, & Bakker, 1987). Test were performed in a pulsating water tunnel with a oscillating period of 2 s. Klein Breteler concluded that for periods of at least 2s the hydraulic critical hydraulic gradients are similar to the values found by de Graauw *et al.*

2.4.3 Design methods open filters

Different design methods for open filter have been developed over the years. Some methods are used for specific situations (e.g. Wörman (1989) developed a design method for bed protections around cylindrical piers). Other methods can be applied in a wider range of situations (e.g. Hoffmans (2012),

who states that his design method can also be applied for situations with additional turbulence. The methods are discussed in this section.

The design philosophy behind the different methods is that all layers are evenly stable. This implies that the base and filter become unstable at the same moment when the hydraulic loading exceeds the critical conditions.

2.4.3.1 (Wörman, 1989)

Wörman (1989) did research to filter protections around bridge piers. The aim was to investigate the use of one layer of riprap instead of the conventional multi-layered riprap design method (as a closed filter). Wörman (1989) derived an analytical description related to the mean flow velocity, which causes initiation of motion of the base material. Note that the situation which is researched by Wörman includes additional turbulence by the bridge pier. With the data of Wörman (1989) the following formula is derived for the stability of open filters (CUR, 2010):

$$\frac{D_f}{d_{f15}} = 0.16 \frac{\Delta_f}{\Delta_b} \frac{n_f}{1 - n_f} \frac{d_{f85}}{d_{b85}} \quad (30)$$

Joustra (2013) and Van de Sande (2012) compared Wörmans formula against the Hoffmans' formula. Van de Sande showed that Wörman is too conservative under uniform flow. Furthermore Joustra suggest that the formula of Wörman should be preferred above the formula of Hoffmans for flows with a cylindrical pier. Thereby, Joustra suggest that the gradient (Or coefficient 0.16[-]) of the linear formula of Wörman should be changed to a gradient in the range between 0.22[-] and 0.33[-].

2.4.3.2 Bakker & Konter (CUR, 161, Filters in de waterbouw, 1993)

This method is developed for a situation with a top layer, underneath a filter layer and also a base layer. Physical experiments are used to derive the interface stability between the top layer and the filter layer, see equation 31 (CUR, 161, Filters in de waterbouw, 1993). The applicability of the formula is limited to flow conditions without additional turbulence.

$$\frac{d_{t15}}{d_{f50}} = \frac{1}{\gamma} \frac{2.2}{e^2 C_0} \frac{\Psi_f \Delta_f}{\Psi_t \Delta_t} \frac{R}{d_{t50}} \quad (31)$$

For the stability between the filter and the base material, another relation is derived (CUR, 161, Filters in de waterbouw, 1993) (see equation 32). Note that this relation is not validated by physical experiments.

$$\frac{d_{t15}}{d_{b50}} = \frac{1}{\gamma} \frac{2.2}{e^2 C_0} \frac{\Psi_b \Delta_b}{\Psi_f \Delta_f} \frac{R}{d_{f50}} \quad (32)$$

And for C_0 :

$$C_0 = 1 + 1.8 \left(\frac{R}{d_{t50cr}} \right)^{0.33} \left(1 - \frac{d}{R} \right)^{0.45} \quad (33)$$

2.4.3.3 (Hoffmans G., 2012)

Since Hoffmans' relation plays a major role in the research described in this report, Hoffmans relation will be explained in more detail in chapter 3. Hoffmans formula is formulated as follows:

$$\frac{D_f}{d_{f15}} = \alpha_{a,H} \ln \left(\frac{\Delta_f d_{f50} \Psi_{cf} (1 - \gamma V_{c,f})}{\Delta_b d_{b50} \Psi_{cb} (1 - \gamma V_{c,b})} \right) \quad (34)$$

2.4.3.4 (Van de Sande, 2012)

Van de Sande's work is explained in more detail in chapter 3. This paragraph briefly outlines his finding.

Van de Sande did research on the validation of Hoffmans formula for uniform flow parallel to the filter structure. Van de Sande concluded that the formula proposed by Hoffmans is in general valid for single layered geometrically open filter structures. Although, Some adjustments were proposed to the formula;

- To use d_{f50} instead of d_{f15} for the relative filter thickness Hoffmans formula (equation 34)
- To use another value for the damping coefficient α_d . The value proposed by Hoffmans is too high.

The adjustment in Hoffmans' formula lead to the new "van de Sande's formula", see equation 35.

$$\frac{D_f}{d_{f50}} = \alpha_{a,S} \ln \left(\frac{\Delta_f d_{f50} \Psi_{cf} (1 - \gamma V_{c,f})}{\Delta_b d_{b50} \Psi_{cb} (1 - \gamma V_{c,b})} \right) \quad (35)$$

With a proposed load damp coefficient of $\alpha_{a,S} \approx 0.82$.

2.5 Previous experimental research to open filters under wave loading

This research aims on the question whether the relatively recent Hoffmans formula can be validated under wave loading. In the past. several experiments are already carried out to investigate the behavior of an open filter under wave loading. This paragraph presents these recent studies.

2.5.1 Halter (1999)

The goal of Halters research was to gain more insight in the behavior of open filters under wave loading. Halter carried out experimental research in a wave flume with regular, non-breaking waves. The goal of Halter's experimental research was to find the critical wave height for which the base material becomes unstable. Halter concluded that:

- The critical hydraulic loading is higher for smaller filter material diameters.
- A thicker filter protects the bed better than a thinner filter; higher critical wave heights were found for thicker filters.
- For larger wave periods, a lower critical wave height was found.
- For large filter material diameters, it was observed that the critical wave height was lower than for a situation without a filter. Halter claims that the roughness of these large stones lead to additional turbulence inside the filter.
- Halter did not find a clear relation between the calculated velocities in the filter and incipient motion of the filter material.
- The calculated critical gradients (corresponding to the critical hydraulic loading and calculated using the linear wave theorem) are lower than the critical gradients calculated with De Grauw's formula (equation 28).

The critical wave conditions found by Halter are summarized in Appendix A.

2.5.2 Jansens (2000)

Jansens research focusses on the relation between the hydraulic conditions upon the filter and the pore velocities within a filter. Jansens used a Laser Doppler Flow Meter (LDFM) to measure the pore velocities and velocity fluctuations. Jansens replicated the model setup and hydraulic conditions used and found by Halter. Jansens did not use base material in his tests. However, Jansens used the critical wave conditions and the same laboratory setup as Halter. Halter did use base material. So the measurements by Jansens are corresponding to the conditions for which the base material would start to become unstable. The main interest was to find the magnitude of the water movements within the filter. Jansens had the following findings:

- The horizontal and vertical velocity in the pores is constant over the thickness of the filter.
- Jansens claims that the horizontal pore velocity is generated by the pressure gradients.
- The pore velocity seems dependent of the orientation and accessibility of the pore. The fluctuations in the pore velocity seem independent of this orientation.
- The measured pore velocities which correspond with the critical hydraulic conditions of Halter are large enough to generate bed instability.
- In the model tests, the measured pore velocities are in the order of 30%-40% of the measured velocities above the filter.
- Jansens measured that the pore velocities, corresponding to Halter's critical hydraulic loading, all have the same magnitude. Between (0.03 and 0.05 m/s).
- Jansens shows that the pore velocity in the filter can be estimated with the following relation:

$$\frac{1}{\rho_w g} \frac{\delta p}{\delta x} \cdot T \cdot 0.4 \equiv \hat{u}_p \quad (36)$$

- measured critical pore velocities were between 0.03 and 0.06 m/s. The nominal diameter of the base material was 100 μ m.

2.5.3 Wolters & Van Gent (2012)

In this research experiments were conducted for granular open filters on a horizontal sand bed under wave and combined wave and current loading. This research is an exploratory study for more extended research effort on open filters. Also, the older dataset of Wolters *et al.* is used (2010).

The research focusses on base material transport. The transported base material was measured for a different hydraulic loading, filter thickness and filter grading. See Appendix A for the test programme and the measurements. The test duration varied between the tests, based on the observed base material transport (1000-12000 waves). During the experiments no filter material transport was observed.

For only wave loading it was observed that bed load transport and suspended load transport of the base material could not be separated. Base material transport could only be realized once the filter velocities were far above the critical velocity and once base material was also suspended in the water column. For all tested filter configurations the base material transport for wave loading alone was very low. Note that during all tests the filter material was stable.

During the tests for wave & current loading was observed that only a fraction of the generated wave height could be realized, because of the interaction between waves and current. An increase of base material transport was observed for increasing current velocities and increasing wave periods.

Despite the hypothesis that combined wave and current action would contribute to an significant increase of base material transport compared to only wave or current loading, this strong increase was not observed.

The filter thickness was expected to have an influence on the hydraulic gradient, although this was not found for the two thicknesses used in the experiments. For the tests with only a wave loading, a larger transport is measured for a thicker filter. This is considered counterintuitive and is not explained.

Wolters & van Gent (2012) conclude that the bed material transport depends on the loading condition, where the transport can be described as function of the hydraulic gradient $\frac{i_{2\%}}{i_{cr}}$.

$$T^* = 1.4 \cdot 10^{-6} \left(\frac{i_{2\%}}{i_{cr}} \right)^{5.8} \quad (37)$$

Wolters & van Gent also found a strong relationship between the KC_f number and the maximum hydraulic gradient $i_{2\%}$. The KC_f number is based on the velocity measured 25 mm above the filter ($u_{2\%}$), the wave period, the porosity of the filter and the filter thickness:

$$KC_f = \frac{u_{2\%} T_m}{n_f D_f} \quad (38)$$

$$i_{2\%} = 0.06 \cdot KC_f^{0.28} \quad (39)$$

Thus, the base material transport can be described as a function of $\frac{i_{2\%}}{i_{cr}}$, where $i_{2\%}$ can be described as a function of KC_f . It should be noted that Wolters & van Gent propose that the latter equation are based on trends which need further verification. Especially the possible influence of variations in filter thickness, since it is expected that the filter thickness is expected to have an influence on the hydraulic gradient.

2.6 Chapter review

In this chapter the differences between a wave loading and a uniform flow were discussed. It is supposed that in particular the accelerations and decelerations of the flow under a wave loading cause the differences in the loading regime on a filter. Sleath (1978) already showed how the oscillatory flow influences the Shields curve.

The main variables that define the loading under waves are the wave height, wave length and the water depth. These variables determine the orbital motion on the bed, thus above the filter. Possible non-linearity of the waves will only have a small influence on the near bed orbital velocity, because the nonlinearities are only large in the upper part of the water column (this will be evaluated in chapter 4).

This chapter also presented different alternatives to use as a stability relation for granular material. It was seen that the velocity, acceleration and turbulence intensity can be taken into account separately in some of these stability relations. Hoffmans formula is based on the shear stress concept, which makes the Shields approach an appropriate method to use for this research. Thereby, the Shields approach can be used under wave loading as well, as was researched by Sleath (1978). Although,

Sleath suggested a modification in the curve. For the determination of the shear stress under waves, the Jonsson-Swart method is used in this research.

This chapter also presents previous research to open filters. Multiple relations and design formulae exist at the moment, but an appropriate design method for an horizontal open filter under wave loading is not available yet. It is supposed that Hoffmans formula can be used for this purpose. However it is not known what the value for the load damp coefficient should be under wave loading. Hoffmans equations is described in more detail in the following chapter. Thereby it should be noted that most of the previous research focused on the hydraulic gradients within the filter material. Hoffmans formula is based on the concept of damping of turbulence energy form the top of the filter. Since the background of Hoffmans' formula is highly relevant for this research, it will be discussed in detail in chapter 3.

Chapter 3

Hoffmans' design formula for open filters

This section gives a background about Hoffmans formula. Also previous research on the validation of the formula is discussed. From there, the possibilities are evaluated to use a similar approach in this research. Eventually, an alternative approach is presented which can be used for the validation under wave loading. For a fully detailed background on Hoffmans design formula is referred to the book "The Influence of Turbulence on Soil Erosion" by Hoffmans (2012).

3.1 Background of Hoffmans' formula

3.1.1 Derivation

Basically, the Hoffmans formula is a strength-load equation. For a stable filter, the strength must be larger than the load. In this case, the strength is represented by a *relative strength between the base and filter layer*. The load is describes as the *relative load between the top of the base and the top of the filter*. Both the strength and load will briefly be discussed.

Strength

As mentioned in chapter 2, the strength of a single grain can be described with the shear stress concept. If the shear stress exceeds a critical value, the grain will start moving Hoffmans uses a description of the relative strength of the base layer. This can be described as the critical shear stress of the base, divided by the critical shear stress of the (much) stronger filter.

$$\eta_c = \frac{\tau_{c,b}}{\tau_{c,f}} = \frac{d_{b50} \Delta_b \Psi_{c,b}}{d_{f50} \Delta_f \psi_{c,f}} \quad (40)$$

However, the critical shear stress of a grain may deviate due to the non-uniformity of the granular material. A characteristic strength can be described, where the influence and uncertainty of the critical stress is included. This characteristic strength can be defined according to the hypothesis of Grass (1970), see equation 41.

$$\tau_{c,k} = \tau_c - \gamma \tau_{RMS,c} \quad (41)$$

Where $\tau_{RMS,c}$ represents the standard deviation of the instantaneous load. This parameter incorporates the influence of the variation of the non-uniformities of the heterogeneity of the soil (represented by $V_{c,f}$ in equation 42).

$$\tau_{RMS,c} = V_{c,f} \tau_c \quad (42)$$

$$V_{c,f} \approx 1 - \frac{d_{15}}{d_{50}} \quad (43)$$

Using the definition for the characteristic strength, the relative strength is expressed as follows:

$$\eta_{c,k} = \frac{\tau_{c,b,k}}{\tau_{c,f,k}} = \frac{d_{b50} \Delta_b \Psi_{c,b} (1 - \gamma V_{c,b})}{d_{f50} \Delta_f \psi_{c,f} (1 - \gamma V_{c,f})} \quad (44)$$

Load

Hoffmans defined a load equation based on the balance of forces, the Forchheimer equation, the hypothesis of Boussinesq and a relation of the eddy viscosity (see Hoffmans (2012)). From this follows a definition for the penetration of turbulence energy, see equation 45 (at the interface of the filter and the bed, $z=0$). k_f represents the load on the filter, k_b represents the load on the base layer, $k_{f,s}$ is the turbulence energy due to gravity (which is negligible in this context), L_d is the load damping length and z is the layer thickness. Hoffmans has derived a definition for the relative load, see equation 47.

$$k_f(z) = k_{f,s} + (k_b - k_{f,s}) \exp\left(\frac{z}{L_d}\right) \quad (45)$$

$$\text{With for uniform flow: } L_d = \alpha_d d_{f15} \quad (46)$$

$$\eta_l = \frac{k_f(z)}{k_b} \approx \exp\left(\frac{z}{L_d}\right) \quad (47)$$

Now the relative load between the interface and the top of the filter can be described, see equation 48. D_f is the thickness of the filter. Combined with equation 46 the relative load can be expressed as:

$$\eta_l \approx \exp\left(\frac{z}{L_d}\right) = \exp\left(\frac{-D_f}{\alpha_d d_{f15}}\right) \quad (48)$$

Hoffmans formula

Logically, for a stable filter the strength must be larger than the load. By combining the relative strength (equation 40) and the relative load (equation 48) the formula of Hoffmans is found, see equation 49. Based on experimental data of Klar (2005), Hoffmans derives for the load damp coefficient a value of $\alpha_d = 1.0$. Thereupon, Hoffmans suggests to use a safety factor for practical purposes and proposes to use a value of $\alpha_d = 1.5$.

$$\frac{D_f}{d_{f15}} = \alpha_d \ln\left(\frac{\Delta_f d_{f50} \Psi_{cf} (1 - \gamma V_{c,f})}{\Delta_b d_{b50} \Psi_{cb} (1 - \gamma V_{c,b})}\right) \quad (49)$$

Hoffmans also proposes a simplified version of his formula. Some basic assumptions are made in this simplification: $\frac{d_{f50}}{d_{f15}} \approx 1.25$, $\frac{\Delta_f}{\Delta_b} \approx 1$, $\frac{\Psi_{cf}}{\Psi_{cb}} \approx 1$, $\frac{\gamma V_{c,f}}{\gamma V_{c,b}} \approx 1$, $\alpha_d \approx 1.5$. This gives:

$$\frac{D_f}{d_{f50}} = 1.2 \ln \left(\frac{d_{f50}}{d_{b50}} \right) \quad (50)$$

3.1.2 The load damping

The load damping length is an important parameter in (the derivation of) Hoffmans formula. Hoffmans mentions that the expression for the load damping length is different for wave loading than for uniform flow. As explained above, for uniform flow the load damping coefficient can be found according to equation 46. Hoffmans calibrated this parameter by applying uniform flow experiments of Klar (2005). For the expression of the load damping under wave loading, Hoffmans and Verheij (2013) have defined an expression based on the work of Bezuijen and Kohler (1996).

The theoretical derived values of the load damping length, and thereby the load damp coefficient α_d are explained in this subparagraph. The next paragraph elaborates on the validation research on these parameters. The expressions for the load damping length are not validated for wave loading yet, it is attempted to do so in this research.

3.1.2.1 Theoretical proposed value of the load damp parameter under uniform flow

Hoffmans used the experiments of Klar (2005) to calibrate the load damp coefficient. In Figure 3-1 the experimental data is shown. It can be seen that the penetration of turbulent energy is decreasing the further it penetrates the filter. Based on this experimental data, Hoffmans derives a value for the load damp coefficient of $\alpha_d = 1.0$. Hoffmans adds a safety factor for his final proposal of the load damp coefficient, this results in: $\alpha_d = 1.5$.

Interesting to point out, is that Klar (2005) observed that the penetration of turbulent energy decreases significantly until 4 to 5 times d_{f50} . However, deeper into the filter, the penetration of turbulent energy decreases and is less effective.

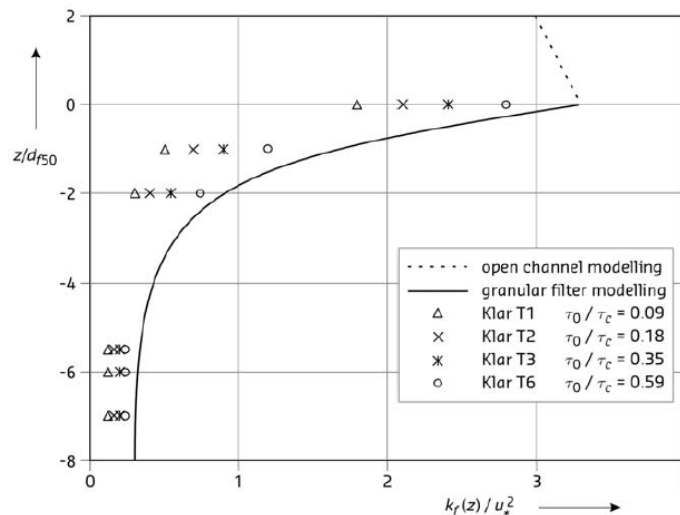


Figure 3-1 experimental data of Klar (Wenka and Köhler 2007)

3.1.2.2 Hypothesis for the load damping length under wave loading

Damping load damping length L_d represents the load penetration in granular filters. The load penetration length was investigated by Bezuijen and Köhler (1996) for wind and ship generated waves in flexible revetment structures. An expression for the load damping length was formulated as in equation 51 (de Groot et al. 1996). Bezuijen and Köhler investigated regular waves in their research.

$$L_{d,Hypothesis I} = \sqrt{\frac{c_v T_p}{\pi}} \quad (51)$$

L_d This load damping length can directly be substituted in Hoffmans formula. The following derivation can be found for the formula under wave loading by combining equations 46, 49 and 51 (Hoffmans & Verheij, 2013):

$$D_f = \sqrt{\frac{c_v T_p}{\pi}} \ln \left(\frac{\Delta_f d_{f50} \Psi_{cf} (1 - \gamma V_{c,f})}{\Delta_b d_{b50} \Psi_{cb} (1 - \gamma V_{c,b})} \right) \quad (52)$$

Now the wave period and the consolidation coefficient of the filter material are also part of the equation. Hoffmans & Verheij state that the consolidation coefficient for filter material is approximately: $c_v = 0.001 \frac{m^2}{s}$.

Hypotheses

“The wave period has an influence on the load damping length L_d ”

“The load damping length L_d increases for a longer wave period.”

“The relation between the load damping length L_d and the wave period is a root square function.”

“the load damping length under wave loading is described by the following expression:

$$L_{d,Hypothesis I} = \sqrt{\frac{c_v T_p}{\pi}}$$

Hoffmans & Verheij (2013) assume that the consolidation coefficient of the filter material is related to the filter diameter by the Kozeny-Carman equation:

$$c_v \equiv K \equiv d_{f15}^2 \quad (53)$$

In the correspondence between Hoffmans & Verheij (2013) some next steps in the derivation are still under discussion. The correlation shown in equation 53 can be used to substitute the consolidation coefficient in equation 51.

$$L_d = \sqrt{\frac{c_v T_p}{\pi}} = \sqrt{\frac{\alpha_{f15} \cdot d_{f15}^2 T_p}{\pi \cdot T_0}} \quad (54)$$

Under uniform flow, it can be assumed that the dominant turbulent eddies have a period of $T_p=0.5s$. Under the assumption that $T_0 = 1s$, it results that $\alpha_{f15} = 2\pi$ (because for uniform flow equation 54 equals $L_d = \alpha_d d_{f15}$, with $\alpha_d \approx 1.0$). This finally results in:

$$L_{d,Hypothesis II} = d_{f15} \sqrt{\frac{2T_p}{T_0}} \quad (55)$$

Now the load damping length depends on the filter diameter. This makes sense, since it can be expected that the damping of the load is dependent of the pores in the material, and thus the size of the grading.

The parameter T_0 has no physical meaning. It was introduced to compensate for the dimensions of the replaced c_v by d_{f15}^2 . This may raise some doubts about physical validity of the hypothesis.

Hypothesis

“the load damping length under wave loading is described by the following expression:

$$L_{d,Hypothesis II} = d_{f15} \sqrt{\frac{2T_p}{T_0}}$$

Equation 52 suggest that the filter thickness needs to increase as the wave period increases. However, it is known that for waves with a very large period (e.g. a tidal wave) the hydraulic conditions are similar to uniform flow. If equation 52 would be used for these very long waves, the filter thickness would become unrealistically large. Therefore the hypothesis is formulated that the range of applicability of equation 52 is limited in a range of wave periods. It is expected that there is a transition zone for the period dependency. Periods higher than this zone will not influence the damping behavior any further, and the damping behavior is likely to be the same as under uniform flow. However, it is not clear for which wave period this transition will happen.

It should also be clear that Bezuijen and Köhler found the damping length for *wind waves, ship generated waves and ship induced water level depressions* against a flexible revetment structure. This is different than the situation considered in this research, where the damping length *under waves* is considered. This brings up some doubt whether equation 51 is applicable. The performance of the rewritten formula is still unproven. This research aims on finding values for the load damping length under wave loading.

3.2 validation of Hoffmans formula

Hoffmans validated his proposed value of the load damp coefficient with experimental data of uniform flow and non-uniform flow. Thereafter, Van de Sande (2012) did additional experimental research and validated the load damp coefficient under uniform flow more thoroughly. Additionally, Joustra (2013) extended the dataset for non-uniform flow and carried out a validation study for Hoffmans formula under flows with additional turbulence by a sill and a cylindrical pier. The validation methods are discussed in this paragraph, thereby an overview of the results is given.

3.2.1 Hoffmans' validation

Hoffmans carried out a validation study with the experimental data of Huijstee & Verheij (1991), Wörman (1989) and Dixen (2008). The data is presented in Figure 3-2. On the y-axis the relative filter thickness is shown. The x-axis gives the ratio between filter material diameter and base material diameter. In this graph, both Hoffmans and Wörmans equation are presented (see respectively equation 30 and 50). Hoffmans included Wörmans method to show the differences, since Wörmans method is one of the most conventional methods.

Theoretically, the regions that lie above the lines of the equation have a filter which is too thick (too conservative), so this is economically and practically undesirable. The regions under the lines of the equations have a relative filter thickness which is too thin, so the base will erode before the filter does.

All shown data points in the graph represent a situation where the filter was not thick enough (thus the base eroded under the filter). It is seen that all data points in the graph are under the line of Hoffmans equation. Herewith, Hoffmans implies that his formula shows satisfying results. The proposed load damp coefficient (of 1.5) was considered to be validated.

The main difference between Hoffmans and Wörman's equation is the difference between the linear and logarithmic relation. Thereby Wörman's equation is more conservative for ratios above $\frac{d_{f50}}{d_{b50}} \approx 50$. Under this ratio, Hoffmans' relation gives more reliable results.

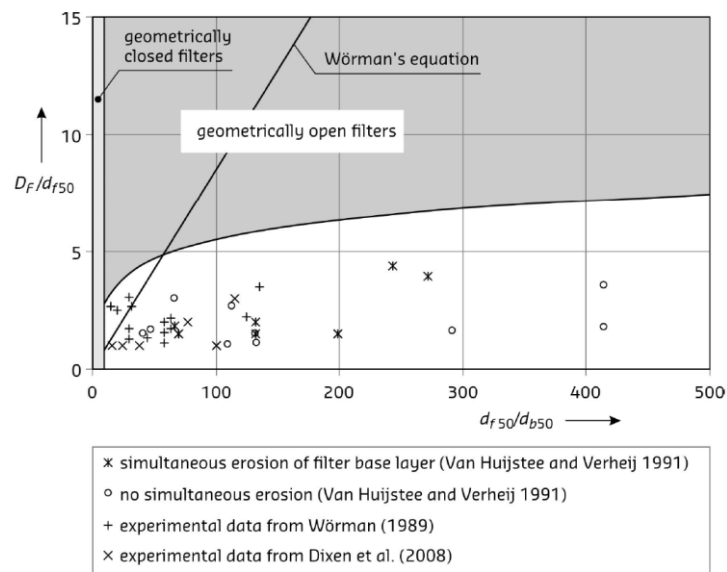


Figure 3-2 D_F/d_{f50} versus the critical d_{f50}/d_{b50} . (Verheij, Hoffmans, Dorst, & van de Sande, 2012)

3.2.2 Van de Sande (2012)

Van de Sande's research aimed on the validation of Hoffmans formula under uniform flow. Compared to Hoffmans' validation, Van de Sande used significantly more data (including his own dataset). Thereby, he also made a suggestion which included the uncertainty and statistics of his found load damp coefficient.

Van de Sande carried out experimental research. For his validation approach, three categories were defined (see Figure 3-3):

- base material moves first
- filter material moves first
- base material and filter material move at the same time

The relation of Hoffmans is based on the philosophy of simultaneous instability of base and filter material. Therefore, Hoffmans formula ideally gives outcomes in the yellow area of Figure 3-3. So when a filter is used which is stable for the given hydraulic loading, Hoffmans formula (2012) then gives the thickness of this filter for which the stability of base material is guaranteed. To classify instability, Van de Sande weighted the transporter filter material and base material separately after each test.

Experiments are carried out with different layer thicknesses and different ratios between base and filter material. This approach resulted in several data points. These points were grouped in the 3 categories.

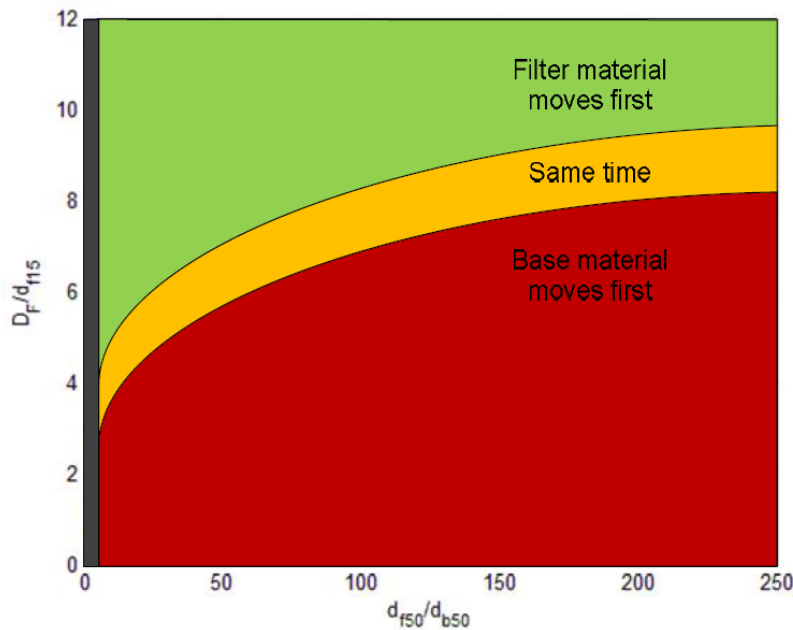


Figure 3-3 movement of filter material and base material (Verheij, Hoffmans, Dorst, & van de Sande, 2012)

Besides his own data, Van de Sande also used other datasets (Bakker (1960), Haverhoek (1968), Wouters (1982), Konter *et al.*(1990), van Huijtee and Verheij (1991), van Velzen (2012)) which were also grouped in the 3 categories. All data is presented in Figure 3-4. All data together was used to calibrate the Hoffmans formula, for which he found a new value for the load damp coefficient. Van the Sande concluded that the value proposed by Hoffmans was too conservative and a lower value could be used.

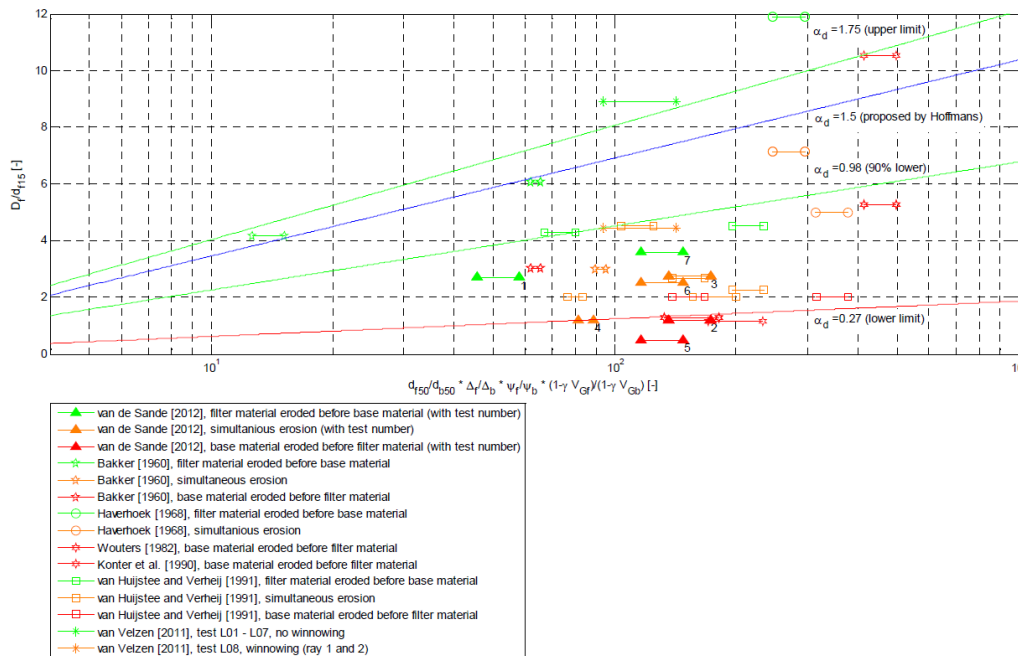


Figure 3-4 Experimental data to validate Hoffmans' load damp coefficient (Van de Sande (2012))

Van de Sande found a load damp coefficient $\alpha_d = 1.75$, and a 90% confidence limit of $\alpha_d = 0.98$. It was observed that the wide graded filter materials gave significantly higher values for the load damp coefficient α_d than the not-wide graded material.

Based on the experimental data, Van de Sande states that Hoffmans formula is valid under uniform flow. Although, Van de Sande makes two proposals:

- Instead of using d_{f15} for the relative filter thickness, d_{f50} should be used for more accurate results. So Hoffmans formula should be rewritten as equation 56. In this report, this rewritten formula will be referred to as “the Van de Sande Formula”.

$$\frac{D_f}{d_{f50}} = \alpha_d \ln \left(\frac{\Delta_f d_{f50} \Psi_{cf} (1 - \gamma V_{c,f})}{\Delta_b d_{b50} \Psi_{cb} (1 - \gamma V_{c,b})} \right) \quad (56)$$

- The proposed alpha value of Hoffmans (1.5) is too high. The following values are suggested (to be used together with the Van de Sande formula):

Table 3-1 proposed load damp parameters by Van de Sande (2012)

Deterministic approach	Probabilistic approach
$\alpha_d = 0.82$: safe upper limit	Log-normal distribution
$\alpha_d = 0.69$: 90% confidence limit	$\mu = -0.86$
	$\sigma = 0.38$
	$E(\alpha_d) = 0.46$
	$Var(\alpha_d) = 0.04$

Van de Sande's incentive to adjust Hoffmans formula was the found inconsistency for the load damp coefficient between narrow and wide graded filter materials. For wide graded filters, d_{f50} seems a better representation than d_{f15} , which sounds logical. However, there is no clear physical explanation why the load damping length gives more accurate results when d_{f50} is used instead d_{f15} . It might be a coincidence. However, it raises the question whether this will be repeated for the validation of the formula under wave loading. Therefore, a hypothesis is defined.

Hypothesis

“Van the Sande's formula gives a more accurate results for the load damp coefficient than Hoffmans formula, also in the tests under wave loading.”

3.2.3 Joustra (2013)

Joustra's research question was formulated as follows: “ To test the validity of the design formula of Hoffmans (2012) for flows with sill-induced additional turbulence, and flows with a cylindrical pier and to test the validity of the design formula of Wörman (1989) for flow velocities over 0.5 m/s and filter layer thicknesses over 0.1 m at flows with cylindrical piers.”

Joustra also collected experimental data. The qualification of filter instability was as presented in Table 3-3. The qualification of filter instability is classified similar to the classification of van Huijstee & Verheij (1991). The classification is based on visual observations.

Table 3-2 classification of base stability in Joustra's research

Class	Description	Stable/Instable	Remarks
F.1	No movement at all	Stable	
F.2	Shaking stones, a single stone rolls	Stable	
F.3	Some stones are rolling	Instable	Corresponds phase 3 defined by Breusers (1977)
F.4	Movement at many locations	Instable	

For the classification of base material Joustra used a stereo photography technique. Using this technique, Joustra was able to identify if the filter replaced by the moving base under the filter layer. However, this technique could only be applied when the filter stones were stable. When the filter stones were unstable, it was not possible to use this technique. See Table 3-3.

Table 3-3 classification of filter stability

Class	Description	Stable/instable
B.1	No filter settlement	Stable
B.2	Minor or small degree of filter settlement	Instable
B.3	Major or large degree of filter settlement	Instable

Joustra results for uniform flow are in agreement with Van de Sande's results. Furthermore, under conditions with sill-additional turbulence, Joustra suggest a value for the load damp coefficients of 1.2 to 2.5. Under flows with a cylindrical pier a load damp coefficient of 2.4 to 3.7 is suggested. Furthermore Joustra suggest that the formula of Wörman should be preferred above the formula of Hoffmans for flows with a cylindrical pier.

3.2.4 Overview of the load damp coefficients

The load damp coefficient is validated for different conditions. The proposed values for the load damping coefficients are presented in Table 3-4.

Table 3-4 Suggested values for the load damp coefficients

Author	Proposed α_d	Loading situation
Hoffmans (2012)	1.5 ¹	Uniform and non-uniform flow
Van de Sande (2012) ²	0.82 ³ (safe upper limit)	Uniform flow parallel to filter structure
Joustra (2013)	1.2 < α_d < 2.5	Flow with sill additional turbulence
Joustra (2013)	2.5 < α_d < 3.7	Flow with cylindrical pier ⁴

3.3 Validation method of Hoffmans formula under wave loading

Hoffmans suggest that his formula is applicable under uniform and non-uniform flow, thus also under a wave loading. However, the validity of the formula under wave loading is not investigated yet. This

¹ Originally, Hoffmans derived a value of 1.0. Hoffmans multiplied this with a safety factor.

² Based on the Van de Sande formula

³ Besides a safe upper limit, Van de Sande also provides statistical values for α_d (see Table 3-1)

⁴ For flows with cylindrical piers Joustra recommends Wörman's formula above Hoffmans' formula

research will aim on the validation on Hoffmans formula under wave loading. Thereby it will be investigated what suggestions can be made for the load damp coefficients. Physical experiments will be carried out to generate data. Thereby data from previous research can be used.

3.3.1 Approach for experiments

A new approach will be introduced to find the values of the load damp coefficients. In the approach of Van de Sande and Joustra (now referred to as the "classical approach"), it was necessary to generate instability of both the base and filter material. In the new approach, where an important assumption is made, only instability of the base material is enough to find the load damp coefficient in the Hoffmans formula. This new approach is introduced to enable experimental modeling in a small wave flume.

3.3.1.1 Applicability of the classical approach

The waves in a wave flume are limited in their height and length. To generate high shear stresses on the filter material, waves with a relative high amplitude need to be generated. There are 3 factors which can be varied to influence the shear stress under waves; the wave height, the wave period and the water depth. An increased wave height gives higher shear stresses. Due to the limited height of the wave flume, the wave amplitudes are relative large to the water depth. Therefore the waves in the flume are non-linear. As a consequence of this non-linearity, the wave peaks are quite steep.

For this reason, the maximum loading in a wave flume is limited. When it is attempted to perform the same approach as Van de Sande and Joustra, it must be possible to generate filter instability. However, with a limited maximum loading, only adjustments can be made in the filter material (Chapter 4 elaborates on the options). Although, it will be very complicated to apply the classical approach under wave loading. Only in a large flume (where high wave loadings can be generated) it will be easier to apply the classical approach.

When filter instability is not generated, only data points in the red area of Figure 3-3 will be found. Therefore it will be possible to suggest a lower limit for the load damp coefficient. However, for a higher limit data with an instable filter is needed.

3.3.1.2 New approach

Although the load in the filter is not critical, this load is still damped out by the filter. For the load damp parameter, it makes no difference what the magnitude of load on top of the filter is. The relative load used to derive Hoffmans formula is nothing more than the relative decrease in the load between the top of the filter and the filter-base interface (equation 47). For this reason, it is assumed that the load on top of the filter does not have to be critical to find the load damping characteristics of a filter. Therefore, in the new approach it is assumed that also the occurring shear stress upon a filter can be used to derive a value for the load damp coefficient, instead of only the critical shear stress.

Assumption

Besides the critical shear stress, also the occurring shear stress in the filter and the base material can be used to find a value of the load damp coefficient.

N.B.: Hoffmans did not make this assumption for his formula. Therefore, theoretically, the method in which this assumption is used differs from Hoffmans method. In this research, this assumption is considered to be very plausible.

To provide more insight which supports this assumption, a visualization is made in figure Figure 3-5. Under the circumstances derived by Hoffmans, both the base and filter are loaded on their critical point. Now, in the new approach, the filter is not loaded by its critical load. However the load will damp out by the same mechanism as in Hoffmans derivation. Only now relative strength is different. On the base, the load is still on the critical point. Only on top the filter, the load does not correspond with the filters critical load, but a value under it's critical load. Therefore the filter has to damp out a smaller relative load.

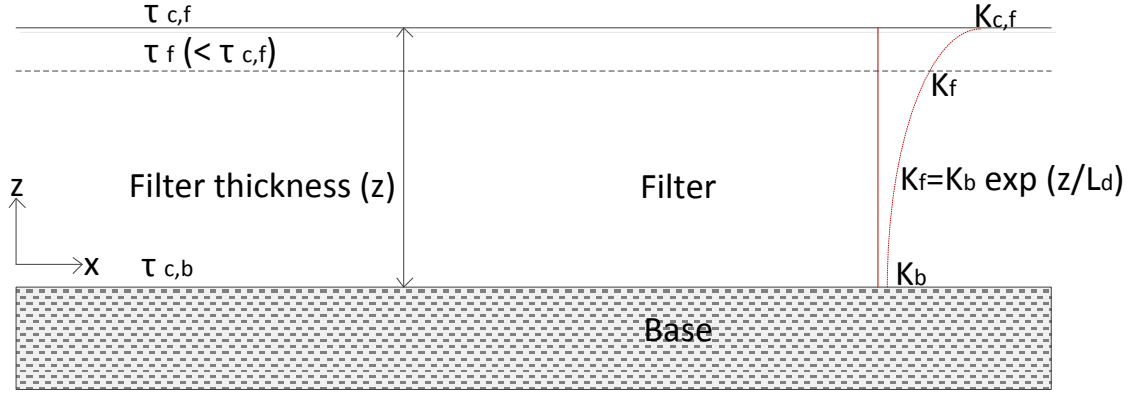


Figure 3-5 visualization of the load damping through the filter

With this assumption the formula can be rewritten. We start with a definition for the relative strength. Note that the shear stresses not represent the critical stresses any more.

$$\eta_c = \frac{\tau_b}{\tau_f} \quad (57)$$

As in the original derivation of the formula, the relative strength is combined with the relative load (equation 47). This gives:

$$D_f' = L_d' \ln \left(\frac{\tau_f (1 - \gamma V_{c,f})}{\tau_b (1 - \gamma V_{c,b})} \right) \quad (58)$$

To find the load damp parameter, the equation can be rewritten to:

$$L_d' = \frac{D_f'}{\ln \left(\frac{\tau_f (1 - \gamma V_{c,f})}{\tau_b (1 - \gamma V_{c,b})} \right)} \quad (59)$$

The latter assumption implies that $L_d' = L_d$.

The parameters which are necessary to find the load damp parameter are presented in Table 3-5. For the approximation of the shear stress, the Jonsson-Swart approximation can be used. To use this approximation, the wave height, period and water depth are used. Thereby, the bottom roughness, density of the fluid and gravitational acceleration are used. Relevant assumptions are found in chapter 6.

Note that a shear stress on the base-filter interface also must be known. There are multiple ways to define the shear stress on the base layer. In this research is chosen to visually qualify when the base layer starts to become unstable. At this point, we know that the threshold for incipient motion is exceeded. Therefore, it can be assumed that the shear stress is on its critical point. By using the Sleath's modified shields curve, the shields number for the start of movement can be found.

Another method to define the shear stress on the base is by measuring the transported sediments and link this to a Shields number. However, it is very complicated to accurately measure the transported sediments in a wave flume. Thereby, the test time needs to be long enough to have significant transport. Due to the complications, it is not chosen to use this method.

Table 3-5 used parameters to find the load damp parameter

Parameter	Defined by:
Layer thickness	measurements
Filter- and base material grading properties	measurements
Shear stress on the filter	Approximated with the Jonsson-Swart approach (equation 20 and 21).
Shear stress on the base	When start of transport is observed, $\tau_{c,b}$ is known from Sleath's modified Shields curve.
γ	=0.625 (from literature (Hoffmans 2012)).

3.3.2 Other datasets which can be used for the validation of Hoffmans' formula

The data of Wolters & van Gent (2012) can be used in the analysis. Wolters & van Gent carried out experiments with waves over an open filter and combined wave & current action. In the tests, the filter material was stable. The transported sand was weighted after the tests. The experiments with waves were carried out with irregular waves.

3.4 Discussion and necessity for further experimental research

Hoffmans suggest that his formula can be applied under uniform flow, non-uniform flows and also under wave loading. However, previous research (Halter, 1999; Jansens, 2000; Wolters & van Gent 2012) does indicate that the stability of the interface is related to the hydraulic gradients within the filter. Hoffmans formula does not include the hydraulic gradients in the equation, nor a term for the pore velocities. The load in Hoffmans formula is solely based on the concept of damping of turbulence energy from the top of the filter. For uniform flow, this concept seemed to be correctly applied, and the Hoffmans formula was validated by van de Sande. For uniform flows, the pore velocities decrease lower inside the filter (see van Os 1998). Under wave loading it is not known what the effects of the penetration of turbulence energy is on the stability of the filter interface. It is known, that under waves, the velocities in the filter are constant (see Jansens, 2000). Jansens claimed that the stability of the interface depends on the pore velocities, which are generated by the hydraulic gradient. However, a variation was seen in the measured velocities on the filter-base interface (the measured pore velocities under the critical hydraulic loading ranged between 0.03 and 0.06 m/s). Also in more recent research (Wolters & van Gent (2012)), the hydraulic gradients were considered to be directly linked to transports under of base material.

It is not known how Hoffmans formula will perform under wave loading. Using the assumption described with equation 59, experimental research can be carried out in a wave flume without generating instability of the filter material. This allows to carry out experimental research in a relatively small flume. Since experimental data in this field of study is scarce, additional research is carried out. Data will be collected with variations in the filter thickness (as recommended by Wolters & Van Gent (2012)), for different filter material diameters and under regular waves (to validate the hypotheses). Especially tests where the filter thickness is varied is desired.

The experimental data of Wolters & Van Gent is obtained under irregular waves. However, this will still be useful in the classical validation approach, which gives an insight in the lower limits for a stable filter thickness.

The experimental data of Halter will also be used in this research. This Data can be used with the new validation approach, since the data is obtained under regular wave loading.

Under the plausibility that the assumption of equation 59 is correct (thus that $L_d' = L_d$), Hoffmans' formula can be validated when the obtained values the load damping length (L_d') are aligned with the hypotheses. Thus for a valid formula, $L_{d,Hypothesis I} = L_d$ or $L_{d,Hypothesis II} = L_d$.

3.5 Chapter review

As explained in this chapter, Hoffmans formula is based on the philosophy that the relative strength must be larger than the relative load. The relative load is related by a load damping length L_d . This load damping length L_d is considered to be different under uniform flow than under wave loading. For uniform flow, the proposed equation is validated and performs well. Under wave loading, only hypotheses are prevailing, but no validation study is carried out yet.

This research aims on the validation on Hoffmans formula under wave loading. Basically, the relation of the load damping length and the wave loading need to be understood for the validation study. Following on in this research, a more general form of the Hoffmans formula is used:

$$D_f = L_d \cdot \ln \left(\frac{\Delta_f d_{f50} \Psi_{cf} (1 - \gamma V_{c,f})}{\Delta_b d_{b50} \Psi_{cb} (1 - \gamma V_{c,b})} \right)$$

For the load damping length L_d are formed some hypotheses. Based the research of Bezuijen & Köhler (1996) an expression for the load damping length L_d under wave loading is suggested. Since the research of Bezuijen & Köhler was based on wave attack on a (flexible) revetment structure, it is debatable whether this will also be a proper expression for the load damping length L_d for a horizontal filter structure under wave loading. Although, it is the most accurate expectation which can be established with the current knowledge. The hypotheses will be verified or falsified with new experimental data.

A new assumption is introduced, which makes it possible to use a new approach for the validation study. This new approach makes it possible to do a validation study in a relatively small wave flume. Using the assumption, it is not necessary to generate filter instability in the experiments. The stresses on the filter are now calculated.

Besides the new validation approach, the classical validation can still be carried out. This will only give insight in the lower limit of the load damp coefficient α_d .

Finally, it is suggested to involve the data of Wolters *et al.* (2010) in this research. Tests with a horizontal open filter under irregular wave loading were carried out.

Chapter 4

Physical model

The model tests are carried out in the wave flume of the Environmental Fluid laboratory at Delft University of Technology. This wave flume has a length of 38m, an effective height of 0.9m and a width of 0.8m. This chapter explains the setup of the physical model, the instruments and the properties of the used materials. Also, the wave conditions are assessed and insight is given in the shoaling and reflection which takes place. Finally, the scaling of the model is discussed.

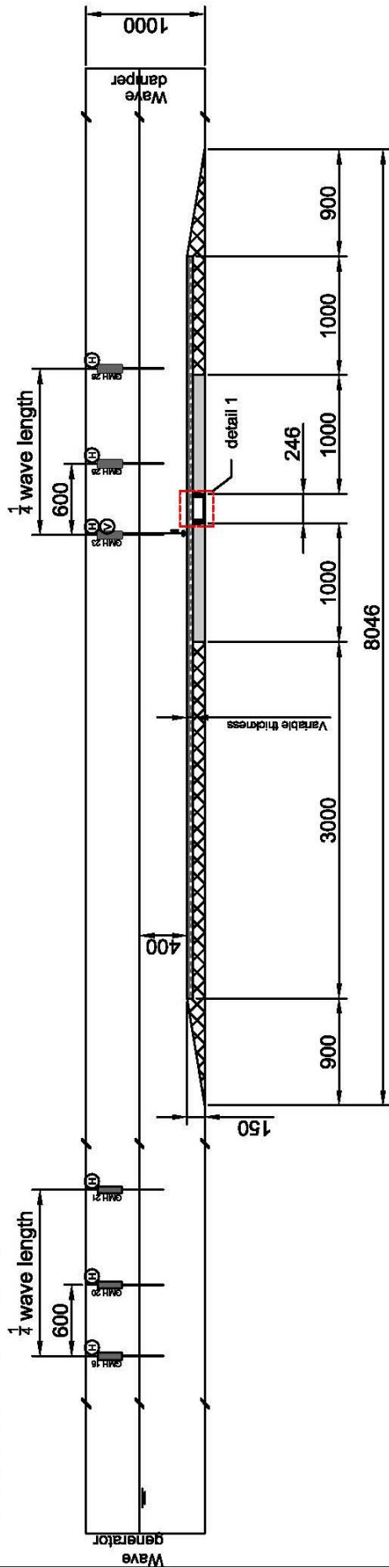


Figure 4-1 the wave flume

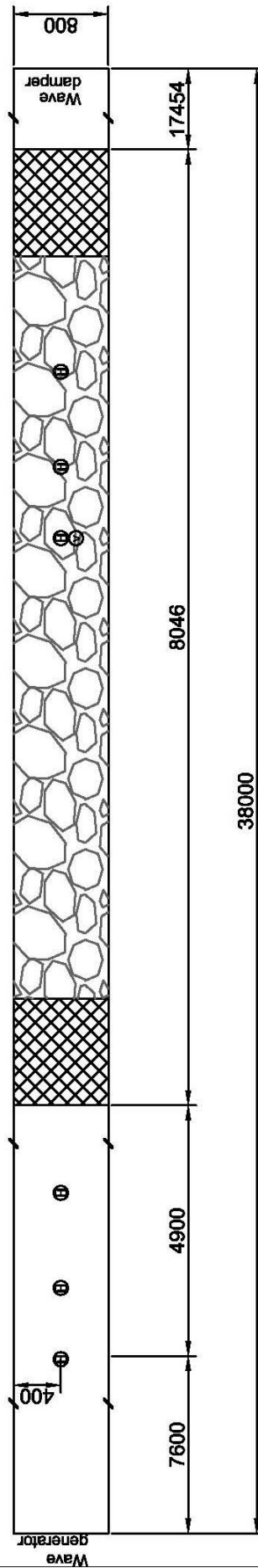
4.1 Model layout

The test setup is inspired by the experiments by Wolters *et al.* (2010). A test section is built with a sand layer under a filter layer. In front and behind the test section a slope is placed, the waves shoal over this slope. The sand layer is not placed over the whole length of the structure. The wave can develop over the first meters behind the slope before it travels over the sand base. Over the whole horizontal length of the structure filter material is placed, so that the rough turbulent conditions over the filter layer can develop.

Cross-section flume



Top view flume



Open filter under wave loading

Test location: Delft University of Technology, Laboratory Fluidmechanics
 Test period: 16 / 8 / 2014 - 01 / 11 / 2014
 Contact: Wessel Hollander, wesselhollander@gmail.com

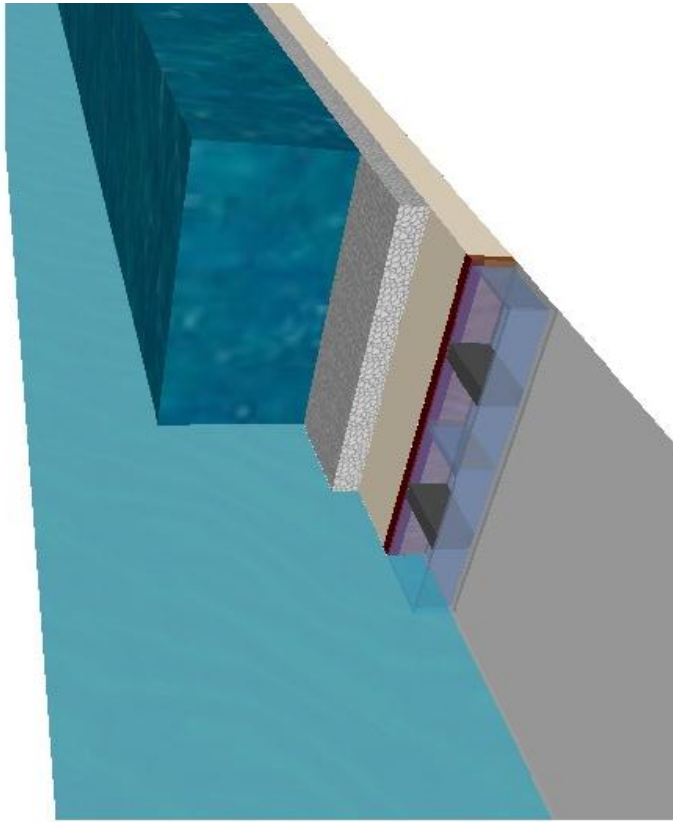
Legend

- ⊗ Wave height meter / wave gauge (GHM)
- ⊙ Flow velocity meter (EMS)
- ▨ Filter material
- ▩ Base Material
- ▧ Wooden model structure
- ↗ Break to next flume section

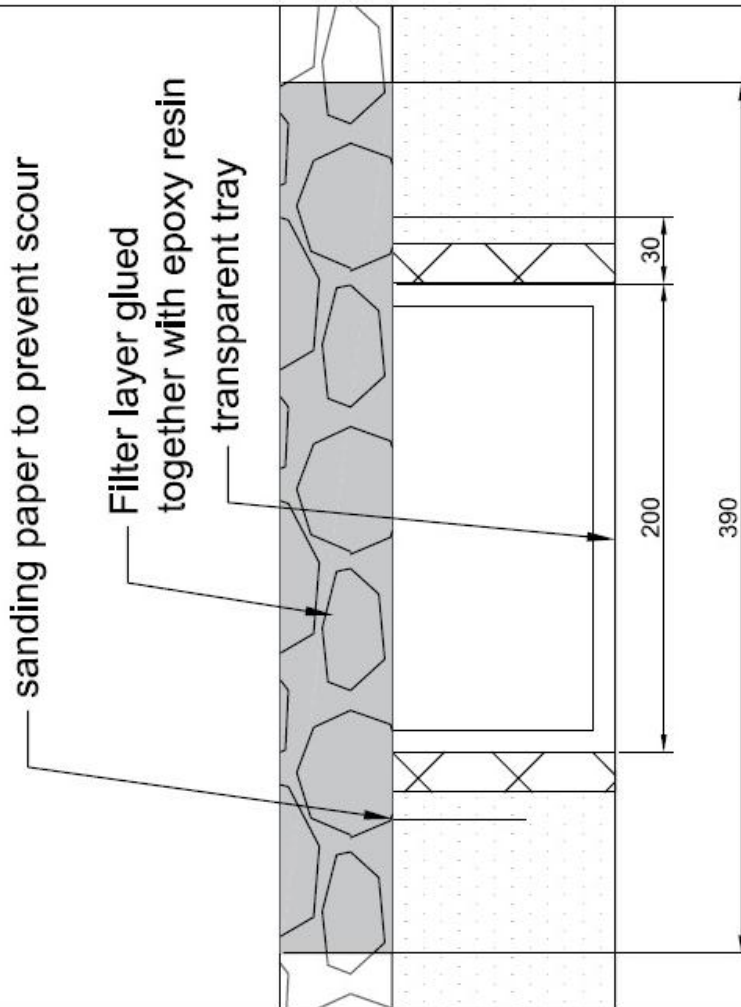
Notes

Units are shown in mm
 Model scale is 1:1

3D visualisation of the flume






Detail 1



Notes

Units are shown in mm

Legend

-  Glued filter section
-  Wooden model structure
-  Filter material

Detail of the tray in the flume

Test location: Delft University of Technology, Laboratory Fluidmechanics
 Test period: 16 / 8 / 2014 - 01 / 11 / 2014
 Contact: Wessel Hollander, wesselhollander@gmail.com

In the middle of the base layer, a transparent tray replaces the sand over the whole width (0.8m) of the flume. This tray is closed at the bottom and edges, but the top side is open. During the model tests, the (unstable) sand particles which travel through the pores of the filter can sink down in this tray. After the tests this tray can be taken out of the flume. Thereby it is possible to visually qualify when base material erosion takes place during the test. Observations through the glass of the flume into the transparent tray can be made. The observations are recorded with a video camera. On top of the tray, the filter is not interrupted. However, to prevent the filter from falling down into the tray (which has an open top), two filter slabs are used. These slabs are made of the filter material, glued together with epoxy resin. A metal wire mesh (with 1cm openings) is used to strengthen the filter slab.



Figure 4-2 fabricated filter slab.

4.2 Instrumentation

During the tests, the wave heights are measured, the fluid velocity above the filter layer is measured and video recordings are made. This section discusses the instrumentation in the flume. This includes the wave generator, the wave height instruments (wave gauges), the fluid velocity instruments (EMS) and the video camera set up.

4.2.1 Wave generator

A wave paddle is installed which is computer driven and is capable of generating regular and irregular waves, linear and second order stokes waves. Thereby the wave paddle automatically compensates for the incoming wave reflections. Behind the wave paddle, inside the generator, a reservoir is filled with water. This volume is also brought in motion when the paddle is generating waves. Under certain conditions, it was noticed that this volume of water resonated. This resonance can be so intense, that the wave generator is not able to continue and stops automatically. This resonance was observed for 4s periods, at a water depth from 0.3m to 0.5m and a wave height of 0.2m and higher. Based on this finding it was chosen to use waves with lower periods for the experiments. The maximum wave period used in the experiments was 3s.

4.2.2 Wave gauges

Two rows of wave gauges are placed in the flume. The first row of wave gauges is placed before the test section, the second row is placed above the test section. Thus it is possible to measure the incoming waves at the first row of gauges. The waves will shoal when they travel over the slope of the laboratory setup, these shoaled waves are measured by the second row of wave gauges. The accuracy and reading error of an individual wave gauge is $\pm 0.2\text{cm}$. The wave gauges are calibrated every day before a model test is carried out.

The wave damper does not damp out the waves completely. By placing the gauges in a row, it is possible to measure the reflected wave. To determine reflections for regular waves, it is necessary to place two gauges at a distance of 0.25 times the wave length. Before the tests, this distance is calculated with the linear wave theory, and the wave gauges are placed in the correct position.



Figure 4-3 wave gauge

4.2.3 Velocity meter (EMS)

EMS stands for "Electromagnetic Flow Meter". This device measures the fluid velocity in the x- and y-direction. The accuracy and reading error is ± 0.02 m/s. Before each tests the offset is noted. It was seen that the offset value was unstable for some after the flume was just filled. The EMS is placed at least 4 hours in a filled flume before the tests are performed, so that the offset value was stable.

4.2.4 Camera set up

Video recordings are made during the experiments. A video camera is placed near the transparent tray. The tray is lightened with a LED which is pushed against the glass of the flume, such that the reflections from the light are minimal.

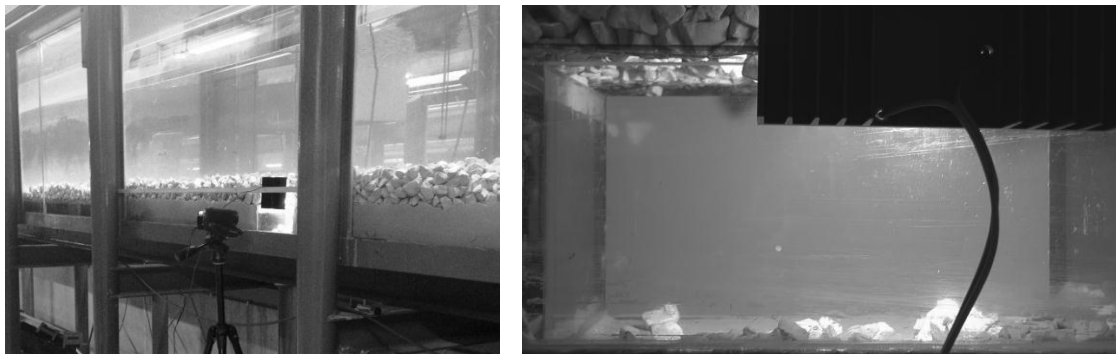


Table 4-1 Left: setup of the camera. Right: a camera shot of the transparent tray.

4.3 Material properties

In Hoffmans relation, the ratio between the filter material and base material is an important parameter. To be consistent with previous research, it is chosen to work in the same range. In previous, the ratio $\frac{d_{f50}}{d_{b50}}$ varied between 50 and 400.

On the other hand, the ratio between the layer thickness and the filter diameter is also of importance. For the filter diameter, there is a practically lower limit; if the diameter is chosen too small, it is not possible to realize a filter thickness with a small ratio of $\frac{D_f}{d_{f15}}$. The accuracy of the placement of the filter layer is approximately 1cm or the value of d_{f50} . Thereby, there is also an upper limit of the filter diameter. For this research, it is desirable to work under wave conditions in which the filter layer is close to instability. When the filter diameter is chosen too large, this is not possible any more.

With these limitations for the filter, it was desirable too chose the sand as fine as possible. This way the $\frac{d_{f50}}{d_{b50}}$ ratio was still in line with previous research. However, the sand may not be cohesive, therefore the particles must be larger than 60 μm . Sand with a median diameter of 113 μm was used in the experiment. This results in ratios of $\frac{d_{f50}}{d_{b50}}$ which vary between 50 and 220.

The density and gran size diameters are determined for this research. In appendix A a full background information about the material properties is given.

4.3.1 Filter material

Three different filter materials were selected for the model tests; “Yellow Sun 8-11 mm” , “Yellow Sun 10-20 mm” and “Yellow Sun 20-40 mm”. The grain size distribution is found by using the weight of the stones. The weight of a stone is related to the nominal diameter, and this nominal diameter is related to the grain size diameter by a shape factor. It is assumed that this shape factor is a constant, a value of 0.88 is used. However, current research at Delft University of Technology shows that this shape factor is not as constant as always was assumed. As a result, an uncertainty is introduced in the found grain size diameter of the filter materials. This uncertainty will be analyzed and taken into account in chapter 6.

Table 4-2 Overview filter properties

Material	d_{15} [mm]	d_{50} [mm]	d_{85} [mm]	d_{90} [mm]	d_{n50} [mm]	$\frac{d_{85}}{d_{15}}$	ρ_f [kg/m ³]
Yellow Sun 8-11 mm	5.39	6.63	8.59	9.02	5.83	1.59	2624
Yellow Sun 10-20 mm	10.88	13.71	17.02	17.76	12.06	1.56	2624
Yellow Sun 20-40 mm	21.09	25.02	29.04	29.55	22.03	1.37	2624

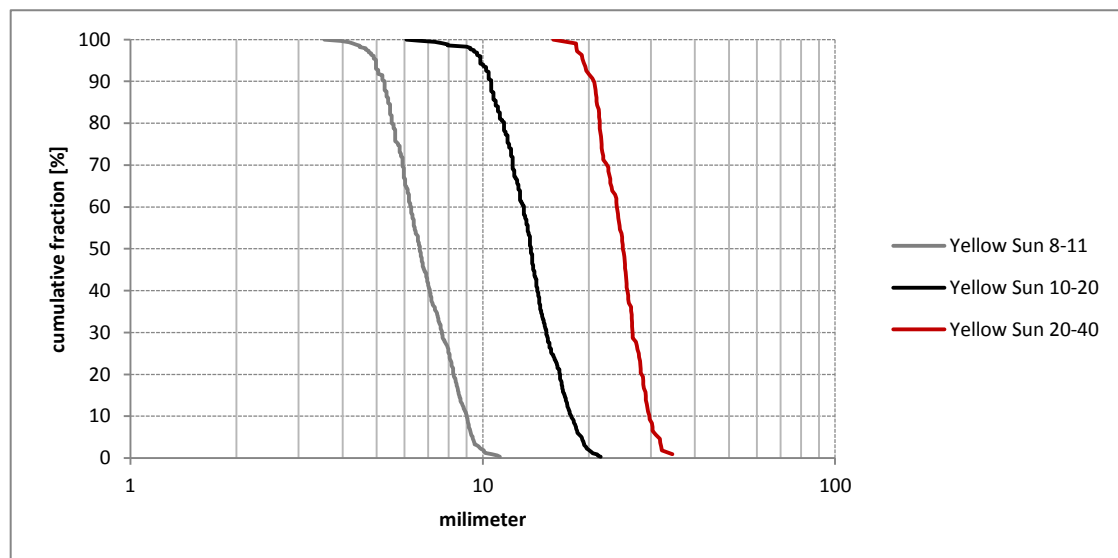


Figure 4-4 grain size distribution of the filter materials

4.3.2 Base material

The base material diameters are obtained by sieving the material. Multiple sieves with different mesh sizes were used. The results are shown in Table 4-3 and Figure 4-5. For a more detailed background is referred to appendix A.

Table 4-3 overview base material properties

Material	d_{15} [μ m]	d_{50} [μ m]	d_{85} [μ m]	d_{90} [μ m]	$\frac{d_{85}}{d_{15}}$	ρ_f [kg/m ³]
Base material	98	113	120	122	1.22	2630

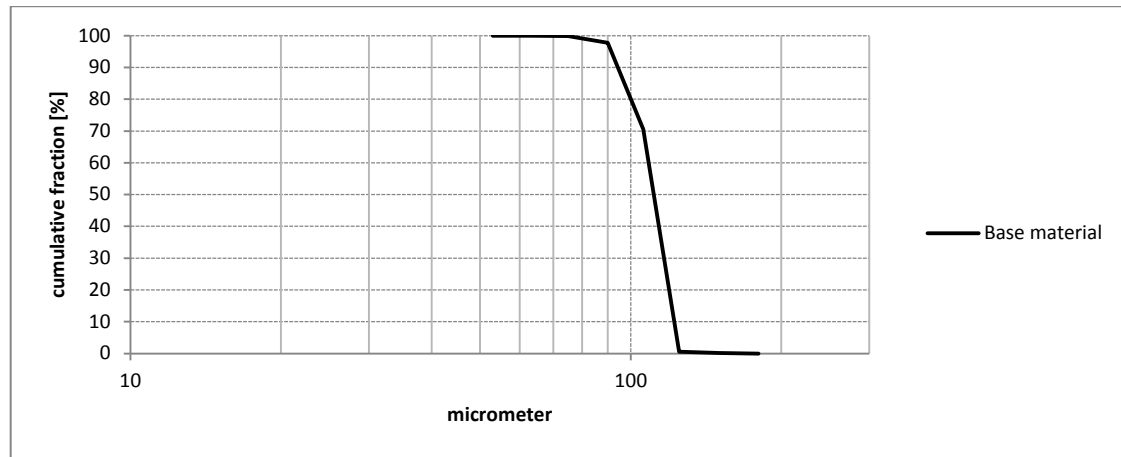


Figure 4-5 Sievedistribution of the base material

4.4 Test program

This research is focused on the validation of Hoffmans relation under wave loading. As explained in chapter 3, it is expected that the wave period has an influence on the damping length. To investigate this, tests with different wave periods will be carried out. Regular waves will be used.

The hydraulic loading is determined by 3 variables: the wave period, the wave height and the water depth. During the tests, the hydraulic loading will be increased until the base layer becomes instable. This increase in the hydraulic loading can be realized by a change in the same 3 parameters. However, it is not desirable to change the value of the wave period for the purpose of increasing the hydraulic loading, because it will be attempted to investigate the effect of the wave period on the load damping of the filter. The water depth is also not ideal to change, because it is very hard to generate exactly the same wave when the water level has changed. Therefore the most logical parameter to increase the hydraulic loading is the wave height. Thus a test will be started with a low wave height, which will be increased until instability of the base material is observed. The water level will not be changed and the wave periods will only vary between 2, 2.5, and 3 seconds. A test is completed when the critical wave height in combination with the 3 different wave periods is found.

Table 4-4 Test program

Test	Test parameters					Loading	
	D_f [mm]	d_{f50} [mm]	d_{b50} [μ m]	$\frac{D_f}{d_{f15}}$ [-]	$\frac{d_{f50}}{d_{b50}}$ [-]	h_f [m]	T [m]
1	20	6,6	113	3.71	58.4	0.4	3.0
2	20	6,6	113	3.71	58.4	0.4	2.0
2	20	6,6	113	3.71	58.4	0.4	2.5
2	20	6,6	113	3.71	58.4	0.4	3.0
3	30	13.7	113	2.76	121.2	0.4	2.0
3	30	13.7	113	2.76	121.2	0.4	2.5
3	30	13.7	113	2.76	121.2	0.4	3.0
4	60	13.7	113	5.51	121.2	0.4	2.0
4	60	13.7	113	5.51	121.2	0.4	2.5
4	60	13.7	113	5.51	121.2	0.4	3.0
5	90	13.7	113	8.27	121.2	0.4	2.0
5	90	13.7	113	8.27	121.2	0.4	2.5
5	90	13.7	113	8.27	121.2	0.4	3.0
6	90	25.0	113	4.26	221.2	0.4	2.0
6	90	25.0	113	4.26	221.2	0.4	2.5
6	90	25.0	113	4.26	221.2	0.4	3.0
7	150	25.0	113	7.11	221.2	0.4	2.0
7	150	25.0	113	7.11	221.2	0.4	2.5
7	150	25.0	113	7.11	221.2	0.4	3.0

The filter layer thickness presented in the test program may deviate in the actual test. An attempt will be made to create a filter with this thickness, but if the thickness is slightly different, that thickness will be used.

Figure 4-6 gives an overview of all tests in a graph. For each point in the graph, the critical wave height will be determined corresponding to a 2, 2.5 and a 3 second wave period.

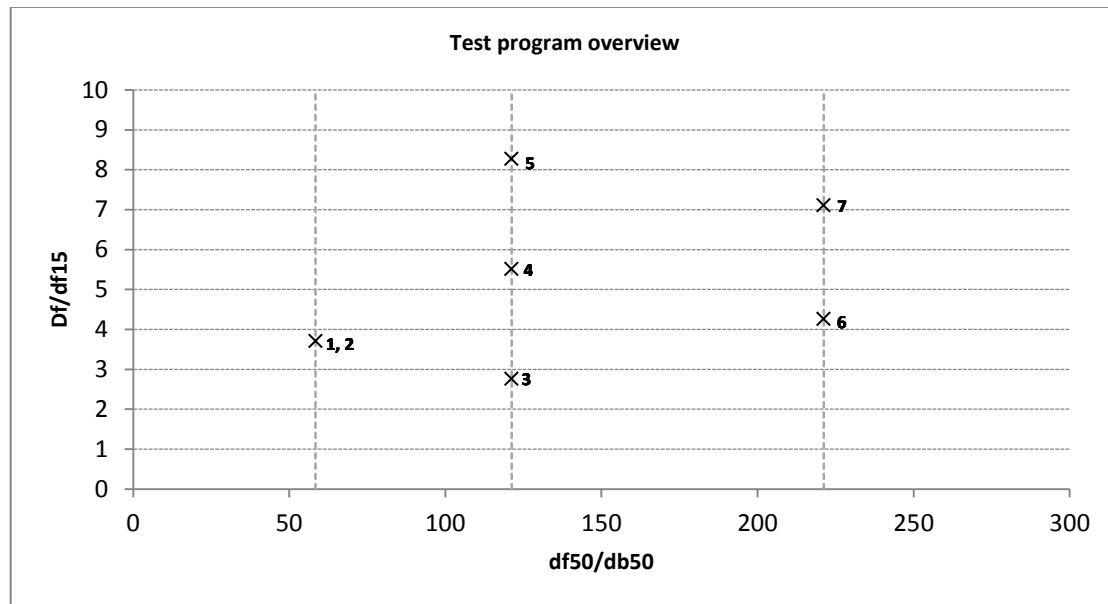


Figure 4-6 Overview of the tests

4.5 Wave behavior and side effects in the flume

4.5.1 Wave linearity

The wave height in the flume is limited. To generate shear stress under waves, an orbital motion needs to be present at the bed. So by its own nature, the waves are in shallow water. For this reason the waves do not behave as linear waves as in deep water, but may be described with nonlinear theories such as the 2nd order Stokes theory. In Figure 4-7 is indicated how the waves used in this research can be described. All waves can be considered non-linear. To reduce spin up time in the flume, the wave generator is set to generate 2nd order waves at all times (instead of linear waves).

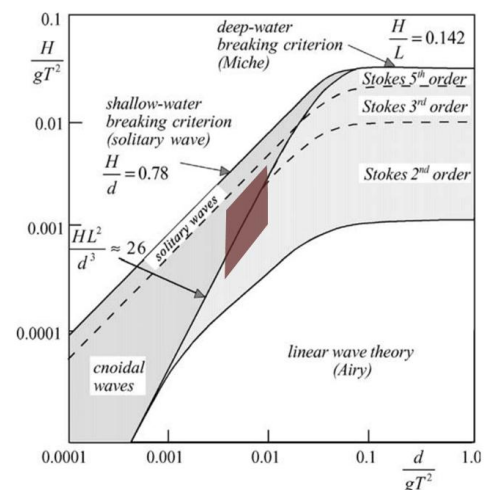


Figure 4-7 red area indicates the work area of this research

The non-linearity of the waves increase as the steepness over the relative depth increases. In figure X two wave patterns in the flume above the filter are shown. The period and water depth is similar, but the wave height is different. It is clear that the higher wave (which is steeper and thus has a larger

Ursell number) has sharper peaks and longer troughs. This is typical for nonlinear waves. Also the orbital velocities under the sharp peak are higher.

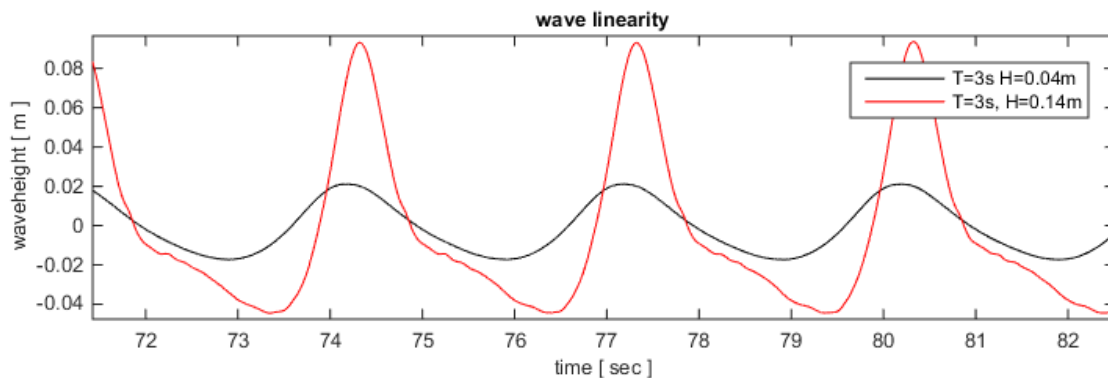


Figure 4-8 Two measured wave profiles in the flume. The red profile shows more nonlinearity than the black profile.

Although the linear wave theory is not perfectly applicable it is still prominently used in the field of shore protections. Compared to the nonlinear theories, the linear wave theory is far more easy to use. Thereby the linear theory gives most of the time an accurate approximation. Also Rance & Warren (1968) and Jonsson (1966) used the linear wave theory as to find their stability relations for granular material under wave loading. LeMéhauté (1968) showed that the linear wave theory predicts the orbital velocities quite well, even far outside the validity range of the linear wave theory. Because Jonsson's approach will be used in the analysis of the results, and in particular the bed velocities are of importance, these are analyzed in Figure 4-9 (this analysis is inspired by Shiereck *et al.* (1994)). A set of wave conditions with a period range of 2s to 3s and a height from 4cm to 14cm is used to generate the data. The different wave conditions are categorized by their steepness. Again, the bed velocities are predicted quite well. Therefore it seems legitimate to apply Jonsson's method for the analysis of the data.

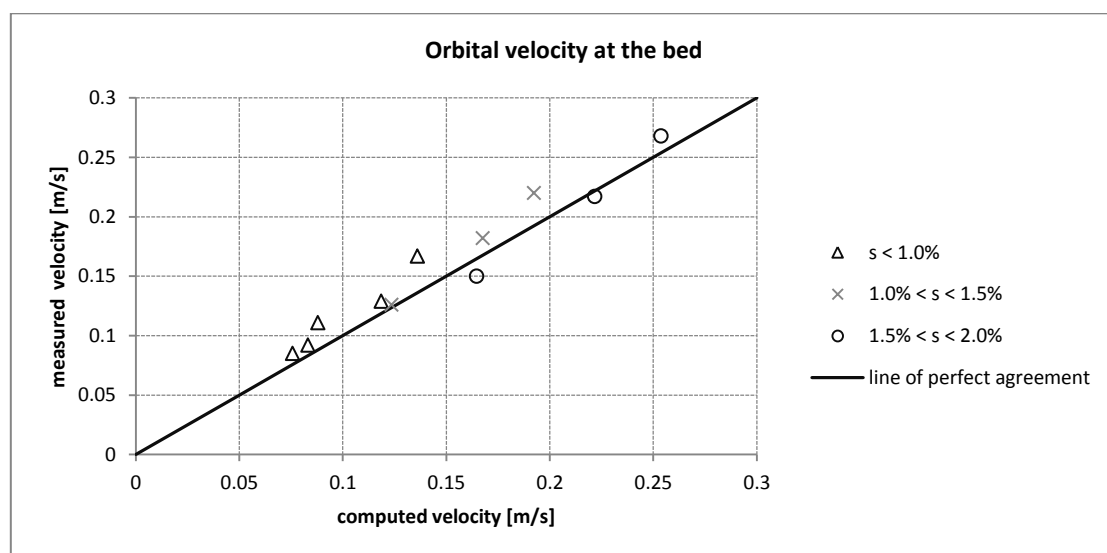


Figure 4-9 analysis of the orbital wave velocity in the flume near the bed

4.5.2 Shoaling & reflection in the flume

As a wave is generated by the wave paddle, it is influenced by the filter-setup and the wave damper. The wave will shoal over the slope in front of the setup. To minimize the reflection, the slope is made very gentle (i.e. 1 to 6). The shoaled wave will travel over the filter setup and consequently pass the second slope. Over the second slope, the wave height will decrease again. Consequently the wave will hit the wave damper where it loses most of its energy. However, the wave damper does not damp all

energy and a part of the wave is reflected. The reflected wave will travel back over the filter and finally it is completely damped out by the wave generator, which compensates for the incoming wave. Figure X gives 2 profiled. The first profile is measured near the wave paddle, and the second profile above the filter. The effect of the shoaling is clear by the increase in the wave height. Also, the effect of the reflected wave can be seen by the curve in the profile of the wave above the filter (the curve between the peak and trough of the wave). The observed reflections for a various condition of waves were in the range of 3% and 11%. In the analysis of the data, the total wave above the filter will be used. So this is the wave which has shoaled including the reflection.

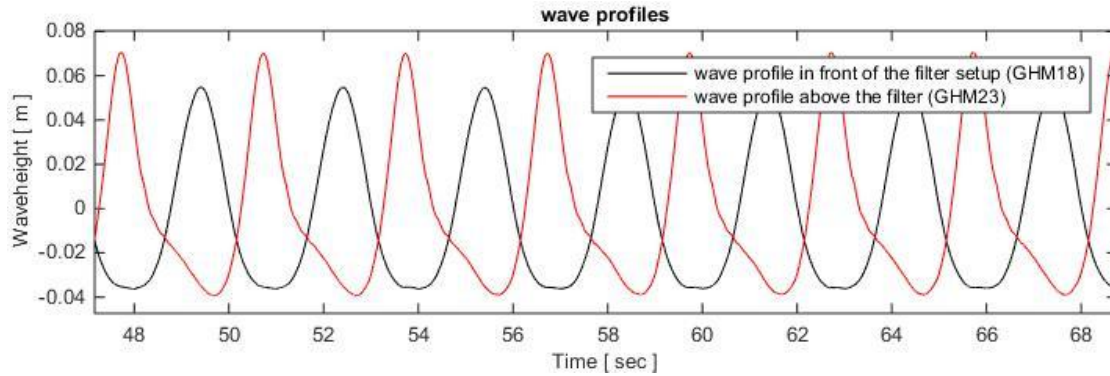


Figure 4-10 wave profiles before and above the filter-setup

4.5.3 Mass flux and return currents

Nonlinear waves are asymmetric over the horizontal axis (skewed). Theoretically, the particles in the peak of the waves have a higher velocity than in the trough. This implies that, when the particles move through their orbits, their velocity is higher when moving in the direction of wave propagation. Therefore the particles do not move in nice circular orbits anymore, but a net transport in the direction of the wave propagation will take place, a mass flux (the Stokes drift). However, the flume is closed at the end, so this mass flux can only be compensated with a water level gradient and a return current. This current influences the orbital velocities near the bed. This might be a reason for the small deviation in the measured and computed velocities shown in Figure 4-9. Overall, the influence is not very dominant, since the computed values are still quite good. Also, research in the past (Schierack *et al* 1994) as shown that the agreement of measured wave velocities and the calculated values is remarkably good. Therefore the effect of the return currents are neglected in the analysis of the data.

4.5.4 Wall friction

The roughness of the wall creates extra turbulence, this is unfavorable. For this reason, it is not possible to directly draw conclusions from observation directly behind the wall.

4.6 Model scaling

Scaled model test are often applied in the field of coastal engineering. In many experiments, the tests are a scaled representative of a full scale design. In this case, the hydraulic conditions in the scale tests must be representative to the conditions in the full scale design. In this field of study, two scale rules can be used; Reynolds scaling and Froude scaling. The philosophy behind the rules is that the values of the Reynolds or Froude parameters are similar to the values on the full scale.

The Froude number gives the ratio between the flow velocity and the wave propagation speed.

$$Fr = \frac{U}{\sqrt{gh}} \quad (60)$$

The Reynolds number gives the ratio between inertial forces and viscous forces. Thereby, the number gives an indication of the degree of turbulence. Reynolds numbers above 2000 are considered to be turbulent. In the formula for the Reynolds number (presented in equation 61), L is length scale.

$$Re = \frac{U \cdot L}{\nu} \quad (61)$$

In this research, where Hoffmans formula will be validated, no full scale design is considered. Hoffmans formula consist of dimensionless parameters and relative dimensions (see equation 34). For this reason, it is assumed that the relation is insensitive for scaling. The physics behind the formula should be independent of the size of the structure. Therefore, this seems a reasonable assumption. The previous validation research (Van de Sande (2012) and Joustra (2013)) was also on full scale in a laboratory setup. The ratio's between the filter and base material are in the same range of the previous validation research.

Chapter 5

Results

In this chapter the results of the physical model tests are presented. It gives background information about the lab results, but also the unexpected occurrences and how is dealt with the undesired effects. In the first subchapter an overview of all results is given. The following subchapters describe how the results were obtained and which inaccuracies are introduced from the lab processes. Finally, a chapter review is given. Detailed background information of the individual test can be found in appendix B.

5.1 Overview of the results

As described in chapter 4, a test program was introduced which is used for the experiments. In the test program a certain layer thickness of the filter was proposed. During the construction of the test, it was not always possible to exactly build a filter with the proposed thickness, therefore these values slightly differ from the values in the test program. Obviously, the measured values in the test will be used for the analysis of the data.

Furthermore, critical data for the analysis are the used materials, the water level and the wave for which the bed material becomes unstable (called: the critical wave height.). Three different wave periods were used during the experiments. For every wave period, the wave height was increased step by step until erosion of the base material was observed through the transparent tray. The wave height for which this occurred is considered to be the *critical wave height for bed erosion* ($H_{c,b}$). After observing the wave height for which the bed began to show instability, the waves were still increased step by step. For a certain wave height it was possible to see the base particles moving through the filter. The wave condition for which this started to occur is referred to as the *critical wave height for winnowing* ($H_{c,w}$). Video recordings are made of every test to support the visual observations. These critical wave heights are important for the analysis of the data. In the experiments it was attempted to find the wave conditions which correspond with initiation of motion of the bed material, therefore it was not necessary to carry the tests for a long duration. It was even desirable to minimize the test duration, because otherwise the test setup would suffer from the bed erosion. The duration was approximately 5 minutes per test. This way, it was possible to find the critical wave

conditions for 3 wave periods, by using the same test configuration. The overview of the results is presented in Table 5-1.

Note that for the first test only waves with a 3 second period were used. For practical reasons, this test was rebuild. It was considered that too much erosion had taken place whereby the base-filter interface was influenced too much to continue testing with other wave conditions on the same set-up. It can also be seen that the critical condition for the observation of bed material is $\leq 0.10\text{m}$. The initial wave height was 0.10m , and base erosion was already be seen for this wave height.

Table 5-1 Overview of the test results

Test	Test parameters					Loading conditions			
	D_f [mm]	d_{f50} [mm]	d_{b50} [μm]	$\frac{D_f}{d_{f15}}$ [-]	$\frac{d_{f50}}{d_{b50}}$ [-]	h_f [m]	T [s]	$H_{c,b}$ [m]	H_w [m]
1	17	6,6	113	3.2	58.4	0.4	3.0	≤ 0.10	0.16
2	17	6,6	113	3.2	58.4	0.4	2.0	0.12	0.15
2	17	6,6	113	3.2	58.4	0.4	2.5	0.09	0.15
2	17	6,6	113	3.2	58.4	0.4	3.0	≤ 0.10	0.13
3	28	13.7	113	2.6	121.2	0.4	2.0	0.05	0.07
3	28	13.7	113	2.6	121.2	0.4	2.5	0.05	0.07
3	28	13.7	113	2.6	121.2	0.4	3.0	0.06	0.08
4	59	13.7	113	5.4	121.2	0.4	2.0	0.08	0.10
4	59	13.7	113	5.4	121.2	0.4	2.5	0.08	0.11
4	59	13.7	113	5.4	121.2	0.4	3.0	0.08	0.08
5	96	13.7	113	8.8	121.2	0.4	2.0	0.11	0.14
5	96	13.7	113	8.8	121.2	0.4	2.5	0.11	0.16
5	96	13.7	113	8.8	121.2	0.4	3.0	0.12	0.15
6	93	25.0	113	4.4	221.2	0.4	2.0	0.06	0.06
6	93	25.0	113	4.4	221.2	0.4	2.5	0.06	0.06
6	93	25.0	113	4.4	221.2	0.4	3.0	0.06	0.08
7	147	25.0	113	7.0	221.2	0.4	2.0	0.06	0.09
7	147	25.0	113	7.0	221.2	0.4	2.5	0.07	0.09
7	147	25.0	113	7.0	221.2	0.4	3.0	0.07	0.09

5.2 Classification of instability

The instability of the bed was visually qualified through the transparent tray. The trays were placed over the entire width of the flume, to prevent that the visual observations would be influenced by wall effects inside the flume. After a test, it was also observed that all compartments of the transparent tray were filled equally with eroded base material. For this reason it is supposed that the wall effect did not had an effect on the visual qualifications of instability.

A situation was qualified as “instable” when many base particles were seen moving into the tray. “Many” is defined as a number which was not possible to count. Sometimes it was able to see very few particles flow around and entering the tray. It was considered that this was not a sign of instability, since these were probably the smallest particles in the grading. For this reason it was chosen qualify the situation as instable when many particles were entering the tray. Although it was not possible to quantify the transport, it was visually clear that the erosion increased for higher wave conditions.

To verify the used criteria for the qualification of bed instability, a number of tests with a long duration were carried out. These long durations tests were carried out at the end of the test series on a model configuration, because significant erosion could take place. The purpose of these test was to check whether the critical wave condition was determined as “critical” righteous. When the wave conditions was critical, significant erosion would occur in 20 hour. The long duration tests lasted for 20 hours. As expected, it was able to see significant erosion after the tests. Therefore it was concluded that the wave conditions did righteous correspond with an instable base layer. The erosion

was observed in two ways: the bed profile observed through the glass wall of the flume, and also by the increased volume of bed material inside the tray before and after the test.

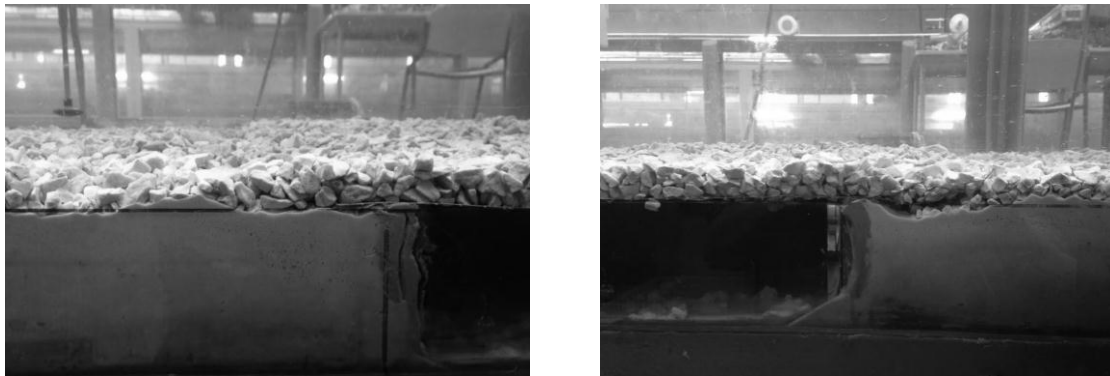


Figure 5-1 Erosion after a long duration test (test 2 T=2.0s H=0.12m)

The qualification of winnowing had a more subjective character than the qualification of base erosion. The observations were made through the glass flume, where the wall effects of the flume might influence the observations. When observations were made of base particles moving out of the top of the filter, the qualification “winnowing” was made. Since the filter material was covered with very fine dirt, the water in the flume was not completely clean (the dirt was clouding the water). This dirt of the filter material hindered the observations for the qualification of winnowing. However, it was always attempted to make this qualification as accurate as possible. Thereby, the dirt was finer than the base material, and could be distinguished from the base material particles. Figure 5-2 shows a snapshot of a test where winnowing was observed. In most test, the critical wave condition for which winnowing occurred was higher than the critical wave condition for which bed material erosion occurred (only in test 6 it was observed that winnowing and bed material erosion occurred for the same critical wave condition).



Figure 5-2 winnowing through the filter (test 6 T=2.5s H=0.08m)



Figure 5-3 Dirt from the filter clouding the water (test 4)

5.3 Unexpected phenomena

This paragraph elaborates on the unexpected occurrences during the model testing. These findings may be useful when a similar experiment will be carried out in the future.

5.3.1 Scour holes

During the first test it was observed that a scour hole was developing next to the tray’s edges, as shown in Figure 5-4. The development of this scour hole was undesirable, since it influenced the base material’s stability. Additional turbulence may be present due to this scour hole.

Two processes may contribute to the development of the scour hole. First, the sediment transport is limited to one direction. This means that particles moving into the tray, cannot move back to their original location. Therefore a hole is formed near the edges of the tray. Secondly, additional turbulence may be present near the edges of the tray. The stream lines of the flow are interrupted by the tray's edge, which causes extra turbulence behind the tray. This effect is undesired, because the aim of this research is to focus on wave loading alone, and not a situation with additional turbulence.



Figure 5-4 scour hole next to the tray (test 1, after a long duration test of 20 hour)

The development of these scour holes cannot be avoided, because they are a result of the instability of the base material. However, the undesirable effects can be limited. Two measures were taken; firstly, the test duration was limited so that the scour hole development was limited (to approximately 5 minutes per tested wave conditions). Secondly, the edges of the tray were protected with a 3 cm wide strip of sanding paper, to protect this area from erosion. The consequence of this strip of sanding paper is also that an unstable base particle now has to move 3 cm to reach the transparent tray where the instability is qualified. Therefore it was undesirable to make this strip very wide, otherwise the base material transport could be measured, instead the start of erosion.

The strip of sanding paper is also seen on the drawing of the model setup in chapter 4.

5.4 Bacteria in the flume

In test 4, it was seen that the experimental model was polluted with a slimy substance. Based on an expert's opinion, it is likely that this substance is the result of a bacterial reaction between the water and the wooden structure of the model setup. The flume was filled for 5 days when this substance was seen. Figure 5-5 shows the pollution in the transparent tray.

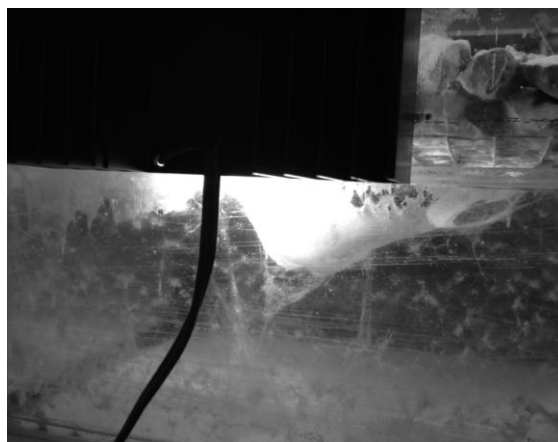


Figure 5-5 bacteria in the flume (test 4)

It was not known if this pollution would affect the experiments. However, no risk was taken and test 4 was repeated with a clean flume. For all following tests the flume was filled no longer than 2 days before a test was rebuild again. This pollution was not seen in any further test.

5.5 Inaccuracies in the experiments

5.5.1 Qualification of instability

Although the best attempts were made to define the instability of the bed as accurate as possible, the visual observations still are a source of subjectivity. As a consequence, this will lead to an inaccuracy in the data analysis. In the analysis of this data, it is assumed that the point where the base starts to erode corresponds with the critical shields number for initiation of motion. However, in reality the erosion might have been slightly larger for one test than the other. Because the classification is visual, this difference is unknown. By assuming that all those critical situation correspond with the critical shields number, an uncertainty arises. The sensitivity of this assumption will be investigated in the analysis of the data (chapter 6).

5.5.2 Thickness of the filter layer

Logically, a filter layer has not a perfect flat top. Therefore, the filter's thickness is also not perfectly equal on every location. The accuracy of the filter layer's thickness depends on the filter material diameter. When the filter material diameter is large, the deviations in the thickness will be larger than for a small filter material diameter.

In the model tests the filter is measured at 20 locations. The average of these measurements is taken as the filter diameter. Figure 5-6 shows how the measured deviations from this average value are distributed. The deviation is expressed in terms of the filter diameter size (on the x-axis). The figure shows that in the most extreme values for the measured deviations are equal to d_{f50} . However, 90% of the measured deviations are in the order of 0.5 time d_{f50} .

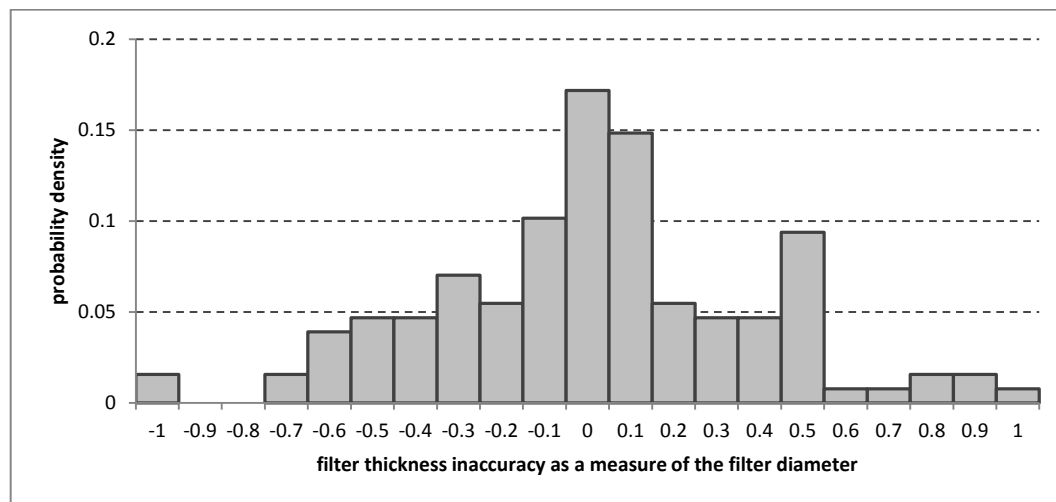


Figure 5-6 distribution of the deviations in the measured filter layer thickness compared with the average value

5.6 Chapter review

It turned out that visual observations became an important tool to classify instability of the base layer. Initially it was an idea to weigh the transported sand in the tray and compare that for different tests. For several reasons it was decided not to weigh the transported sand after each test. To start with, sand is transported into the tray when filling the flume. Thereby only small amounts of sand are transported during the tests. Long tests with considerable transport are needed to draw conclusions

from the transported amount of sand. Thereby it is extremely time consuming to remove the tray of sand after a test, since the whole experiment has to be recovered due to the collateral damage of removing the tray.

Video recordings are made of each test, thus the visual observations can be extensively reviewed. For the purpose of qualifying instability of the base layer, the model tests do not have to run for a long time. A few minutes was enough to make the video recordings and collect all data.

The development of the scour hole near the edges of the tray is considered as an inaccuracy in the test. Therefore the development of this scour hole was limited as much as possible. Thereby, it cannot completely be avoided that this scour occurs, since it was a result of the eroding base layer in the first place. Thereby a test was rebuild when the scour hole had grown too large.

Chapter 6

Analysis

6.1 Classical validation approach

The same approach as Van de Sande (2012) and Joustra (2013) used can be applied in this research. As already discussed in chapter 3, this approach will only give a lower limit for the load damp parameter, since only data points are found with a stable filter layer. Still, this lower limit may provide interesting insights. In Figure 6-1, this analysis is shown. Also the data of Halter (1999) and Wolters & Van Gent (2012) is included in the figure. The y-axis shows the relative filter thickness, the x-axis shows a major part of Hoffmans formula. According to Hoffmans formula, the two components on the axis are related by the load damp coefficient α_d .

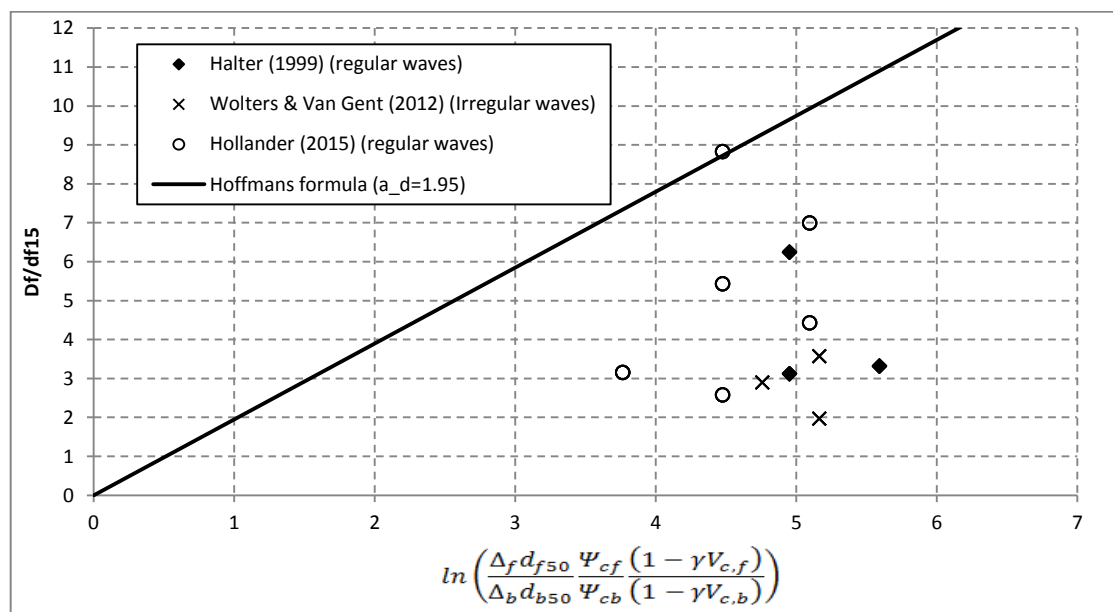


Figure 6-1 Classical validation approach (for shown data points are classified as "only base erosion"). The following assumptions are made for the data of Wolters & Van Gent (2012): $\frac{\Delta_f}{\Delta_b} \approx 1$, and $\frac{\gamma V_{c,f}}{\gamma V_{c,b}} \approx 1$.

All data points in this analysis represent a situation where the base material eroded first, without any filter material erosion. Thus, the relative filter thickness was too thin for a stable open filter. Therefore, the load damp coefficient α_d has a value for which all the data-points are in the area under the line drawn in Figure 6-1. From this analysis follows that the load damp parameter should at least have a value of 1.95. This can be considered as the lower limit for the load damp coefficient α_d . Besides this lower limit, no other clues can be given for the load damp parameter. It cannot be told what the actual value of the load damp parameter will be, this requires tests with simultaneous erosion or filter erosion. Although, from this analysis can be concluded that, for a stable filter, the relative filter thickness is larger under wave loading than under uniform flow.

It should be noted that this classical validation approach is doubtful to validate Hoffmans' formula under wave loading, since it is hypothesized that the load damping length L_d depends on the wave period. Using the classical validation approach, it is assumed that $L_d = \alpha_d d_{f15}$, which is proposed for uniform flow. However, this classical validation approach does give insight in the stability of a filter under wave loading compared with uniform flow. From the fact that the found values of the load damp coefficient α_d is higher under wave loading than uniform flow (for which $\alpha_d \approx 1.00$) follows that a stable open filter has to be thicker under wave loading than for uniform flow. This is a valuable insight which indicates the difference between the performance of an open filter under wave loading and under uniform flow.

6.2 New approach (using the assumption that $L_d' = L_d$)

6.2.1 Overview of the results

Using the new validation approach (which is explained in paragraph 3.3.1.2), it is possible to find the value load damp parameter, instead of a lower limit. For this analysis it is not necessary to have experimental data with "only base erosion", "simultaneous erosion" and "only filter erosion". The experimental data with only base erosion is sufficient. Although, in the new approach it is necessary to define the load on the filter and the base layer.

The load of the filter layer is determined with the Jonsson/Swart approach. This approach gives the bed shear stress on the bed under wave loading. Using this approach, it is necessary to define a roughness coefficient for the bed. It is assumed that the roughness coefficient is twice the nominal diameter of the filter material.

For the determination of the load on the base material, it is assumed that the critical shear stress is exceeded when base transport is observed. During the tests the wave height was increased step by step. For the wave condition for which the first base material transport was observed, it was assumed that the loading on the base was critical. From the modified Shields curve under waves (Sleath, 1978), the critical shields number is found. Using this Shields number, the shear stress is calculated. In this research, it was assumed that the critical Shields parameter was 0.073 for the critical hydraulic condition where base material erosion was observed.

As explained in chapter 3, the load damping lengths are calculated with the following equation:

$$L_d' = \frac{D_f'}{\ln\left(\frac{\tau_f (1 - \gamma V_{c,f})}{\tau_b (1 - \gamma V_{c,b})}\right)}$$

Where was assumed that $L_d' = L_d$. Under uniform flow, the load damping length L_d was related to the load damp coefficient α_d as follows:

$$L_d = \alpha_{d,H} d_{f15}$$

It is also investigated how the expression for the load damping length by van de Sande performs. Van de Sande suggested to use d_{f50} instead of d_{f15} to calculate the load damping length.

$$L_d = \alpha_{d,S} d_{f50}$$

The results of this analysis are shown in Table 6-1. Undoubtedly, the experimental data and the used methods in the analysis contain errors or uncertainties. The effect of these errors and uncertainties are discussed in the following paragraph.

Table 6-1 overview of the calculated values for the load damping length and the load damp coefficients per test

Test	D_f [mm]	$\frac{D_f}{d_{f15}}$ [-]	$\frac{d_{f50}}{d_{b50}}$ [-]	T [s]	L_d'	$\alpha_{d,H}$	$\alpha_{d,S}$
1	17	3.2	58.4	3.0	0.006	1.162	0.945
2	17	3.2	58.4	2.0	0.005	1.015	0.826
2	17	3.2	58.4	2.5	0.006	1.201	0.977
2	17	3.2	58.4	3.0	0.006	1.162	0.945
3	28	2.6	121.2	2.0	0.013	1.184	0.940
3	28	2.6	121.2	2.5	0.013	1.215	0.964
3	28	2.6	121.2	3.0	0.012	1.109	0.880
4	59	5.4	121.2	2.0	0.021	1.891	1.501
4	59	5.4	121.2	2.5	0.021	1.927	1.530
4	59	5.4	121.2	3.0	0.021	1.974	1.567
5	96	8.8	121.2	2.0	0.029	2.642	2.097
5	96	8.8	121.2	2.5	0.029	2.686	2.132
5	96	8.8	121.2	3.0	0.029	2.636	2.092
6	93	4.4	221.2	2.0	0.033	1.585	1.383
6	93	4.4	221.2	2.5	0.034	1.617	1.411
6	93	4.4	221.2	3.0	0.035	1.657	1.446
7	147	7.0	221.2	2.0	0.053	2.505	2.186
7	147	7.0	221.2	2.5	0.050	2.359	2.058
7	147	7.0	221.2	3.0	0.051	2.413	2.106

6.2.2 Sensitivity analysis

There are two types of inaccuracies in the analysis: measurement errors and uncertainties in the analysis of the data. For the analysis of the data, it is important to know what the influence of these uncertainties are on the results. Therefore, a sensitivity analysis is carried out. An overview of the sources of errors and uncertainties is given in Table 6-2. Background information about the uncertainty of each parameter is given in appendix D. It should be noted that a substantiated attempt is made to estimate these uncertainties as accurate as possible, but a source of subjectivity will always remain in the determination of the error.

Table 6-2 Uncertainty of the parameters

Parameter	Standard deviation
water depth	$0.02 \cdot d$
wave period	$0.001 \cdot T$
wave height	$0.02 \cdot H$
density water	$0.001 \cdot \rho_w$
Wn15 filter	$0.01 \cdot W_{n15}$
Wn50 filter	$0.01 \cdot W_{n50}$
density filter material	$0.01 \cdot \rho_f$
density base material	$0.001 \cdot \rho_h$
thickness filter	$0.5 \cdot d_{f50}$
db15	$0.05 \cdot d_{b15}$
db50	$0.05 \cdot d_{b50}$
bottom roughness	$0.25 \cdot k_r$
gravitational acceleration	0
shape factor F_s	$0.05 \cdot F_s$

loading coefficient	$0.05 \cdot \Upsilon$
Shields stress critical base	$0.20 \cdot \Psi_b$
Friction factor under waves c_f (Jonsson-Swart)	$0.5 \cdot c_f$

In the analysis the parameters are used to calculate other values (e.g. the shear stress on the filter, the load damping length L_d , etc.) Thus the parameters following from these calculations do also have an error. The obtained load damping length from the experiments will be compared with the hypotheses. Therefore it is necessary to have an insight in the error of the load damping length. Table 6-3 shows the calculated standard deviation for the load damping length. It is shown that the standard deviation is in the range of 0.16-0.34 times the value of the obtained load damping length.

Table 6-3 standard deviation of L_d'

Test	D_f [mm]	$\frac{D_f}{d_{f15}}$ [-]	$\frac{d_{f50}}{d_{b50}}$ [-]	T [s]	L_d'	Standard deviation L_d'
1	17	3.2	58.4	3.0	0.006	0.0017
2	17	3.2	58.4	2.0	0.005	0.0014
2	17	3.2	58.4	2.5	0.006	0.0018
2	17	3.2	58.4	3.0	0.006	0.0017
3	28	2.6	121.2	2.0	0.013	0.0044
3	28	2.6	121.2	2.5	0.013	0.0045
3	28	2.6	121.2	3.0	0.012	0.0040
4	59	5.4	121.2	2.0	0.021	0.0044
4	59	5.4	121.2	2.5	0.021	0.0045
4	59	5.4	121.2	3.0	0.021	0.0047
5	96	8.8	121.2	2.0	0.029	0.0048
5	96	8.8	121.2	2.5	0.029	0.0050
5	96	8.8	121.2	3.0	0.029	0.0048
6	93	4.4	221.2	2.0	0.033	0.0074
6	93	4.4	221.2	2.5	0.034	0.0077
6	93	4.4	221.2	3.0	0.035	0.0080
7	147	7.0	221.2	2.0	0.053	0.0105
7	147	7.0	221.2	2.5	0.050	0.0094
7	147	7.0	221.2	3.0	0.051	0.0098
Halter (1999)						
	0.12	3.3129	377.1118	1.03	0.0379	0.0091
	0.12	3.3129	377.1118	1.33	0.0374	0.0089
	0.12	3.3129	377.1118	1.9	0.0385	0.0093
	0.12	3.3129	377.1118	2.41	0.0405	0.0100
	0.12	6.2429	200.1207	1.03	0.0309	0.0050
	0.12	6.2429	200.1207	1.33	0.0364	0.0066
	0.12	6.2429	200.1207	1.9	0.0357	0.0064
	0.12	6.2429	200.1207	2.41	0.0382	0.0071
	0.06	3.1214	200.1207	1.03	0.0176	0.0043
	0.06	3.1214	200.1207	1.33	0.0181	0.0044
	0.06	3.1214	200.1207	1.9	0.0195	0.0049
	0.06	3.1214	200.1207	2.41	0.0207	0.0053

Additionally to the calculated errors presented in Table 6-3, it is also investigated which parameters have a large influence on the magnitude of the error of L_d' . By adjusting every parameter individually, insight was obtained in the influence in the calculated value for the load damping length. This way, uncertainty of an individual parameter could be expressed in the influence on the obtained value for the load damping length. An example of one of these calculations is shown in Figure 6-2. This is an example based on test 4. An overview of this analysis on all test can be found in the appendix. It was found that the uncertainty in the layer thickness and the uncertainty of in the friction factor (found with Jonsson-Swart's method) have most influence on the calculated error of L_d' .

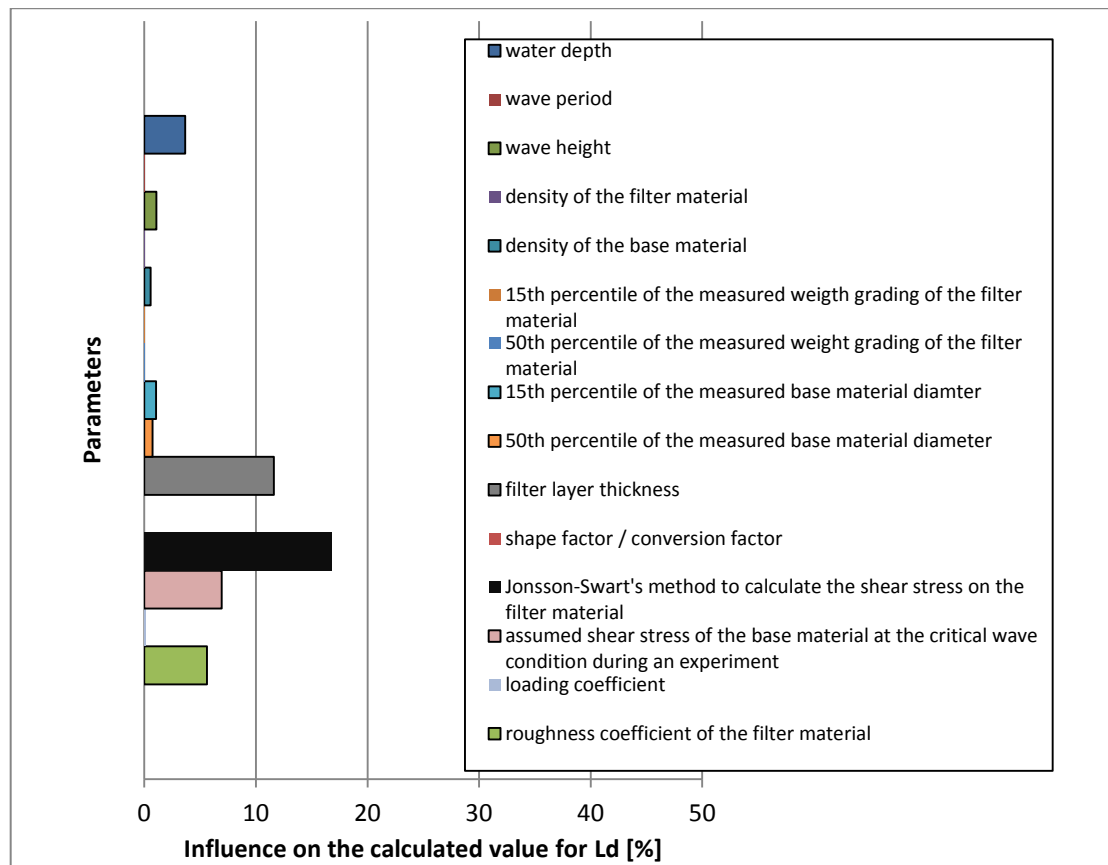


Figure 6-2 Influence of the individual uncertainties on the obtained value for the load damping length (based on test 4)

In the analysis shown above only gives a first insight in the influence of the individual uncertainties. No insight is gained how several individual uncertainties can magnify or eliminate each other when they are combined. For a more detailed insight, it is advised to carry out a FORM analysis. This is a more thorough approach which gives more insight in the individual influenced. For this research, it was considered that the rough indication presented above was sufficient.

6.2.3 Validity of the original Hoffmans formula under wave loading

The original Hoffmans formula, as presented in Hoffmans (2012) is formulated as follows:

$$\frac{D_f}{d_{f15}} = \alpha_{d,H} \ln \left(\frac{\Delta_f d_{f50} \Psi_{cf} (1 - \gamma V_{c,f})}{\Delta_b d_{b50} \Psi_{cb} (1 - \gamma V_{c,b})} \right)$$

As shown in Table 6-1, the range in $\alpha_{d,H}$ is quite wide. The values range from 1.0 to 2.7. Theoretically, the value of the load damp coefficient is a constant. Therefore it is concluded that the latter expression of the Hoffmans formula is not valid and should not be used under wave loading.

This conclusion is not unexpected, since this definition of the Hoffmans formula was derived using equation 46 (which is an assumption for uniform flow).

6.2.4 Validity of the van de Sande formula under wave loading

The Van de Sande Formula is formulated as follows:

$$\frac{D_f}{d_{f50}} = \alpha_{d,S} \ln \left(\frac{\Delta_f d_{f50} \Psi_{cf} (1 - \gamma V_{c,f})}{\Delta_b d_{b50} \Psi_{cb} (1 - \gamma V_{c,b})} \right)$$

Van de Sande showed that use of this expression gives improved results compared to the expression proposed by Hoffmans. This improvement was seen for very wide graded filters in particular. In this research, the filter grading was not very wide, and values for $\alpha_{d,S}$ show no significant improvement compared to $\alpha_{d,H}$. The value for $\alpha_{d,S}$ ranges between 0.8 and 2.2. Therefore it is concluded that the Van de Sande formula is also not a valid under wave loading. This is not unexpected, since this formula was suggested for uniform flows.

6.2.5 Testing of the hypotheses of Hoffmans and Verheij (2013)

As was already suggested in chapter 3, it is more convenient to formulate the Hoffmans formula slightly different, where the layer thickness is a function of the load damp parameter. This is a more general form for the Hoffmans formula, since it is hypothesized that the load damp parameter is dependent on the type of loading. For wave loading, two hypotheses were formed.

$$D_f = L_d \cdot \ln \left(\frac{\Delta_f d_{f50} \Psi_{cf} (1 - \gamma V_{c,f})}{\Delta_b d_{b50} \Psi_{cb} (1 - \gamma V_{c,b})} \right)$$

The first hypothesis for the load damping length under wave loading

Hoffmans (2012) formed a hypothesis based on the research of Bezuijen and Köhler (1996). It is formulated as follows:

$$L_{d,Hypothesis I} = \sqrt{\frac{c_v T_p}{\pi}}$$

Note that this hypothesis suggests that the load damping length under wave loading is not dependent of the filter material diameter. Although, the damping length does depend on the consolidation coefficient of the filter material. It is assumed that this consolidation coefficient has a constant value of 0.001 for filter material.

The hypothetical load damping length is compared with the load damping length which were based on the experimental results. The results are presented in Figure 6-3. It is shown that the range of the calculated values is much higher than the hypothetical values. Hypothesis I does not give reliable results. Thereby, the load damping parameter does not seem to depend on only the wave period.

For the purpose of the readability of the graph, the error bars are left out of the graph. The same graph including the error bars can be found in appendix E.

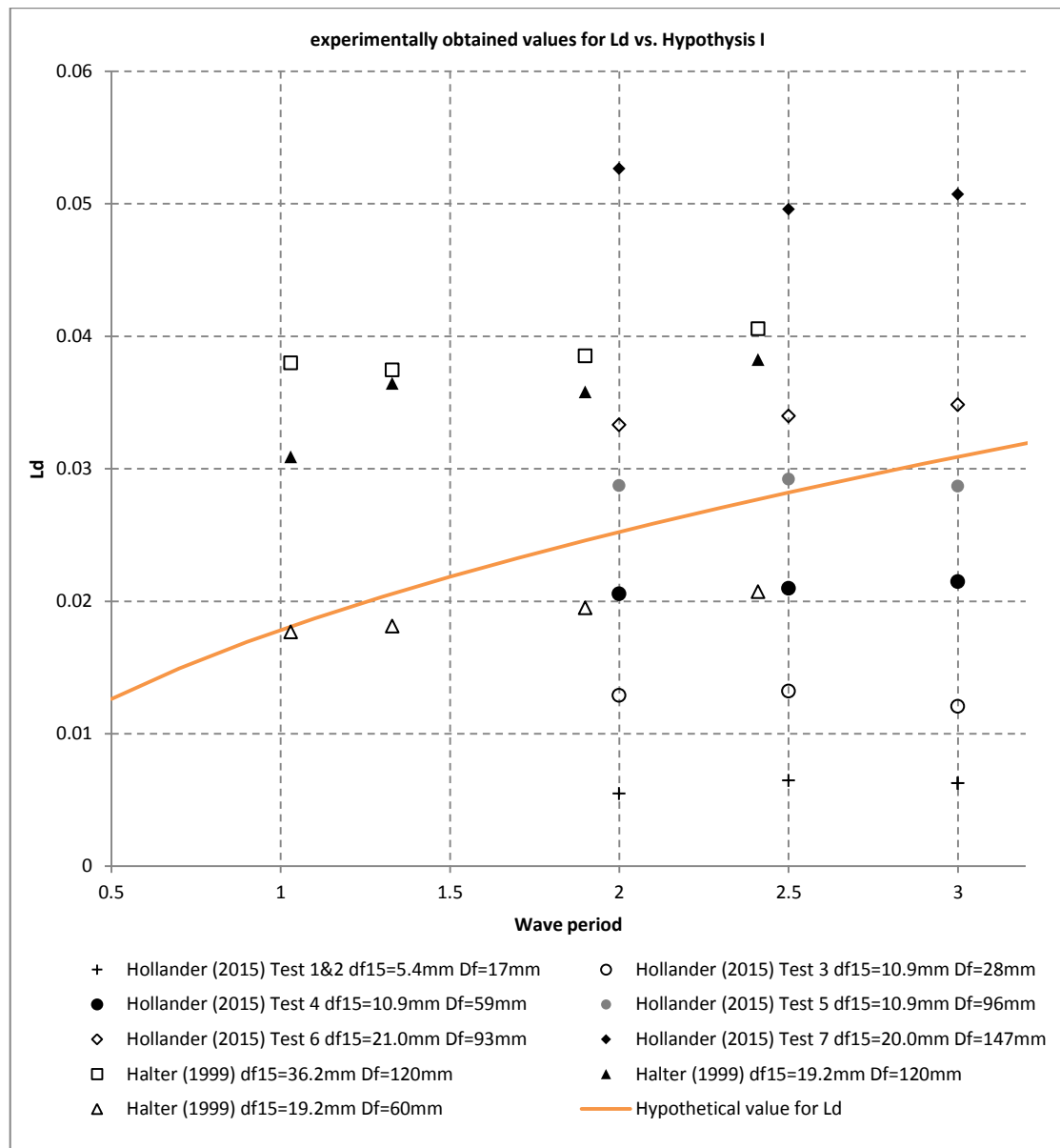


Figure 6-3 Hypothetical values (obtained by hypothesis I) for Ld and the Ld values obtained in the experiments

The second Hypothesis for the load damping length under wave loading

Also a second hypothesis was formulated by Hoffmans & Verheij (2013):

$$L_{d,Hypothesis II} = d_{f15} \sqrt{\frac{2T_p}{T_0}}$$

The results are presented in Figure 6-4. The hypothesized values now give a better approximation for the load damping length. Looking at the data of test 1 & 2, the hypothesized values are conservative, while the hypothesized values are too low for test 7.

Figure 6-4 contains a large amount of data points. In Appendix D the figure is separated for different filter size diameters. This might give a clearer overview.

Based on the hypotheses, the load damping length is expected to be dependent of the wave period. Larger wave periods would lead to higher load damp parameters. This tendency is not seen in the load damp parameters which are found in the experiments. It is supposed that the inaccuracies in the

experimentally found values for L_d are too large to draw conclusions about the wave dependency. For further research it is suggested to carry out experiments with a wide range of wave periods, so that the inaccuracies are less dominant over the influence of the wave length, or to find a method to reduce the uncertainties in the experiments.

For the purpose of the readability of the graph, the error bars are left out of the graph. The same graph including the error bars can be found in appendix E.

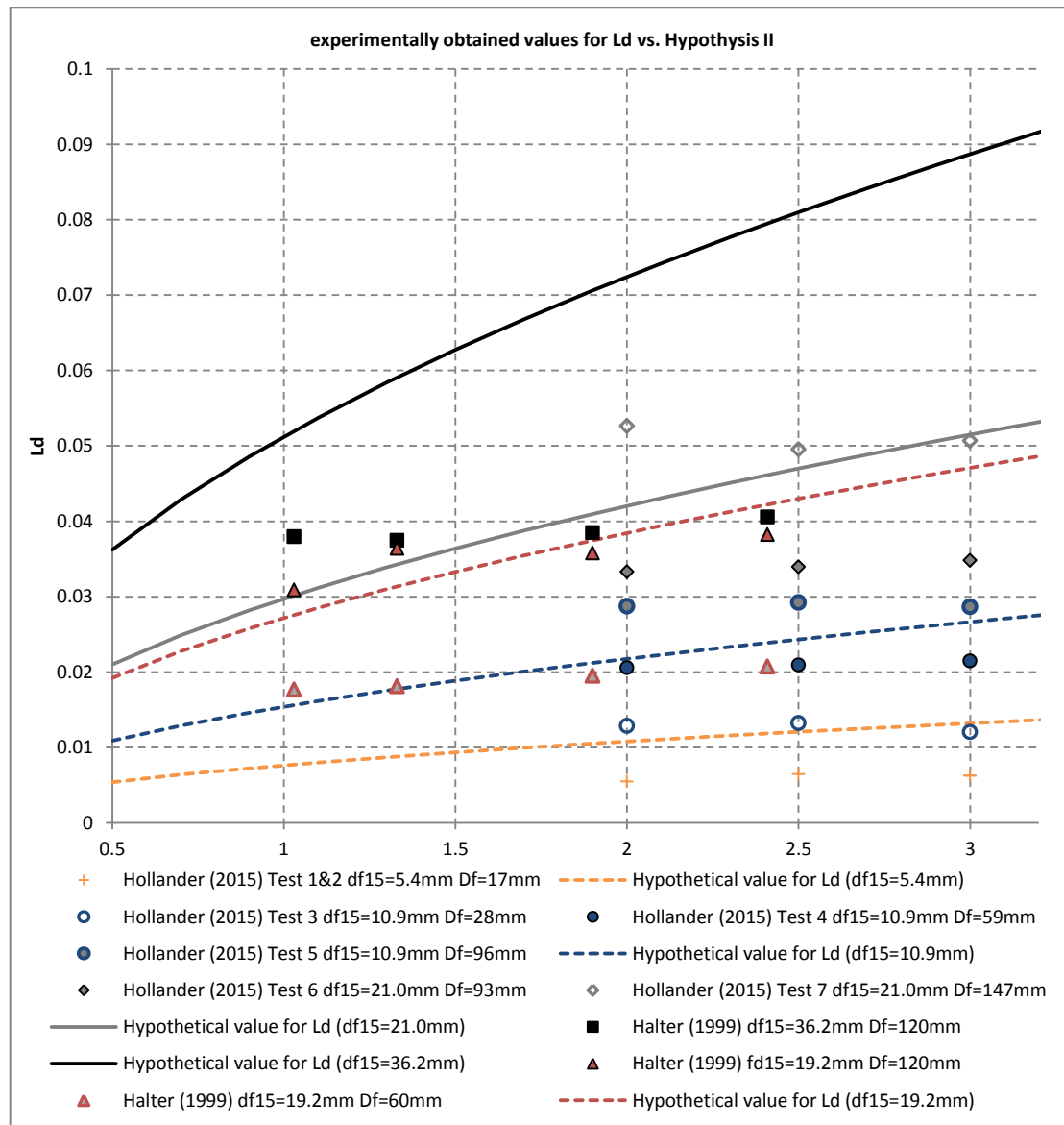


Figure 6-4 Hypothetical values (obtained by hypothesis II) for L_d and the L_d values obtained in the experiments

On first sight, hypothesis II for the load damping length seems to perform better than hypothesis II. However, the obtained values with hypothesis II do not seem to be correct, large differences are seen between the experimentally obtained values and the hypothesized values. It is unlikely that the inaccuracies are the only reason behind the differences between the hypothetical values for the load damp parameter and the experimentally found values. It seems that the layer thickness itself also influences the value for the load damping length. This finding was not expected. This finding implies that the damping efficiency of the filter decreases when the filter thickness increases. Thus a thicker filter is still able to damp out a larger loading, but the efficiency of the damping process decreases. Since it was expected that the damping of the filter material was related to the material properties

and the wave loading, it is remarkable that the layer thickness also seems to have influence on the damping efficiency.

Note that the difference in Halter's data (where $d=36.2\text{mm}$ and $D_f=120\text{mm}$) and the hypothetical values corresponding to this data is very large.

Under the assumption that $L_d'=L_d$, it can be concluded that hypothesis II is falsified. The hypothesis does not describe the values for L_d accurately, large deviations are seen. Thereby, the L_d seems to be influenced by the layer thickness itself. This finding is counterintuitive, and implied that the concept of the damping of turbulence energy is not the only forcing in an horizontal granular open filter under wave loading.

6.3 Chapter review

The research question was whether the Hoffmans formula can be applied under wave loading. Experiments were carried out where the critical hydraulic conditions for wave loading were found for different layer thicknesses and filter materials. For the analysis of the data a method was used which assumed that the Hoffmans formula was valid, and the values for the load damp coefficient α_d and load damping length L_d were traced back.

The Hoffmans formula could be considered valid if the found values for α_d would be constant or L_d would be aligned with the hypotheses.

The analysis of the results showed that α_d was not constant. Not for the Hoffmans formula, nor for the Van de Sande formula. The version of the Hoffmans with α_d is derived for uniform flow. It is concluded that the formula's for uniform flow cannot be applied for wave loading.

Two hypotheses were stated for the value of the load damping length L_d . However, the calculated values were not aligned with the hypotheses. The value of L_d may be a function of the filter material and the wave period, as suggested in one of the hypotheses, but it appears that this value also depends on the filter thickness.

It is concluded that, under the assumption that $L_d'=L_d$, Hoffmans formula cannot be validated for wave loading. None of the hypotheses for the load damp parameters seem to give reliable results or describe the trends of the value of the load damping length correctly.

Chapter 7

Discussion

It is concluded that for a horizontal formula under wave loading, using the assumption that $L_d' = L_d$, the Hoffmans formula could not be verified. This chapter discusses this finding, where it is attempted to find an explanation why the Hoffmans formula was not validated. Feedback is given on the assumption made in this research, the hypotheses and on the philosophy behind Hoffmans formula.

7.1 Assumption $L_d' = L_d$

Compared to previous validation studies of Hoffmans formula (Joustra (2013), Van de Sande (2012)), no filter material instability was generated in this research. Initially, it was attempted to apply the same methodology as Joustra and van de Sande. However, the flume was not large enough to generate instability of the chosen filter material. However, it was possible to generate base material instability. Using the assumption that the damping length can also be found under conditions for which the filter material is stable (see paragraph 3.3.1.2), the hypotheses were tested. Although this assumption is considered to be very plausible, it is not proven yet.

The essence of the assumption entails that the use of Hoffmans formula is not limited to the critical shields values for the filter and base material, but that also Shields values under or above the critical value can be used. The damping efficiency of the filter material, characterized by L_d , is considered to be independent of the magnitude of the load.

This assumption is considered to be very plausible, but not proven. The conclusions in this research are made under the condition that this assumption is valid. Therefore, it will be necessary to carry out further research to this assumption.

The verification of this assumption will also have value for design purposes. For example, it can be estimated how much erosion will take place under an unstable open filter, since it is possible to relate Shields values to entrainment rates (Paintal, 1971). It is proposed to validate this assumption for uniform flow, for which the Hoffmans formula is already successfully validated (Van de Sande (2012)).

7.2 Source term in Hoffmans formula

In the derivation of his formula, Hoffmans used a definition to describe the damping of turbulence energy (see below). This definition incorporates the “local turbulence energy in the filter layer (k_b)” and a “source term ($k_{f,s}$)”.

$$k_f(z) = k_{f,s} + (k_b - k_{f,s}) \exp\left(\frac{z}{L_d}\right)$$

Hoffmans (2015) states that the source term is related to the hydraulic gradient. The measurements of Klar (2005) indicate that for uniform flow the hydraulic gradients (and thus the pore velocities) are negligible. For this reason, Hoffmans also states that the source term under uniform flow is negligible. Using this assumption, the original Hoffmans formula is found (as presented in chapter 3, equation 49).

For the experiments in this research the same assumption was made. However, values for the load damping length L_d were obtained which seemed to be dependent of the filter thickness. This might have been the result of the (potentially incorrect) assumption that the source term was negligible under wave loading. Since the hydraulic gradients under waves are larger than under uniform flow, this source term $k_{f,s}$ may have had a contribution to the instability of base material under wave loading.

This implies that two mechanisms influence the stability of the filter interface:

- The penetration of turbulence energy from the top of the filter
- The hydraulic gradient, which generates pore velocities inside the filter and influences the source term $k_{f,s}$

Suppose that this source term was not negligible under wave loading. This would have influence on the obtained values of the load damping length. It is not known what the exact value of the source term $k_{f,s}$ might have been in the tests under wave loading. However, an insight can be given about the effect on the obtained values of the load damping length L_d .

Hoffmans (2015) shows how the load damping length is influenced when the source term is not negligible:

$$k_{f,without\ source\ term}(z) = k_b \cdot \exp\left(\frac{z}{L_d}\right) \quad (62)$$

$$k_{f,with\ source\ term}(z) = k_{f,s} + (k_b - k_{f,s}) \cdot \exp\left(\frac{z}{L_d}\right) \quad (63)$$

Then:

$$\frac{dk_{f,without\ source\ term}(z)}{dz} = \frac{k_b}{L_d} \cdot \exp\left(\frac{z}{L_d}\right) \quad (64)$$

$$\frac{dk_{f,with\ source\ term}(z)}{dz} = \frac{(k_b + k_{f,s})}{L_d} \cdot \exp\left(\frac{z}{L_d}\right) \quad (65)$$

For $z=0$ yields:

$$k_{f,without\ source\ term}(0) = k_b \quad (66)$$

$$k_{f,with\ source\ term}(0) = k_b \quad (67)$$

$$\frac{dk_{f,without\ source\ term}(0)}{dz} = \frac{k_b}{L_d} \quad (68)$$

$$\frac{dk_{f,with\ source\ term}(0)}{dz} = \frac{(k_b + k_{f,s})}{L_d^*} \quad (69)$$

To compare L_d against L_d^* , $k_{f,without\ source\ term}(0)$ must equal $k_{f,with\ source\ term}(0)$ and $\frac{dk_{f,without\ source\ term}(0)}{dz}$ must equal $\frac{dk_{f,with\ source\ term}(0)}{dz}$.

Thus:

$$\frac{k_b}{L_d} = \frac{(k_b + k_{f,s})}{L_d^*} \quad (70)$$

This results in the following comparison between L_d and L_d^* :

$$L_d^* = L_d \left(1 - \frac{k_{f,s}}{k_b} \right) \quad (71)$$

For uniform flow $k_{f,s} \ll k_b$, so that $L_d^* \approx L_d$. Suppose that under wave loading the source term $k_{f,s}$ is not negligible, then $L_d^* < L_d$. This implies that the correct values for the load damping length -which would be found if the source term would be incorporated in the analysis- is smaller than the values obtained in this research.

When the source term $k_{f,s}$ (which is somehow related to a hydraulic gradient) exceeds the critical conditions for the base material erosion, a thicker filter will not be very effective.

In chapter 6 was concluded that the obtained load damping lengths were influenced by the layer thickness. This might be an artifact resulting from the neglected source term! Further research is necessary to validate this statement.

It is recommended to evaluate the latter insight for uniform flow. The source term $k_{f,s}$ is in some way related to the hydraulic gradient (or the filter velocity). The obtained results for the values of the load damp coefficient may be redefined (more accurate results or new insights may be found).

7.3 Feedback on the validity of Hoffmans formula under wave loading and the hypotheses (feedback on Bezuijen and Kohler)

The concept that only the penetration of turbulence energy influences the stability of the filter interface seems not applicable for wave loading. Therefore, the obtained values for the load damping length L_d are not correct. When the hydraulic gradient is included in Hoffmans formula (which is related to the source term $k_{f,s}$), other values for the load damping length L_d would be found. Equation 71 shows that a smaller value for the load damping length would be found when the source term is incorporated in Hoffmans formula. Therefore, it is uncertain that the hypotheses were tested correctly, since other (smaller) values for L_d had to be used.

Thus, if the source term $k_{f,s}$ would be incorporated in the analysis, other values for the load damping length L_d would be found. Accordingly, it might be questioned how this influences the validity of the hypotheses. Possible, when the source term $k_{f,s}$ would be incorporated in the analysis, it is found that

the hypotheses give a better approximation of the value for the load damping length than is now presented in this research. Some speculations can be made about this scenario. When the source term $k_{f,s}$ would be incorporated in the analysis, the obtained values for the load damping length can only become lower, since $L_d^* = L_d \left(1 - \frac{k_{f,s}}{k_b}\right)$. However, the hypothesized values for the load damping length under wave loading (which are based on Bezuijen and Köhler), did not give an underestimation for the load damping length. Thus it is not plausible that the hypotheses give more accurate results when the source term $k_{f,s}$ is incorporated. In other words, when incorporating the source term $k_{f,s}$, the values found for L_d will be lower than the values found in this report. The hypothetical values for the load damp coefficient give an overestimation for most of the tests.

Although, it is advised to evaluate the hypotheses again against the correct values for the L_d . As explained in paragraph 7.2, it is possible that the influence of the filter thickness on the value of the load damping length L_d is an artifact resulting from the neglected source term $k_{f,s}$. It would be valuable if this statement could be proven.

Nonetheless, some doubts are placed to the hypotheses. For hypothesis I, the assumed value for the consolidation coefficient of filter material ($c_v = 0.001$) can be more accurate.

$$L_{d,Hypothesis\ I} = \sqrt{\frac{c_v T_p}{\pi}}$$

Some doubts are also present about the second hypothesis for the load damping length L_d . The parameter T_0 has no physical meaning and was introduced for the missing dimensions. A value of $T_0 = 1\text{ s}$ was assumed. A physical explanation for this parameter would be necessary to completely understand the hypothesis.

$$L_{d,Hypothesis\ II} = d_{f15} \sqrt{\frac{2T_p}{T_0}}$$

7.4 Comparison of the data with Jansens (2000)

The pore velocity is related to the filter velocity. The velocity inside a filter is forced by the hydraulic gradient. Jansens (2000) did measure the pore velocity under wave loading. Since Hoffmans states that the source term $k_{f,s}$ is related to the hydraulic gradient, the pore velocities in this research are estimated according to the relation found by Jansens.

Jansens found that the pore velocity was constant over the thickness of the filter. Jansens found in his experiments that the pore velocities inside the filter had a range between 0.03 m/s and 0.06 m/s for the critical hydraulic conditions. The base material which was used to determine the critical hydraulic conditions (by Halter (1999)) had a nominal diameter of 100 μm , thus was similar to the base material used in this research. Jansens found the following relation between the average pore velocities and the hydraulic conditions:

$$\frac{1}{\rho_w g} \frac{\delta p}{\delta x} \cdot T \cdot 0.4 \equiv \hat{u}_p \quad (72)$$

So the pore velocities are related to the wave period and the hydraulic gradients. This relation can be used to estimate the pore velocities in this research. The gradients on the filter interface are calculated using the linear wave theory (which was also done by Jansens in his research). The results are shown in Table 7-1.

The pore velocities are in the same range as in Jansens research. The estimated pore velocities in this research range between 0.03 and 0.07 m/s. This finding indicates that the experimental method to determine instability in this research (visual observations) correspond quite well with the results from Halter's (1999) research (Jansens copied Halter's experimental set-up). Halter did not use a visual method to classify base material instability, but measured the scour holes under the filter to determine the critical wave conditions.

Table 7-1 estimated pore velocities for the critical hydraulic conditions. The pore velocity is estimated with equation 73

Test	D_f [mm]	$\frac{D_f}{d_{f15}}$ [-]	$\frac{d_{f50}}{d_{b50}}$ [-]	T [s]	d_{f50} [mm]	$i_{max,calculated}$ [-]	$\hat{u}_{p,estimated}$ [m/s]
1	17	3.2	58.4	3.0	6.63	0.048	0.058
2	17	3.2	58.4	2.0	6.63	0.079	0.063
2	17	3.2	58.4	2.5	6.63	0.050	0.050
2	17	3.2	58.4	3.0	6.63	0.048	0.058
3	28	2.6	121.2	2.0	13.70	0.032	0.026
3	28	2.6	121.2	2.5	13.70	0.028	0.028
3	28	2.6	121.2	3.0	13.70	0.029	0.035
4	59	5.4	121.2	2.0	13.70	0.050	0.040
4	59	5.4	121.2	2.5	13.70	0.044	0.044
4	59	5.4	121.2	3.0	13.70	0.038	0.045
5	96	8.8	121.2	2.0	13.70	0.067	0.053
5	96	8.8	121.2	2.5	13.70	0.058	0.058
5	96	8.8	121.2	3.0	13.70	0.056	0.067
6	93	4.4	221.2	2.0	24.08	0.036	0.029
6	93	4.4	221.2	2.5	24.08	0.032	0.032
6	93	4.4	221.2	3.0	24.08	0.028	0.034
7	147	7.0	221.2	2.0	24.08	0.034	0.027
7	147	7.0	221.2	2.5	24.08	0.036	0.036
7	147	7.0	221.2	3.0	24.08	0.032	0.038

Thus, the estimated pore velocities are in the range for which erosion of the base material occurs. Assumed that the source term $k_{f,s}$ is related to the pore velocities, it is plausible that this term was not negligible in the model tests.

As seen in the results of the tests, the critical hydraulic loading was larger for a thicker filter. Thus, a thicker filter did offer more protection to the bed. It is speculated that this can be explained by the ratio $\frac{k_{f,s}}{k_b}$, which was not constant over the test. For a thinner filter, the influence of the penetration of turbulence energy bed is larger than for a thicker filter. Thus, when comparing a thin and a thick filter under the critical hydraulic wave conditions for which the base material is unstable, it is plausible that the source term $k_{f,s}$ is smaller for the thin filter (since the influence of the penetrated turbulence energy is larger). For a thick filter the influence of the penetration of the turbulence energy becomes negligible, and the instability is fully assigned to the influence of the source term $k_{f,s}$. Test 3, 4 and 5 show increased estimated pore velocities for thicker filters, and support the latter speculation. Enlarging the filter thickness will not be effective to protect a bed more efficiently in the scenario that the source term $k_{f,s}$ is dominant over the influence of the penetrated turbulence energy.

7.5 Comparison of the data with Wolters & Van Gent (2012)

In comparison to Hoffmans, Wolters & Van Gent consider that the stability of an open filter can be described by only the hydraulic gradient. Wolters & Van Gent have empirically found a relation between the gradients and transport under a filter for irregular wave loading.

For practical purposes it is interesting to compare the experimental results with Wolters & Van Gent's approach.

Wolters & van Gent claim that the base material transport can be described as a function of the hydraulic gradient $\frac{i_{2\%}}{i_{cr}}$. Furthermore, the hydraulic gradient can be described using the modified Keulegan-Carpenter number KC_f . These relations were found under irregular waves. For wave loading, dimensionless transport rates were found in the range 0.0019-0.007 (which related in Wolters & Van Gent's test to 0.033-0.161 g/m/s).

$$KC_f = \frac{u_{2\%} T_m}{n_f D_f} \quad (73)$$

$$i_{2\%} = 0.06 \cdot KC_f^{0.28} \quad (74)$$

$$T^* = 1.4 \cdot 10^{-6} \left(\frac{i_{2\%}}{i_{cr}} \right)^{5.8} \quad (75)$$

Since this research focused on the start of instability, it is expected that the transport rate is very small for the critical wave condition. Using Wolters & Van Gent's relations, the transport rates are estimated and presented in Table 7-2. Since regular waves were used in this research, the maximum values for the near bed velocities (u_{max} , which is calculated with the linear wave theorem) were used instead of the 2% upper limit ($u_{2\%}$) used by Wolters & Van Gent. A porosity of 0.4 [-] is assumed for the used filter materials. The i_{cr} is calculated with de Graauw (1983), (see chapter 2, equation 28).

Table 7-2 Transport rates using Wolters and Van Gent's (2012) formula (with the use of the relation between KC_f and $i_{2\%}$).

Test	D_f [mm]	$\frac{D_f}{d_{f15}}$ [-]	$\frac{d_{f50}}{d_{b50}}$ [-]	T [s]	KC_f [-]	$i_{2\%}$	i_{cr}	T^*
1	17	3.2	58.4	3.0	105.46	0.221	0.050	0.00755
2	17	3.2	58.4	2.0	79.42	0.204	0.050	0.00477
2	17	3.2	58.4	2.5	77.59	0.203	0.050	0.00459
2	17	3.2	58.4	3.0	105.46	0.221	0.050	0.00755
3	28	2.6	121.2	2.0	20.09	0.139	0.040	0.00167
3	28	2.6	121.2	2.5	26.17	0.150	0.040	0.00257
3	28	2.6	121.2	3.0	38.42	0.167	0.040	0.00479
4	59	5.4	121.2	2.0	15.26	0.129	0.031	0.00515
4	59	5.4	121.2	2.5	19.87	0.139	0.031	0.00791
4	59	5.4	121.2	3.0	24.31	0.147	0.031	0.01097
5	96	8.8	121.2	2.0	12.89	0.123	0.028	0.00666
5	96	8.8	121.2	2.5	16.79	0.132	0.028	0.01023
5	96	8.8	121.2	3.0	22.41	0.143	0.028	0.01634
6	93	4.4	221.2	2.0	7.26	0.105	0.034	0.00081
6	93	4.4	221.2	2.5	9.46	0.113	0.034	0.00124
6	93	4.4	221.2	3.0	11.57	0.119	0.034	0.00173
7	147	7.0	221.2	2.0	4.59	0.092	0.033	0.00049
7	147	7.0	221.2	2.5	6.98	0.103	0.033	0.00097
7	147	7.0	221.2	3.0	8.54	0.109	0.033	0.00134

The obtained dimensionless transport rates fall in the same range as in Wolters & Van Gent's research. This is counterintuitive, the values were expected to be lower. Wolters & Van Gent clearly measured transports for the base material ($\Psi_{b,tests\ Wolters\ \&\ Van\ Gent} > \Psi_{b,critical}$), while the experiments in this research were focused on incipient motion of the base material ($\Psi_{b,tests\ Hollander} \approx \Psi_{b,critical}$).

Thus Wolters & Van Gent do not give plausible results for the experiments in this research. The reason for this may lie in the different loading conditions. In this research regular waves were used. Every time a wave travels over the filter, The filter is loaded by the same maximum gradient. Thus for every wave passing by, the base material is instable. Wolters & Van Gent used irregular waves in their research. Thus in Wolters and Van Gent's experiments, the maximum hydraulic gradient

($i_{2\%}$) may be the results of only a few waves in the whole spectrum. Therefore, it is possible, that most of the transports only occurred under a few waves.

Thereby, the proposed formula of KC_f is doubtful. The gradients which result from this formula are too large under regular waves. Suppose the filter layer does not have any influence on the wave properties, then the gradients on the interface can be estimated according to the linear wave theorem (see the results in Table 7-3). Obviously, It is not plausible that the filter layer does not influence the wave properties, the gradient is probably reduced inside the filter. However, the calculated gradients on the interface using Wolters & Van Gent's relation (with KC_f) give higher gradients than calculated with the linear wave theorem! This is counterintuitive. It is recommended to validate equation 73 for regular wave loading.

Based on the latter finding, It is supposed that the gradients calculated with the linear wave theorem give more reliable results when used to calculate the transports (using equation 75). The obtained values are shown in Table 7-3. The calculated dimensionless transport rates are much smaller than in Wolters & Van Gent's research. This is a plausible result since it is expected that the transport rates would be smaller for the experiments in this research, since in this research only incipient motion was generated ($\Psi_b \approx \Psi_{b,critical}$).

Table 7-3 Transport rates using Wolters and Van Gent's (2012) formula (where i_{max} is calculated using the linear wave theorem)

Test	D_f [mm]	T [s]	KC_f [-]	$i_{2\%}$	i_{max}	i_{cr}	$T_{i_{max}}^*$
1	17	3.0	105.46	0.221	0.048	0.050	1.115E-06
2	17	2.0	79.42	0.204	0.079	0.050	1.903E-05
2	17	2.5	77.59	0.203	0.050	0.050	1.415E-06
2	17	3.0	105.46	0.221	0.048	0.050	1.115E-06
3	28	2.0	20.09	0.139	0.032	0.040	3.642E-07
3	28	2.5	26.17	0.150	0.028	0.040	1.468E-07
3	28	3.0	38.42	0.167	0.029	0.040	1.830E-07
4	59	2.0	15.26	0.129	0.050	0.031	2.237E-05
4	59	2.5	19.87	0.139	0.044	0.031	9.595E-06
4	59	3.0	24.31	0.147	0.038	0.031	4.301E-06
5	96	2.0	12.89	0.123	0.067	0.028	1.921E-04
5	96	2.5	16.79	0.132	0.058	0.028	8.899E-05
5	96	3.0	22.41	0.143	0.056	0.028	6.901E-05
6	93	2.0	7.26	0.105	0.036	0.034	1.799E-06
6	93	2.5	9.46	0.113	0.032	0.034	8.281E-07
6	93	3.0	11.57	0.119	0.028	0.034	3.863E-07
7	147	2.0	4.59	0.092	0.034	0.033	1.612E-06
7	147	2.5	6.98	0.103	0.036	0.033	2.040E-06
7	147	3.0	8.54	0.109	0.032	0.033	1.017E-06

Chapter 8

Conclusions & recommendations

8.1 Conclusions

In the introduction of this report the research question is formulated along with three sub questions. First the sub questions will be answered, followed by the answer to the main research question.

To validate Hoffmans formula, experiments were carried out with a horizontal open filter structure. For the analysis of the results, Hoffmans formula was used to find the values for the load damp length of the filter. Hoffmans formula can be considered valid, if the experimentally obtained load damping lengths would be aligned with the load damp coefficient α_d in original Hoffmans formula or with the hypotheses for the damping length under wave loading.

The first sub question: *“What can be said about the value for the load damp coefficient under wave loading?”*

For uniform flow, Hoffmans used the following expression in the derivation of his formula:

$$L_d = \alpha_d d_{f15}$$

Under wave loading, it is suggested to use another expression for the load damping length. Thus in fact, the load damp coefficient α_d is only relevant for uniform flow. The parameter α_d is therefore not useful for wave loading.

This finding is supported by the analysis, which shows that no constant value of α_d is found under wave loading. The calculated values range from 1 to 2.7. The fact that the values for α_d are quite high does indicate that a stable filter under wave loading needs to be thicker than for uniform flow.

The second sub question: *“Is it possible to verify or falsify the hypotheses for the load damping length?”*

For the load damping length under wave loading two hypothesis were formed. The first was formed by Hoffmans (2012), and the second was formed by Hoffmans & Verheij (2013). Both hypotheses were based on Bezuijen and Köhler (1996).

$$L_{d,Hypothesis I} = \sqrt{\frac{c_v T_p}{\pi}}$$

The value for the load damping length was calculated from the experiments and compared with the hypothetical values. The hypothetical values for the load damp parameter did not correspond correctly with the values found in the experiments. The experimentally obtained values of the load damping length gave a strong indication that the value depends on the layer thickness. The relation of the load damping length is not described in the Hoffmans formula, nor in the formulated hypothesis. Thus, under the assumption that $L_d = L'_d$, it is concluded that the hypothesis that the load damping length is a function of only $\sqrt{T_p}$ is incorrect.

The second hypothesis was stated as follows:

$$L_{d,Hypothesis II} = d_{f15} \sqrt{\frac{2T_p}{T_0}}$$

This hypothesis did also not predict the obtained values for the load damp parameter accurately and does also not incorporate the effect of the filter layer thickness. Therefore, under the assumption that $L_d = L'_d$, it is concluded that the hypothesis is only a function of d_{f15} and $\sqrt{T_p}$ is also incorrect.

The third sub question: *“What is the difference between an oscillating flow and an uniform flow regarding the stability of an open filter?”*

It is supposed that the stability of an open filter is influenced by the pore velocity, and the penetration of turbulence energy from the top of the filter. For wave loading, the flow on top of the filter is oscillating, therefore the turbulence intensity will be different than for uniform flow. The velocity of the fluid through the filter (pore velocity) is forced by the hydraulic gradient. For waves, the hydraulic gradient depends on the water depth, wave height and wave period. Compared to uniform flow, the hydraulic gradients under waves can be quite high.

The main question of this research was formulated as:

“Is the design formula of Hoffmans (2012) valid under wave loading for horizontal filter structures?”

The results showed that no constant value for α_d was found under wave loading. Thus it can be concluded (under the assumption that $L'_d = L_d$) that the original formulation of Hoffmans formula, as validated for uniform flow, is not applicable under wave loading.

The two hypothesis for the load damping length under waves in combination with Hoffmans were also tested. Based on the experiments carried out in this research, it was not possible to validate the relation between the wave period and the damping length, since the uncertainties were too large. However, it was seen that the obtained values of the load damping length L'_d were influenced by the filter thickness. This finding is counterintuitive and indicate that the hydraulic gradient should be incorporated in Hoffmans formula (which might be possible via the source term $k_{f,s}$). It is concluded

that (under the assumption that $L_d' = L_d$) the hypotheses are not applicable in combination with the Hoffmans formula when the source term $k_{f,s}$ is neglected.

Thus, the philosophy of Hoffmans formula is not rejected. A valid form of the formula may be found when the source term $k_{f,s}$ is incorporated. Until more insight is acquired about the influence of the source term $k_{f,s}$, speculations are prevailing.

This leads to recommendations for further research.

8.2 Recommendations

First of all, it is recommended to verify the assumption that $L_d = L_d'$, which was important in this research. The essence of the assumption entails that the use of Hoffmans formula is not limited to the critical shields values for the filter and base material, but that also Shields values under or above the critical value can be used. The damping efficiency of the filter material, characterized by L_d , is considered to be independent of the magnitude of the load. This assumption is considered to be very plausible, but not proven. The conclusions in this research are made under the condition that this assumption is valid. Therefore, it will be necessary to carry out further research to this assumption. The verification of this assumption will also have value for design purposes. For example, it can be estimated how much erosion will take place under an unstable open filter, since it is possible to relate Shields values to entrainment rates. It is proposed to validate this assumption for uniform flow, because the Hoffmans formula is successfully validated (Van de Sande (2012)) for this type of loading.

Secondly, it is recommended to carry out more research on the source term $k_{f,s}$. It is plausible that two processes (both the damping of turbulence energy under wave loading as the hydraulic gradients) generate the instability of the filter interface. The turbulence energy which penetrates from the top of the filter is decreasing inside the filter, thus for very thick filters this loading will become negligible compared with the hydraulic gradients. Therefore, it is expected, above a certain filter thickness, instability will only be generated by the hydraulic gradient. It is recommended to carry out model research where the filter thickness is increased step by step. Thereby the gradients on the interface must be measured. It is hypothesized that for above a certain filter thickness the critical hydraulic gradient is constant, and under this thickness the gradient is lower than this constant value (since the penetration of turbulence energy will affect the instability). It is recommended to carry out this research under regular waves.

Hoffmans claims that the source term $k_{f,s}$ depends on the hydraulic gradient. However, it is not known how these two are exactly related. For a design purposes, it is important to know the value of the source term $k_{f,s}$ or the ratio $\frac{k_{f,s}}{k_b}$, otherwise the Hoffmans formula cannot be used for design purposes. It is recommended to carry out research to the relation between the source term and the hydraulic gradients.

It is also recommended to evaluate the influence of the gradient under uniform flow. Theoretically, the source term $k_{f,s}$ increases for a larger hydraulic gradient. This can also be evaluated for uniform flow. It is recommended to measure the hydraulic gradients on the interface, and carry out tests where the hydraulic gradient is varied. If it turns out that the hydraulic gradient also plays a role under uniform flow, the load damp coefficients under uniform flow can be evaluated again. This might lead to new insights.

The influence of the wave period is still unknown. It is assumed that for very long waves, the loading conditions will be similar to uniform flow. It is suggested to investigate the effect of the wave period on the stability of an open filter in more detail. It is suggested to use a wider range of wave periods than applied in this research.

In this research is suggested that the gradients calculated with the formula of Wolter & Van Gent (2012) do not give plausible results under regular wave loading. It is recommended to do more validation research to the formula of KC_f under regular wave loading.

Bibliography

Bezuijen, A., Klein Breteler, M., & Bakker, K. J. (1987). Design criteria for placed block revetments and granular filters. *Second International Conference on Coastal and Port Engineering in Developing Countries*. Beijing.

CUR. (1993). *161, Filters in de waterbouw*. Gouda.

CUR. (2010). *233, Interface stability of granular filter structures*. Gouda.

de Graauw, A. F., van der Meulen, T., & van der Does de Bye, M. R. (1984). Granular Filters: Design Criteria. *Journal of Waterway, Port, Coastal, and Ocean Engineering*, 80-94.

Dessens, M. (2004). *The influence of flow acceleration on stone stability*. *MS.c. Thesis*. Delft University of Technology.

Detert, M., Weitbrecht, V., & Jirka, G. (2010). Laboratory Measurements on Turbulent Pressure Fluctuations in and above Gravel Beds. *Journal of Hydraulic Engineering, Volume 136, issue 10*, 779–789.

Halter, W. (1999). *(in dutch) "Het gedrag van zakkingsfilters onder de invloed van golfbelasting"*. *MSc. Thesis* Delft University of Technology.

Hoan, N. T. (2008). *Stone stability under non-uniform flow*. *PhD thesis*. Delft University of Technology.

Hoffmans, G. (2012). *The influence of turbulence on soil erosion*. Delft: Eburon Academic Publishers.

Hoffmans, G. (2015, January 27). Internal communication Deltares (memo). *(in dutch) filterinstabiliteit*. Delft.

Hoffmans, G., & Verheij, H. (2013, January 27). Internal communication Deltares. *geometrisch-open filters*.

Holthuijsen, L. H. (2007). *Waves in oceanic and coastal waters*. New York: Cambridge university press.

- Huijsmans, M. A. (2006). *The influence of flow acceleration on the stability of stones*. MSc. Thesis. Delft University of Technology.
- Jansens, R. (2000). (in dutch) "*Het doordringen van golven in een filterlaag*". MSc. Thesis Delft University of Technology.
- Jongeling, T. H., Blom, A., Jagers, H. R., Stolker, C., & Verheij, H. J. (2003). *Design method granular protections. Technical report*. WL Delft Hydraulics, rapport schaalmodelonderzoek, numerieke simulaties en bureaustudie.
- Jonsson, I. G. (1966). Wave Boundary layers and friction factors. *Proceedings on the 10th conference of coastal engineering, tokyo, japan* (pp. 127-147). New York: ASCE.
- Joustra, R. (2013). *Interface stability in granular open filters in unidirectional flows*. MSc. Thesis University of Twente.
- Kaminsky, G. M., & Kraus, N. C. (1993). Evaluation of depth-limited wave breaking criteria. *Int. Symp. Ocean Wave Measurement and Analysis WAVES 93* (pp. 180-193). New Orleans: ASCE.
- Klar, M. (2005). *Design of an endoscopic 3-D particle-tracking velocimetry system and its application in flow measurement within a grave layer (Doctoral Thesis, University of Heidelberg, Germany)*.
- Klein Breteler, M., den Adel, H., & Koenders, M. A. (1992). (in dutch) "*Taludbekleding van gezette steen: ontwerpregels voor het filter*". Waterloopkundig Labratorium, Oriënterende bureaustudie N603.
- LeMéhauté, B. (1968). Shallow water waves: A comparison of theories and experiments. *Conference on Coastal Engineering*, (pp. 86-107). London.
- Morison, J. R., O'Brian, M. P., Johnson, J., & Schaaf, S. A. (1950). The force exerted by surface waves on piles. *Petrol. Trans AIME*, (pp. 149-154).
- Papadopoulos, D. (2012). *Scour below the toe of breakwaters*. MSc. Thesis Delft University of Technology.
- Rance, P. J., & Warren, N. F. (1968). The threshold of movement of coarse material in oscillatory flow. *Proceedings of the 11th conference on coastal engineering, London, United Kingdom* (pp. 487-491). ASCE.
- Schiereck, G. J., & Verhagen, H. (2012). *Introduction to bed, bank and shore protection*. Delft: VSSD.
- Schiereck, G. J., Fontijn, H. L., Grote, W. V., & Siermans, P. G. (1994). Stability of rock on beaches. *Proceedings of the 24th conference on coastal engineering, Kobe, Japan* (pp. 1553-1567). ASCE.
- Schiereck, G. J., & Fontijn, H. L. (1996). Pipeline protection in the surf zone. *Proceedings of the twenty-fifth international conference on Coastal Engineering, Orlando, Florida* (p. 4228). New York: ASCE.
- Shields, A. (1936). *Application of similarity principles and turbulence research to bed load movement (translated from "Anwendung der aehnlichkeitsmechanik und der turbulenzforschung auf die geschiebebewegung")*. Preußischen Versuchsanstalt für Wasserbau.
- Sleath, J. F. (1978). Measurements of bed load in oscillatory flow. *Journal of the waterway, port, coastal and ocean division, Vol 104, No. 3* (pp. 291-307). New York: ASCE.

- Steenstra, R. (2013). *Incorporation of the effects of acceleration flow in the design of granular bed protections*. Delft: TU Delft Msc. Thesis.
- Tromp, M. (2004). *Influences of fluid accelerations on the threshold of motion*. MSc. Thesis Delft University of Technology.
- Van de Sande. (2012). *stability of open filter structures under waves*. MSc. Thesis Delft University of Technology.
- van Os, P. (1998). *(in dutch) Hydraulische belastingen op een geometrisch open filterconstructie*. MSc. Thesis Delft University of Technology.
- van Rijn, L. (1984). Sediment transport, part 1: bed load transport. *journal of hydraulic engineering*, 1432-1456.
- Verheij, H., Hoffmans, G., Dorst, K., & van de Sande, S. (2012). Interface stability of granular filter structures under currents. *6th International Conference on Scour and Erosion*. Paris.
- Wolters, G., & van Gent, M. R. (2012). Granular open filters on a horizontal bed under wave and current loading. *Proceedings of the 33rd international conference on Coastal Engineering, Santander, Spain*. Coastal Engineering Research Council.
- Wolters, G., Rudolph, D., Hofland, B., & Verheij, H. (2010). On the behaviour of open filters under wave loading. *5th international conference on Scour and Erosion* (pp. 142-151). San Francisco: ASCE.
- Wörman, A. (1989). Riprap protection without filter layers. *journal on hydraulic engineering*, 1615-1630.

Appendices

Appendix A

A Background information of previous experimental research

This appendix shows more background information of relevant previous research to granular open filters. Background data of Halter (1999), Jansens (2000) and Wolters & Van Gent (2012) is presented.

A1 Halter (1999)

Halter carried out research to find the critical wave condition for which incipient motion of the base material occurs. His results are presented in table A1.

Table A1 Critical hydraulic conditions for which the base material erodes (Halter, 1999)

dikte filterlaag [cm]	D_{n50F} [cm]	golfperiode T [s]	golfhoogte H [cm]	u_{max} (2cm boven filter) [m/s]
12	3,75	1,03	8,2	0,08
12	3,75	1,33	6,7	0,09
12	3,75	1,9	6	0,11
12	3,75	2,41	5,6	0,14
12	1,99	1,03	16,7	0,16
12	1,99	1,33	8,9	0,14
12	1,99	1,9	8,8	0,17
12	1,99	2,41	7,9	0,19
6	1,99	1,03	12	0,12
6	1,99	1,33	9	0,13
6	1,99	1,9	7,3	0,13
6	1,99	2,41	6,7	0,17
0	-	1,03	11,7	0,09
0	-	1,33	7	0,09
0	-	1,9	6,3	0,10
0	-	2,41	5,1	0,12

Table A2 Properties of the used materials in the experimental research of Halter

	basismateriaal	filtermateriaal A	filtermateriaal B
soort materiaal	zand	stenen	Stenen
nominale diameter	100 μm	3,75 cm	1,99 cm
wijde (D_{85}/ D_{15})	1,54	1,25	1,28
dichtheid	2650 kg/m^3	2550 kg/m^3	2540 kg/m^3
porositeit	$\pm 0,4$	0,42	0,39
vormfactor (l/t)	n.v.t.	2,5	2,5

To use Halter's data in this research, information was needed for the water depth above the filter, the value of d_{f15} and the conversion factor between d_{f50} and d_{nf50} . The used values are presented in table A3.

Table A3 Other relevant parameters which are used to interpret Halter's data. (shape factors and ratio's are plausible assumptions)

Parameter	Used value in this research
Water depth above filter	38 cm
Shape factor F_s	0.88 [-]
Ratio d_{f15} and d_{f50}	0.85 [-]

A2. Jansens (2000)

Jansens (2000) found a relationship to estimate the measured pore velocities inside the filter. This relationship was formulated as follows:

$$\frac{1}{\rho_w g} \frac{\delta p}{\delta x} \cdot T \cdot 0.4 \equiv \hat{u}_p$$

Jansens compared the calculated pore velocities against the measured pore velocities. See table A4. In the calculations of the pore velocity, Jansens used the orbital velocity which was measured during the experiments of Halter (1999). Jansens states that Halter made a mistake for loading situation A. Using the correct orbital velocity, Jansens calculates a pore velocity of 0.046 m/s. Thus the calculated velocities are in the same order as the measured velocities. Figure A1 shows the ratio between the orbital velocity and the pore velocity for Jansens experiments.

Table A4 Measured and calculated pore velocities by Jansens (2000)

Loading situation	$i \cdot T$	factor	calculated velocity	measured velocity
A	0.144	0.4	0.058	0.04-0.08
B	0.106	0.4	0.042	0.03-0.05
C	0.114	0.4	0.046	0.03-0.06
D	0.121	0.4	0.048	0.03-0.05

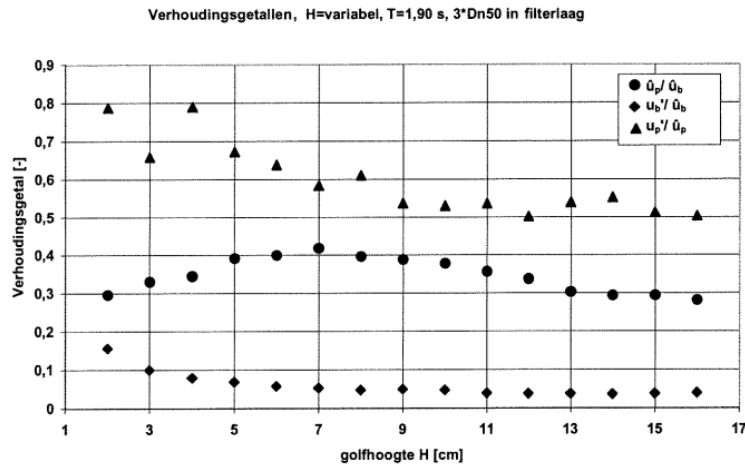


Figure A1 Ratios between velocities (Jansens, 2000)

A3. Wolters & van Gent (2012)

The test program of Wolters & Van Gent’s research is presented in table A5. Wolter & Van Gent found a relation between the transport rate of base material and the hydraulic gradient. Thereby, the maximal value (2% upper limit) for the hydraulic gradient was related to the KC_f number. The relations are presented in figure A2. Note that Wolters & van Gent used irregular waves in their experiments.

Table A5 Test program and observed base material transport (Wolters & van Gent, 2012)

Table 2. Test programme.												
Test	Loading	Test parameters			Loading conditions					Measured		
		$D_{n50,f}$ (mm)	d_f (m)	h_f (m)	H_s (m)	T_p (s)	S_{wp} (-)	u_m	t_{Tot} (hrs)	$u_{2\%}$ (m/s)	T (g/m/s)	T^* (-)
T01	current	22	0,055	0,4	-	-	-	1,25	8,48	1,00	0,062	0,0029
T02	current + waves	22	0,055	0,4	0,06	1,98	0,009	0,83	0,50	0,68	-	-
T03	current + waves	22	0,055	0,4	0,11	2,51	0,011	0,13	6,00	0,35	0,008	0,0004
T04	current + waves	22	0,055	0,4	0,15	3,01	0,011	0,13	6,00	0,71	0,007	0,0003
T05	current + waves	22	0,055	0,4	0,12	2,99	0,008	0,83	6,00	1,03	0,031	0,0014
T06	current + waves	22	0,055	0,4	0,12	5,08	0,003	0,83	6,00	0,92	0,043	0,0020
T07	current + waves	22	0,055	0,4	0,14	5,69	0,003	0,83	6,00	1,14	0,063	0,0029
T08	current	22	0,055	0,4	-	-	-	1,06	6,00	1,02	0,052	0,0024
T09	current + waves	22	0,055	0,4	0,10	5,07	0,002	1,06	4,18	1,43	0,203	0,0094
T10	current	22	0,055	0,4	-	-	-	0,83	6,00	0,60	0,006	0,0003
T11	current	22	0,055	0,4	-	-	-	1,06	6,00	0,91	-	-
T12	current + waves	22	0,055	0,4	0,10	5,08	0,002	1,06	2,00	1,20	0,331	0,0153
Reference tests (without filter)												
T13	current	-	-	0,455	-	-	-	0,55	0,50	0,65	12,265	0,5684
T14	current + waves	-	-	0,455	0,13	5,10	0,003	0,55	0,50	1,13	33,553	1,5550
Wave tests (Wolters et al. 2010)												
T05	waves	30	0,1	0,4	0,10	2,09	0,015	-	6	0,26	0,102	0,0047
T06	waves	30	0,1	0,4	0,14	2,52	0,014	-	6	0,38	0,079	0,0037
T07	waves	30	0,1	0,4	0,17	5,41	0,004	-	2	0,88	0,161	0,0075
T08	waves	30	0,055	0,4	0,14	2,52	0,014	-	6	0,43	0,063	0,0029
T09	waves	30	0,055	0,4	0,14	1,80	0,027	-	6	0,32	0,063	0,0029
T10	waves	30	0,055	0,4	0,16	5,10	0,004	-	2	0,86	0,068	0,0031
T11	waves	20	0,055	0,4	0,14	2,52	0,014	-	6	0,41	0,035	0,0016
T12	waves	20	0,055	0,4	0,14	1,81	0,027	-	6	0,32	0,033	0,0015
T13	waves	20	0,055	0,4	0,16	5,10	0,004	-	2	0,88	0,040	0,0019

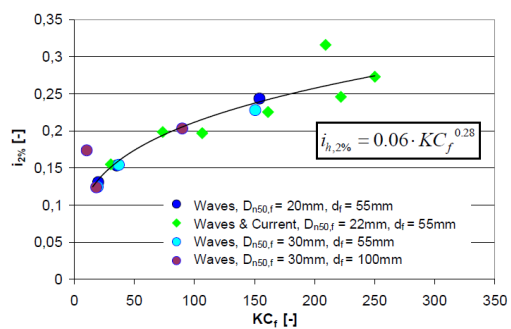
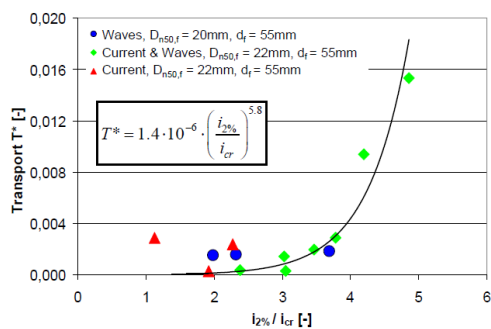


Figure A2 Relation between dimensionless transport rate and hydraulic gradient (left), relation between maximal hydraulic gradient and KC_f number (right)

Appendix B

B Material properties

B1. Filter materials

Three different filter materials were selected for the model tests; “Yellow Sun 8-11 mm” , “Yellow Sun 10-20 mm” and “Yellow Sun 20-40 mm”. For this research, the density and the grading of the materials must be known. The density is determined by weighing a sample of the material. Subsequently the volume of the material is determined by placing the sample in a measuring beaker. When a measuring beaker filled with water is used, the volume of the filter material sample is easily found. This test is repeated several times and the average off all test is used as representative density. A value of 2624 kg/m³ was found.



Figure B1 Filter materials. Left: Yellow Sun 8-11. Middle: Yellow Sun 10-20. Right: Yellow Sun 20-40

Weight distribution of the filter materials

Several properties can be determined from the grain size distribution of the material, such as the nominal diameter and the grading width. To find the grain size distribution, a batch of the filter material is taken to create a sieve curve (in this research the batch counted between 110 and 350 stones). Every stone is individually weighed. This results in the weight distribution.

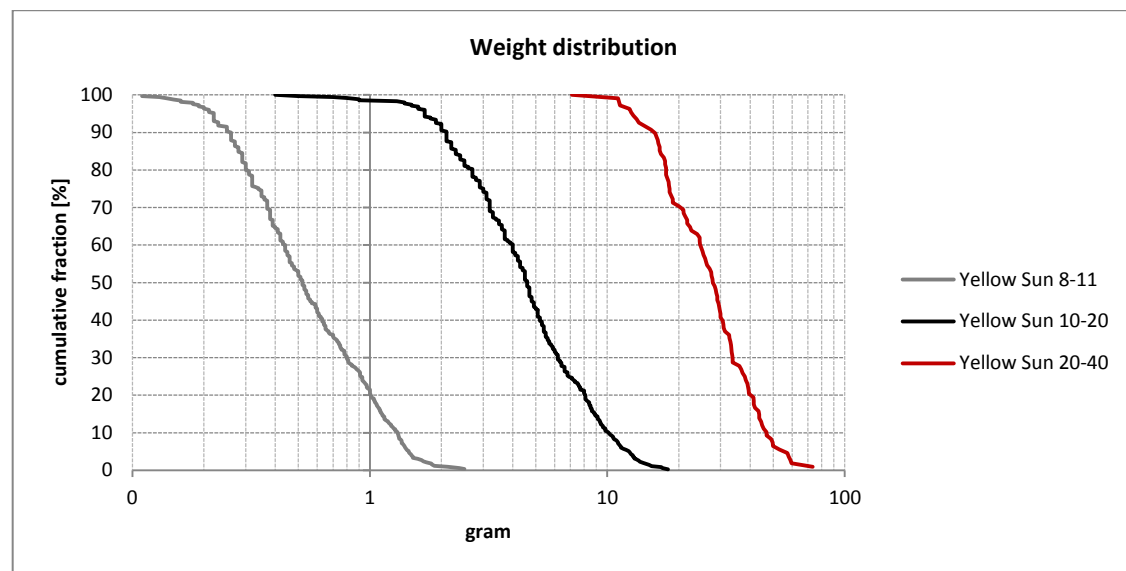


Figure B2 Weight distribution of the filter materials

Grain size distribution of the filter materials

Two methods are possible to obtain the grain size distribution of granular materials. One way is by making a sieve curve. Multiple sieves with a different mesh size can be used to find the distribution of the material. The smaller the difference between the mesh size of the different sieves, the more accurately the distribution will be. During this research, the amount of sieves was limited, therefore it was chosen to determine the grain size distribution with another method. In this research, the weight distribution is used to find the grain size distribution.

The weight of a stone is related to the nominal diameter, see equation 76. Subsequently, the nominal diameter is related to the grain size diameter by equation 77. F_s is a shape factor, which determines how the nominal diameter is related to the grain size diameter. Mostly, this value has a range from 0,7 to 0,9. A value of 0,88 is used in this research (CUR, 233, Interface stability of granular filter structures, 2010). It should be noted that this used value is seen as a constant. However, recent research shows that the value for F_s is not a very reliable value (Witteveen, 2015), and may deviate. Therefore, the choice of this method to determine the grain size distribution introduces an error which will be evaluated in the analysis of the results.

$$d_{n50} = \sqrt[3]{\left(\frac{W_{50}}{\rho_f}\right)} \quad (76)$$

$$d_{n50} = F_s \cdot d_{50} \quad (77)$$

The found grain size distribution is presented in figure B3. An overview of the filter material properties is presented in table 9-1. The ratio $\frac{d_{85}}{d_{15}}$ gives an indication of the width of the material grading, a value below 1.5 means that the grading is narrow, and above 1.5 that the grading is wide (Schierck & Verhagen, Introduction to bed, bank and shore protection, 2012). As shown in table 9-1, it can be seen that the grading is wide, but not very wide.

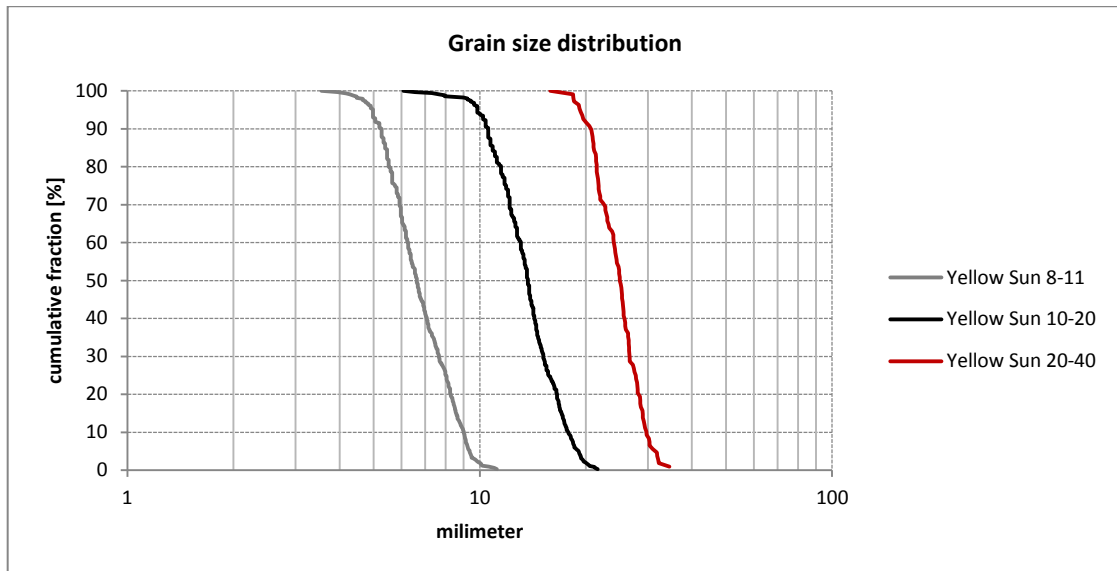


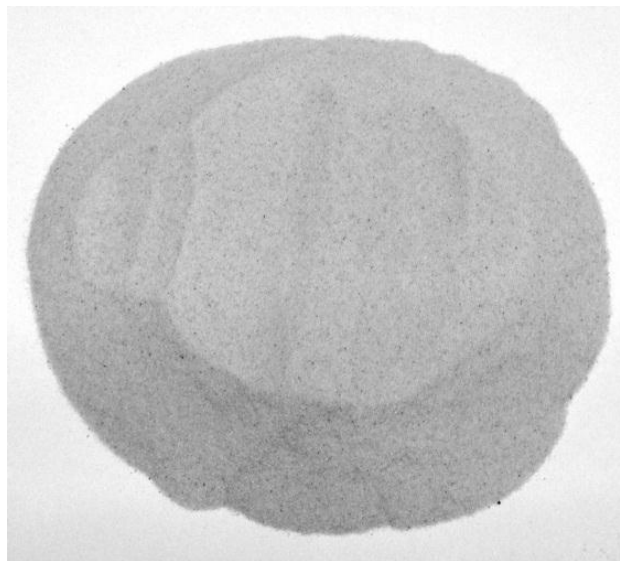
Figure B3 Grain size distribution of the filter materials

Table B1 Overview filter properties

Material	d_{15} [mm]	d_{50} [mm]	d_{85} [mm]	d_{90} [mm]	d_{n50} [mm]	$\frac{d_{85}}{d_{15}}$	ρ_f [kg/m ³]
Yellow Sun 8-11 mm	5.39	6.63	8.59	9.02	5.83	1.59	2624
Yellow Sun 10-20 mm	10.88	13.71	17.02	17.76	12.06	1.56	2624
Yellow Sun 20-40 mm	21.09	25.02	29.04	29.55	22.03	1.37	2624

B2. Base material

The density of the base material is determined similar to the filter material, which gives a value of 2630 kg/m³. The grading is determined using the method with the different sieves. A series of six sieves is used to find the grain size distribution of the base material. The size of the sieve mesh is directly a measure for the sand grains which fall through the mesh. The analysis results in the sieve distribution presented in figure 9-5. An overview of the base material properties is presented in table 9.2.



Base material

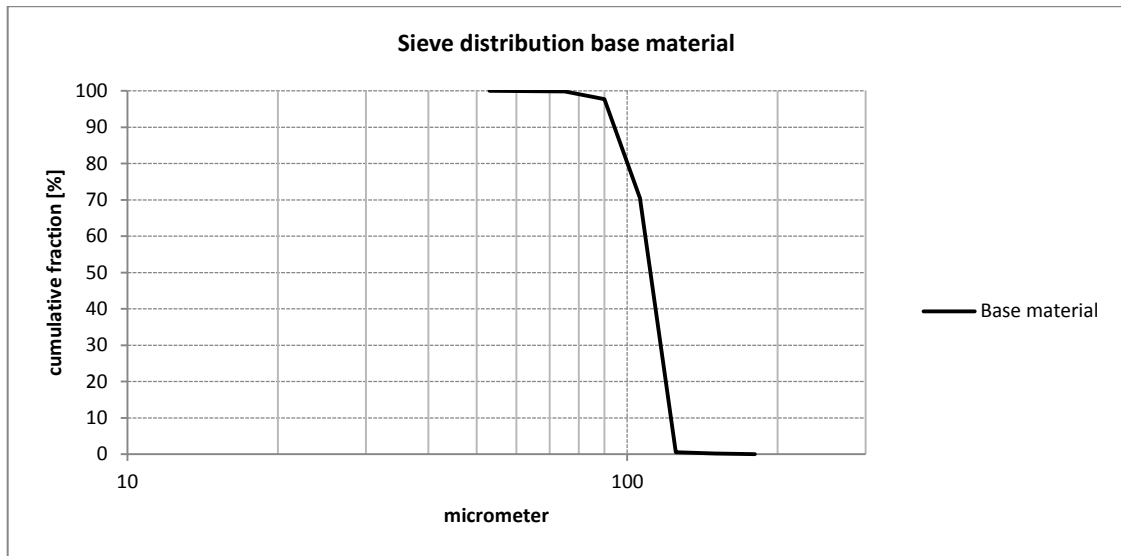


Figure B4 Grain size distribution of the base material

Table B2 Overview base material properties

Material	d_{15} [μm]	d_{50} [μm]	d_{85} [μm]	d_{90} [μm]	$\frac{d_{85}}{d_{15}}$	ρ_f [kg/m^3]
Base material	98	113	120	122	1.22	2630

Appendix C

C Experimental results

C1 Overview


In the test overview all parameters of importance are presented. These are: the thickness of the filter layer, the diameter of the filter and base material, the water depth above the filter and the critical wave conditions for that set-up. The critical wave condition is defined as the condition for which the base material is instable and moved into the transparent tray. The wave height was increased in steps of 2 cm until instability of the bed was observed. Obviously, all wave heights above the critical height ($H_{c,b}$) also generated bed instability. Also, the wave conditions is given for which winnowing of particles through the filter was observed (H_w). For all test video recordings are made of the transparent tray. On these videos the bed instability can be reviewed.

Test	Test parameters					Loading conditions			
	D_f [mm]	d_{f50} [mm]	d_{b50} [μ m]	$\frac{D_f}{d_{f15}}$ [-]	$\frac{d_{f50}}{d_{b50}}$ [-]	h_f [m]	T [m]	$H_{c,b}$ [m]	H_w [m]
1	17	6,6	113	3.2	58.4	0.4	3.0	≤ 0.10	0.16
2	17	6,6	113	3.2	58.4	0.4	2.0	0.12	0.15
2	17	6,6	113	3.2	58.4	0.4	2.5	0.09	0.15
2	17	6,6	113	3.2	58.4	0.4	3.0	≤ 0.10	0.13
3	28	13.7	113	2.6	121.2	0.4	2.0	0.05	0.07
3	28	13.7	113	2.6	121.2	0.4	2.5	0.05	0.07
3	28	13.7	113	2.6	121.2	0.4	3.0	0.06	0.08
4	59	13.7	113	5.4	121.2	0.4	2.0	0.08	0.10
4	59	13.7	113	5.4	121.2	0.4	2.5	0.08	0.11
4	59	13.7	113	5.4	121.2	0.4	3.0	0.08	0.08
5	96	13.7	113	8.8	121.2	0.4	2.0	0.11	0.14
5	96	13.7	113	8.8	121.2	0.4	2.5	0.11	0.16
5	96	13.7	113	8.8	121.2	0.4	3.0	0.12	0.15
6	93	25.0	113	4.4	221.2	0.4	2.0	0.06	0.06
6	93	25.0	113	4.4	221.2	0.4	2.5	0.06	0.06
6	93	25.0	113	4.4	221.2	0.4	3.0	0.06	0.08
7	147	25.0	113	7.0	221.2	0.4	2.0	0.06	0.09
7	147	25.0	113	7.0	221.2	0.4	2.5	0.07	0.09
7	147	25.0	113	7.0	221.2	0.4	3.0	0.07	0.09

Table C1 Test overview

Test 1

Parameter	Value	Unit
Base material d_{b50}	113 (fine sand)	μm
Filter material d_{f50}	6.6 (Yellow Sun 8-11)	mm
D_f	17	mm
D_f/d_{15}	3.2	-
d_{f50}/d_{b50}	58.4	-
Depth above filter	0.4	m
T	3	s
$H_{c,b}$	≤ 0.10	m
H_w	0.16	m



Only waves with a period of 3 seconds were tested in the first test. While filling the flume, it was observed that the base material eroded. The transparent trays were already filled with water during the test setup (thus before the flume was filled), to prevent the erosion during the filling of the flume as much as possible. Thereby the flume was filled very slowly.

Movement of the filter material was not observed during the tests. Only some rocking of filter stones was observed at several locations, but this cannot be classified as filter instability.

Around the tray some interesting observations were made. It was possible to see the base material erode under the filter. The sand particles sink down slowly in the tray. It seemed that scour holes were formed under the filter, near the edges of the tray. During the tests, these scour holes seem to enhance the instability of the base material; sand was stirred up in the pore under the filter layer and moved into the tray. The base layer was classified as unstable when it was able to see sand particles moving into the tray, at both sides of the flume.

Two processes may contribute to the development of the scour hole. First, the sediment transport is limited to one direction. This means that particle moving into the tray, cannot move back to their original location. Therefore a hole is formed near the edges of the tray. Secondly, additional turbulence may be present near the edges of the tray. The oscillatory flow through the tray is interrupted by the tray's edge, which causes extra turbulence behind the tray. This effect is undesired, because the aim of this research is to focus on wave loading alone, and not a situation with additional turbulence. Unfortunately, it is not possible to quantify the contribution to the instability of each of these two processes. In further tests, measures are taken to minimize the effect of additional turbulence.

Beside the observations in the tray, it was also possible to observe entrainment of sediment in the flume. However, it can be hard to distinguish base material entrainment from the dirt of the filter material. Even after washing the filter material, some very fine dirt is present in the water column.

The tests were started with a wave height of approximately 10 cm. During the analysis of the video data after the tests, it was seen that the bed was already instable for this wave height. Therefore it is concluded that the critical wave height to generate bed instability must be lower or equal to 10 cm.

A wave height of 12 cm was considered to generate bed instability. To be certain that this observation was correct, and check the credibility of the visual observations in general, a test was carried out with a long duration (20 hours). After the test fluctuations in the bed had formed. However, it should be noted that the visual observation were made through the window and might therefore be subjected to wall effects of the glass. However, the scour holes next to the tray have also grown extensively. A

large amount of sand was found in the trays over the whole length of the flume. Therefore it seems acceptable to qualify this test as “instable bed”.

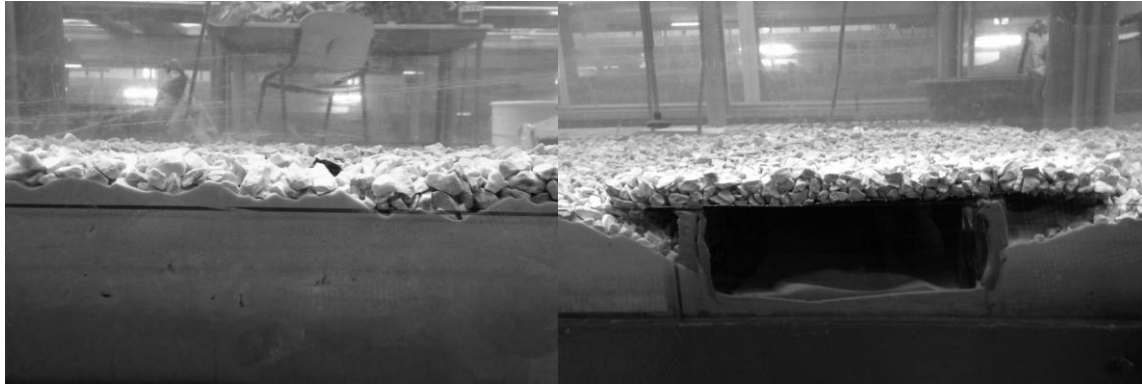
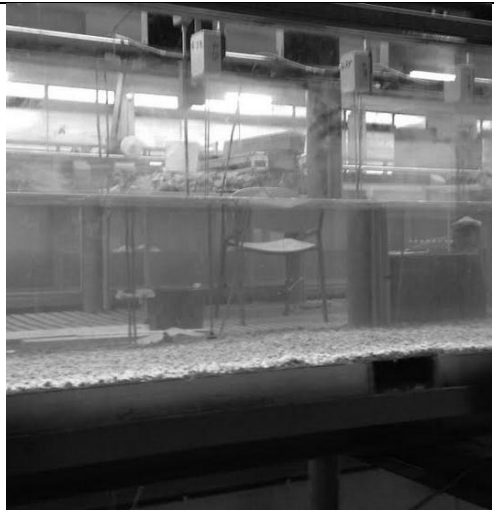


Figure C1 Results after the 20-hour test. Left: ripple formation at the interface. Right: scour holes near the tray's edges.

Test 2

Parameter	Value	Unit
Base material (d_{50})	113 (fine sand)	μm
Filter material (d_{50})	6.6 (Yellow Sun 8-11)	mm
D_f	17	mm
D_f/d_{15}	3.2	-
d_{f50}/d_{b50}	58.4	-
Depth above filter	0.4	m
T	2	s
$H_{c,b}$	0.12	m
H_w	0.15	m
T	2.5	s
$H_{c,b}$	0.09	m
H_w	0.15	m
T	3.0	s
$H_{c,b}$	≤ 0.10	m
H_w	0.16	m



In the second test it was attempted to reduce the undesired effects seen in test 1. Thereby tests with several wave periods were carried out. To prevent scour holes near the edges of the tray, measures were taken. The edges of the tray were protected with a 3 cm strip of sand paper. Thereby the time of each test was minimized to several minutes, to prevent the development of a scour hole. It was observed that the scour hole was not formed as quick as in the earlier test. It seemed that inaccuracies in the set-up of the test (i.e. little openings under the glued filter near the tray) seem to enhance the development of the scour hole. At one side of the tray, the filter was placed perfectly upon the sand layer, where at the other side still very little pores could be seen. During the tests, the development of the scour hole on the irregular edge seemed to be much stronger, indicating that the inaccuracy of the set-up contributes to the development of the scour hole.

Again, the base material was classified as unstable when erosion was observed at both sides of the tray, at both sides of the flume. This time also a 20 hour test was carried out, but now with a wave condition which was considered to be *just* instable. The idea was to confirm whether the base was unstable. After 20 hours with a 2 second wave of 0.12 meter, it was observed that the scour holes had further developed. The development was not as much as in the previous 20 hour test (where $T=3.0\text{s}$ and $H=0.12\text{m}$). However, it was not observed that bed forms were developed.

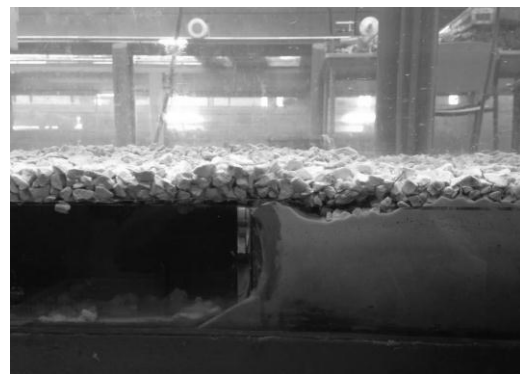


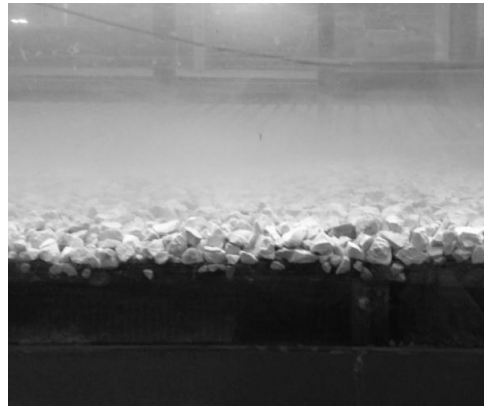
Figure C2 Scour holes after the 20 hour test ($T=2.0\text{s}$ $H=0.12\text{m}$)



Figure C3 Interface after the 20 hour test

Test 3

Parameter	Value	unit
Base material (d_{50})	113 (fine sand)	μm
Filter material (d_{50})	13.7 (Yellow Sun 10-20)	mm
D_f	28	mm
D_f/d_{15}	2.6	-
d_{f50}/d_{b50}	121.2	-
Depth above filter	0.4	m
T	2	s
$H_{c,b}$	0.05	m
H_w	0.07	m
T	2.5	s
$H_{c,b}$	0.05	m
H_w	0.07	m
T	3.0	s
$H_{c,b}$	0.06	m
H_w	0.08	m




A larger filter diameter was tested in test 3. Again the edges of the tray were protected with sand paper. For the higher wave conditions, entrainment of sand particles through the filter was clearly observed. The filter material itself was stable during all tests. No movement was observed at all.

Again, it was attempted to classify instability through observations in the transparent tray. However, some observations are considered to be doubtful because the observed transport was extremely small. For these conditions, also no entrainment through the layer was observed. Therefore, these hydraulic conditions will be classified as “doubtful instability”.

No 20h test is carried out, because it is avoided to distort the sand layer too much. The filter layer will be enlarged for the following test, thus it is undesirable to distort the sand layer any further.

Test 4

Parameter	Value	unit
Base material (d_{50})	113 (fine sand)	μm
Filter material (d_{50})	13.7 (Yellow Sun 10-20)	mm
D_f	57	mm
D_f/d_{15}	5.2	-
d_{f50}/d_{b50}	121.2	-
Depth above filter	0.4	m
T	2	s
$H_{c,b}$	0.11	m
H_w	-	m
T	2.5	s
$H_{c,b}$	0.10	m
H_w	-	m
T	3.0	s
$H_{c,b}$	0.08	m
H_w	-	m



The same filter material is used as in test 3, but now the filter is twice as thick. After placement of the stones, a lot of dirt was stirred up by the waves in the flume. It was attempted to remove this dirt before the experiment was carried out. A low wave condition ($T=2\text{s}$, $H=04\text{ cm}$) was generated for an hour to transport this dirt to the end of the flume. However, it is not possible to transport all dirt from the stones to the end of the flume. During the model test, it seemed that some dirt was still entrained in the water column. The presence of the dirt complicates the qualification of entrained sand in the water column.



Figure C4 Dirt of the stones above the filter layer

Another unexpected element in this test was the presence of dirt in the transparent tray. When the flume was emptied, water had still been standing in the transparent tray, since it is water tight. A slimy substance had developed in the tray, which is probably a reaction of the wood and water in the flume. The presence of this dirt complicates the visual observations in the tray. After the test, it was carefully examined if the slimy substance was also present in or under the filter or in the sand bed. No detections were made of affections in the sand or filter layer.



Figure C6 Dirt in the tray




Figure C7 Examination of dirt elsewhere in the model

Despite the dirt in the tray, test were carried out. It is observed that the critical wave heights were larger than in test 3. After the test it was decided to repeat the experiments with a cleaned tray. Also a large part of the sand layer was rebuild for this repeated test, to be sure that the slimy substance would not be present anywhere in the test. See test 5 for the results.

Test 4 (repeated)

Parameter	Value	unit
Base material (d_{50})	113 (fine sand)	μm
Filter material (d_{50})	13.7 (Yellow Sun 10-20)	mm
D_f	59	mm
D_f/d_{15}	5.4	-
d_{f50}/d_{b50}	121.2	-
Depth above filter	0.4	m
T	2	s
$H_{c,b}$	0.08	m
H_w	0.10	m
T	2.5	s
$H_{c,b}$	0.08	m
H_w	0.11	m
T	3.0	s
$H_{c,b}$	0.08	m
H_w	0.08	m

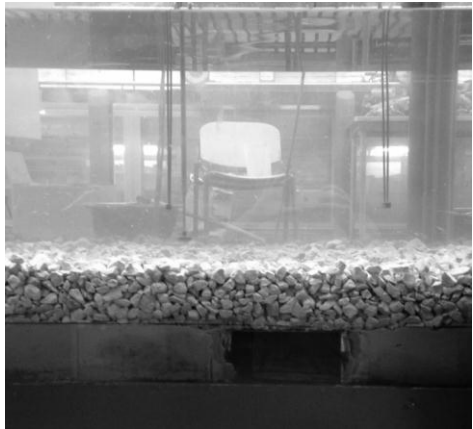


After test 4, the transparent tray was removed and cleaned. The sand layer was partly replaced (at both ends of the tray) to remove the slimy substance completely. Although, during this process of rebuilding, no dirt was detected in the sand layer. The replacement of the sand was considered as a precautionary measure, to prevent any possible negative effect from the slimy substance.

During the testing, the results are quite similar as in test 4. However, for the 3 second wave it was noticed that instability was observed for a 8cm wave height. This was not clearly seen in test 4. This difference probably lies in the fact that the visual observations were hindered by the dirt in test 4.

Test 5

Parameter	Value	unit
Base material (d_{50})	113 (fine sand)	μm
Filter material (d_{50})	13.7 (Yellow Sun 10-20)	mm
D_f	96	mm
D_f/d_{15}	8.8	-
d_{f50}/d_{b50}	121.2	-
Depth above filter	0.4	m
T	2	s
$H_{c,b}$	0.11	m
H_w	0.14	m
T	2.5	s
$H_{c,b}$	0.11	m
H_w	0.16	m
T	3	s
$H_{c,b}$	0.12	m
H_w	0.15	m



Test 5 was executed with the same filter material as in test 4, only with a thicker filter layer. It is observed that the protective efficacy of the filter layer has increased compared to the previous test. Higher wave conditions were needed to generate bed instability.

To remove the dirt from the filter material a small current in combination with very low wave action ($H=3\text{cm}$) was generated in the flume for several minutes. The dirt from the stones was transported in the direction of the wave damper. No transport in the tray was seen during the cleaning of the flume. A 20 hour test was carried out with the following wave conditions: $H=0.14$ and $T=2\text{s}$. After the test it was clear that the base layer was instable, because the amount of sand in the tray was clearly larger after the test than before. Although, the bed forms had not clearly changed during the test, while winnowing was observed during the test. Probably the amount of sand transported by winnowing is very small compared with the transport at the interface.

Test 6


Parameter	Value	unit
Base material (d_{50})	113 (fine sand)	μm
Filter material (d_{50})	13.7 (Yellow Sun 20-40)	mm
D_f	93	mm
D_f/d_{15}	4.4	-
d_{f50}/d_{b50}	221.2	-
Depth above filter	0.4	m
T	2	s
$H_{c,b}$	0.06	m
H_w	0.06	m
T	2.5	s
$H_{c,b}$	0.06	m
H_w	0.06	m
T	3	s
$H_{c,b}$	0.06	m
H_w	0.08	m



Test 6 was carried out with a large filter material diameter. It was observed that the critical wave height for all periods was small compared to the previous test. Therefore it seems that the efficiency to damp the wave loading is smaller for a larger filter diameter. Conclusions based on this observation will be elaborated in chapter 6. Furthermore the filter layer was stable during all tests. No movements of the individual stones were observed. The filter layer is classified as stable (phase 0 according to Breusers).

Test 7

Parameter	Value	unit
Base material (d_{50})	113 (fine sand)	μm
Filter material (d_{50})	13.7 (Yellow Sun 20-40)	mm
D_f	147	mm
D_f/d_{15}	7.0	-
d_{f50}/d_{b50}	221.2	-
Depth above filter	0.4	m
T	2	s
$H_{c,b}$	0.06	m
H_w	0.09	m
T	2.5	s
$H_{c,b}$	0.07	m
H_w	0.09	m
T	3	s
$H_{c,b}$	0.07	m
H_w	0.09	m



Test 7 is carried out with the thickest filter layer of all tests. Although, the critical wave height for which bed instability was observed was not as high as in the tests with other filter materials. For practical reasons the filter thickness was only partly on its correct thickness. See figure C8.

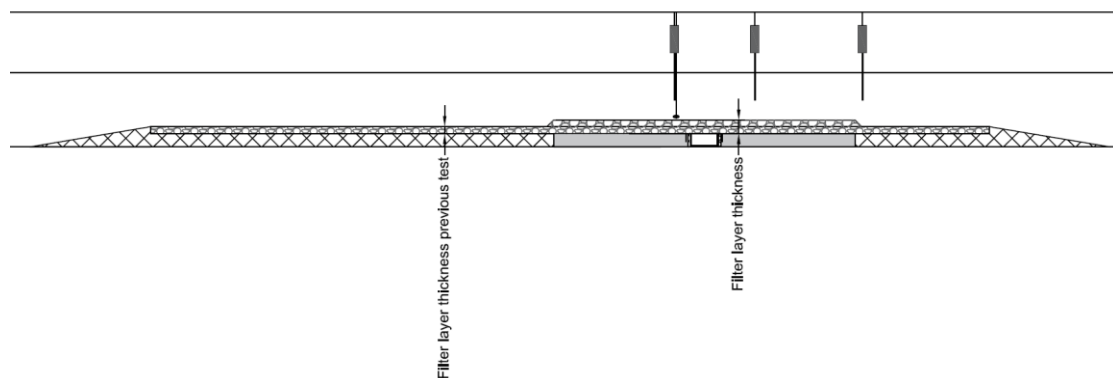


Figure C8 Filter thickness test 7

The last test in the series with this configuration was again a 20 hour test. The wave period was 2 seconds and the wave height was 0.06 meter. During the test, a small amount of base material entering the transparent tray was observed. Visually, it was clear that the tray had been filled with sand, since the amount of sand at the bottom of the tray after the 20 hours was clearly larger than before the test. Therefore it seems justified to classify these wave conditions as “critical”. However, entrainment was not observed. Thereby no indicators of a lowering of the bed was observed, so it is concluded that there is no presence of entrainment for this wave condition.

On figure C9 a shot is shown of the video recordings. A single stone is lying in the tray. This stone fell down in the tray during the placement of the filter layer and has no further meaning.

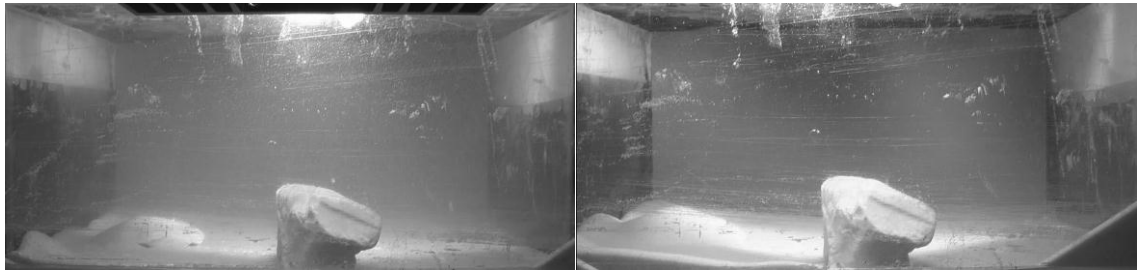


Figure C9 Left: tray before the 20h test. Right: after the 20h test

After the 20 hour test the filter layer was carefully removed to investigate the bed forms on the base layer. It seemed that the Filter layer had “sunk down” into the base layer. The stones in the bottom of the filter layer were covered by sand. An explanation for this observation might be that the pores in the filter have slowly filled with sand. The sand makes movements back and forth, and is dynamically stable. However, when the sand particles under the stones are moving into the pores of the filter, and the filter sinks down, the effective filter thickness reduces. This phenomenon is interesting for further research. Long test will be necessary to investigate how far the filter can sink down into the base layer, and how the protective efficacy of the filter layer is affected.

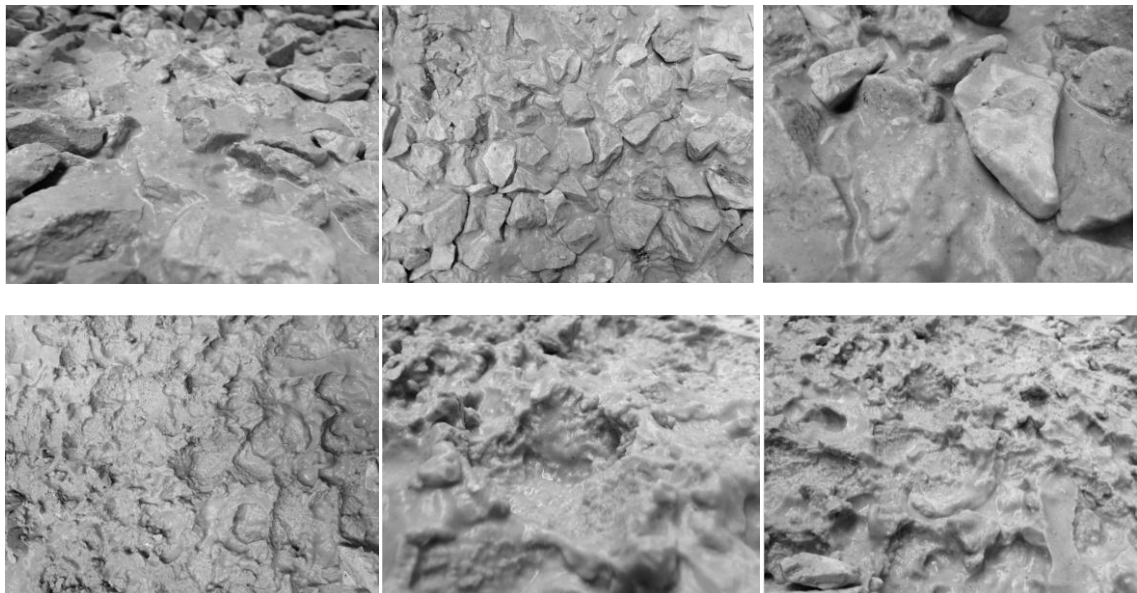


Figure C10 Row above: stones in the bottom of the filter sunk into the sand layer. Row below: all stones removed.

Test 8 (no filter layer)

The purpose of test 8 was to illustrate the vulnerability of an unprotected bed. Therefore, a test without a filter layer was performed to investigate the stability of the bed material. A wave with a period of 2 seconds and a height of 4.2 cm was generated. The water depth was 0.4 meter. The generated shear stress by the waves was in the range of the critical shear stress for the base material ($\Psi=0.044$, which is in the critical area according to the modified Shields diagram for waves (see Sleath 1978).) The test was performed for 20 minutes, no studies were made to bed form developments. Thereby, the bed was already influenced during the filling of the flume.

As expected, instability of the bed was observed. Particles were rolling over the bed back and forth. Thereby it was also observed that the particles were suspended in the water column. Probably only the smaller particles from the bed material grading were suspended, because suspension coincides with larger shields values. The shields value is larger for the smaller particles since the strength of those particles is smaller. According to the transport stages of Breusers this can be classified as stage 2 / stage 3 (frequent particle movement at some locations / frequent particle movement at many locations).

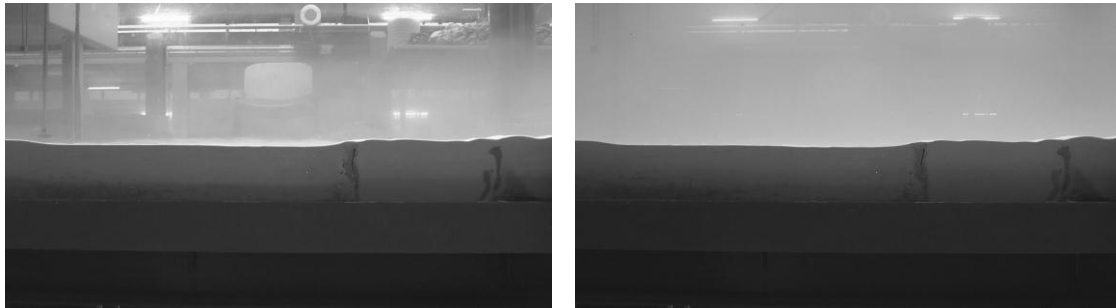


Figure C11 Pictures during the test. Left: at the start of the test. Right: after 15 minutes of testing. It can be seen that base material had been brought in suspension. A change in the bed forms is not observed.

Appendix D

D Sensitivity analysis

D1 Base parameters and uncertainty

For the analysis of the data several calculations were made in this research. Most of these calculations are made with parameters which were measured in the lab. Other parameters were known from literature. The used parameters for the calculations (the base parameters) contain uncertainties. This chapter explains the magnitude of uncertainty of each parameter and shows a sensitivity analysis of these uncertainties on the calculations. Table D1 gives an overview of the uncertain parameters.

Table D1 Magnitude of uncertainty of the base parameters

Parameter	Standard deviation
water depth	$0.02 \cdot d$
wave period	$0.001 \cdot T$
wave height	$0.02 \cdot H$
density water	$0.001 \cdot \rho_w$
Wn15 filter	$0.01 \cdot W_{n15}$
Wn50 filter	$0.01 \cdot W_{n50}$
density filter material	$0.01 \cdot \rho_f$
density base material	$0.001 \cdot \rho_b$
thickness filter	$0.5 \cdot d_{f50}$
db15	$0.05 \cdot d_{b15}$
db50	$0.05 \cdot d_{b50}$
bottom roughness	$0.25 \cdot k_r$
gravitational acceleration	0
shape factor F_s	$0.05 \cdot F_s$
loading coefficient	$0.05 \cdot \Upsilon$
Shields stress critical base	$0.20 \cdot \Psi_b$
Friction factor under waves c_f (Jonsson-Swart)	$0.5 \cdot c_f$

The magnitude of the standard deviation is based on the uncertainties in the measurements or the uncertainties known from literature. An explanation for the uncertainties of some of these parameters is found below.

Thickness filter

The filter's thickness is also not perfectly equal on every location. The accuracy of the filter layer's thickness depends on the filter material diameter. When the filter material diameter is large, the deviations in the thickness will be larger than for a small filter material diameter.

In the model tests the filter is measured at 20 locations. The average of these measurements is taken as the filter diameter. Figure 5-6 shows how the measured deviations from this average value are distributed. The deviation is expressed in terms of the filter diameter size (on the x-axis). The figure shows that in the most extreme values for the measured deviations are equal to d_{f50} . However, 90% of the measured deviations are in the order of $0.5 \cdot d_{f50}$.

If a normal distribution would be fitted to the measurements of the filter layer thickness, the standard deviation would approximate $0.35 \cdot d_{f50}$, since the values $0.35 \cdot d_{f50}$ of the mean account for 65% of the whole set. A standard deviation of $0.5 \cdot d_{f50}$ is assumed, which is conservative.

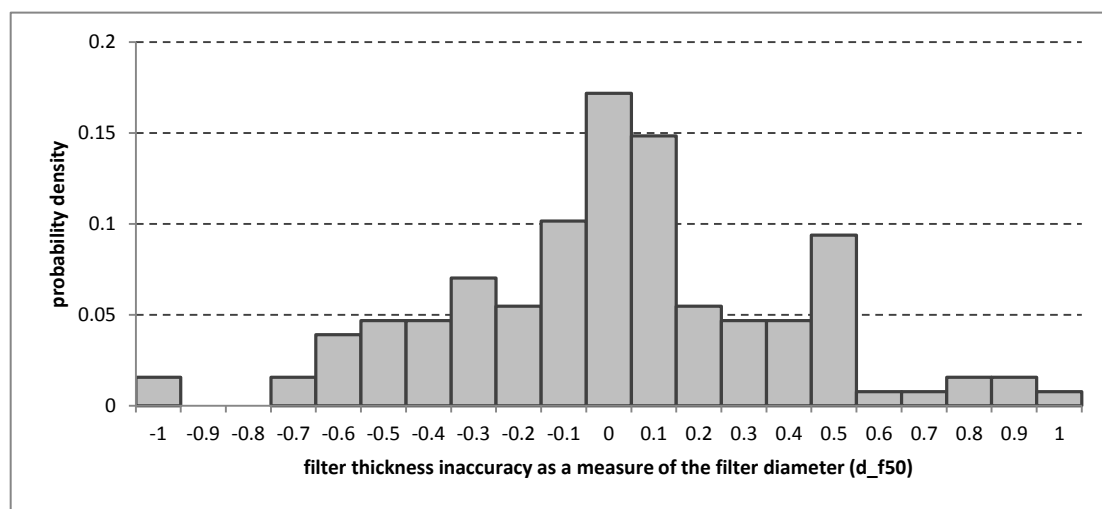


Figure D1 Distribution of the measurements of the filter layer thickness

Shields stress critical base

In the experiments critical wave height was found. The critical wave height, is the height for which the base material becomes unstable. Theoretically, this corresponds with a Shields value of $\Psi_b = 0.073$ (based on Sleath's graph). Two sources of uncertainty are introduced by this method. First, is the found critical wave height accurate? Secondly, is the critical shields parameter for the base material exactly 0.073?

In this research, it is assumed that the critical wave height was correct. Although, the corresponding shields value of the base was uncertain. For one critical wave conditions, slightly more mobility was seen than another critical wave height. It is assumed that the observations for the instability were in phase 5, 6 or 7 according to Breusers (1968). This corresponds with an 20% error for the assumed critical shields value of $\Psi_b = 0.073$.

Friction factor under waves c_f (Jonsson-Swart)

Jonsson (1966) found an empirical relation for the friction factor under wave loading. This relation was based on experimental data. The empirical relation does not fit the experimental data perfectly, and is therefore not completely certain.

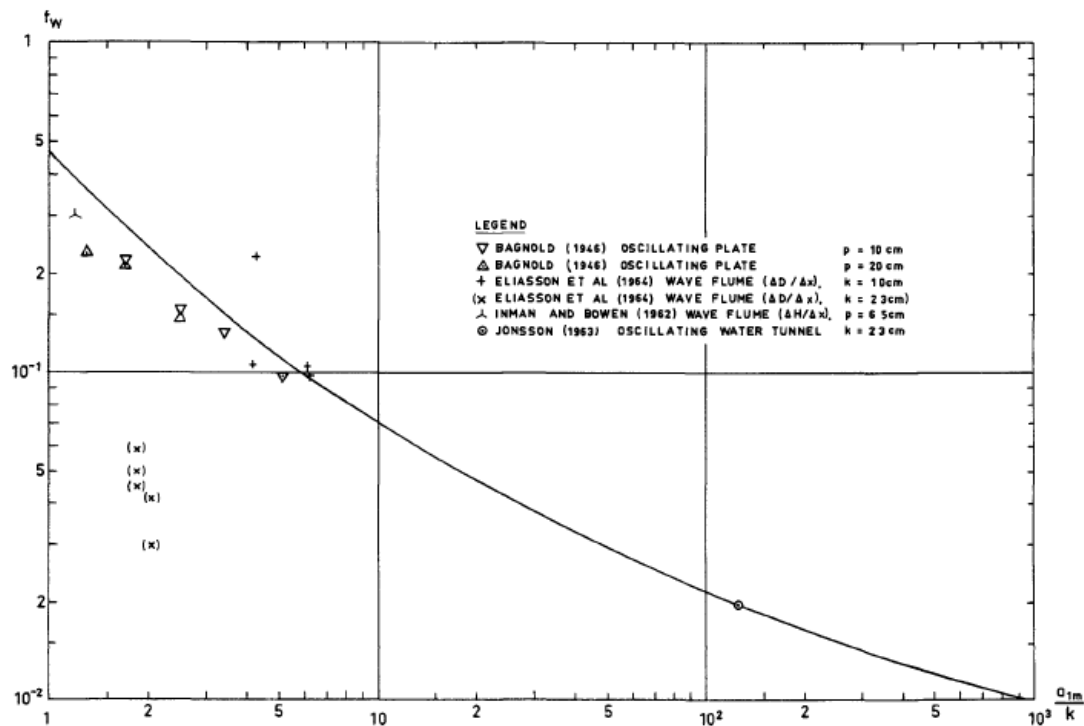


Figure D2 Measured wave friction factors in rough turbulent regime (Jonsson, 1966)

Figure D2 shows the regression line through the experimental data. Since the axis are on a logarithmic scale, large relative errors are seen between the experimental values and the curve fit. Based on this graph, an uncertainty of 50% of the value for the friction factor is plausible.

Other parameters

The uncertainties of all other parameters are plausible assumptions based on the measurement method or from literature.

D2 Propagation of uncertainty

All base parameters are considered to be independent, without a covariance. In the analysis, all calculations are made with the use of these base parameters. Using the rules for the propagation of uncertainty, the standard deviation of the obtained load damping length is found.

Table D2 Progression of errors on the calculation of L_d'

Test	D_f [mm]	$\frac{D_f}{d_{f15}}$ [-]	$\frac{d_{f50}}{d_{b50}}$ [-]	T [s]	L_d'	Standard deviation L_d'
1	17	3.2	58.4	3.0	0.006	0.0017
2	17	3.2	58.4	2.0	0.005	0.0014
2	17	3.2	58.4	2.5	0.006	0.0018
2	17	3.2	58.4	3.0	0.006	0.0017
3	28	2.6	121.2	2.0	0.013	0.0044
3	28	2.6	121.2	2.5	0.013	0.0045
3	28	2.6	121.2	3.0	0.012	0.0040
4	59	5.4	121.2	2.0	0.021	0.0044
4	59	5.4	121.2	2.5	0.021	0.0045
4	59	5.4	121.2	3.0	0.021	0.0047
5	96	8.8	121.2	2.0	0.029	0.0048
5	96	8.8	121.2	2.5	0.029	0.0050
5	96	8.8	121.2	3.0	0.029	0.0048
6	93	4.4	221.2	2.0	0.033	0.0074
6	93	4.4	221.2	2.5	0.034	0.0077
6	93	4.4	221.2	3.0	0.035	0.0080

7	147	7.0	221.2	2.0	0.053	0.0105
7	147	7.0	221.2	2.5	0.050	0.0094
7	147	7.0	221.2	3.0	0.051	0.0098
Halter (1999)						
	0.12	3.3129	377.1118	1.03	0.0379	0.0091
	0.12	3.3129	377.1118	1.33	0.0374	0.0089
	0.12	3.3129	377.1118	1.9	0.0385	0.0093
	0.12	3.3129	377.1118	2.41	0.0405	0.0100
	0.12	6.2429	200.1207	1.03	0.0309	0.0050
	0.12	6.2429	200.1207	1.33	0.0364	0.0066
	0.12	6.2429	200.1207	1.9	0.0357	0.0064
	0.12	6.2429	200.1207	2.41	0.0382	0.0071
	0.06	3.1214	200.1207	1.03	0.0176	0.0043
	0.06	3.1214	200.1207	1.33	0.0181	0.0044
	0.06	3.1214	200.1207	1.9	0.0195	0.0049
	0.06	3.1214	200.1207	2.41	0.0207	0.0053

The calculated errors of the obtained load damp length is in the range of 0.15 - 0.30 times L_d' .

D3 Influence of the individual parameters

Besides the total error in the obtained damping length, an analysis is carried out to the influence of each individual parameter. The influence of the error of each individual base parameter is calculated. The results are shown in figure D3. The figure shows what influence the range of uncertainty of every parameter has on the calculated value of the load damping length (the values presented in Table 6-1). This influence is expressed in a percentage. For example: the range of uncertainty of the measured water depth (2%) has a range of uncertainty of 3.6% on the calculated value of the load damping length in test 1.

Note that this analysis is only carried out for the experimental data of Hollander (2015).

It is shown that in every test the uncertainty of the filter layer thickness and the uncertainty of the Jonsson-Swart method has most impact. When a similar analysis will be carried out for further research, it is recommended to focus on the reduction of the uncertainty of these parameters.

Furthermore, it is advisable to carry out a FORM analysis for the uncertainties in further research. This will provide more accurate insight in the influence of the uncertainties of the individual parameters.

D4 Critical note to the reflection analysis

It should be noted that the estimations and assumptions made about the uncertainties of the base parameters influence the sensitivity analysis. Although a substantiated attempt is made to estimate these uncertainties as accurate as possible, a source of subjectivity will always remain.

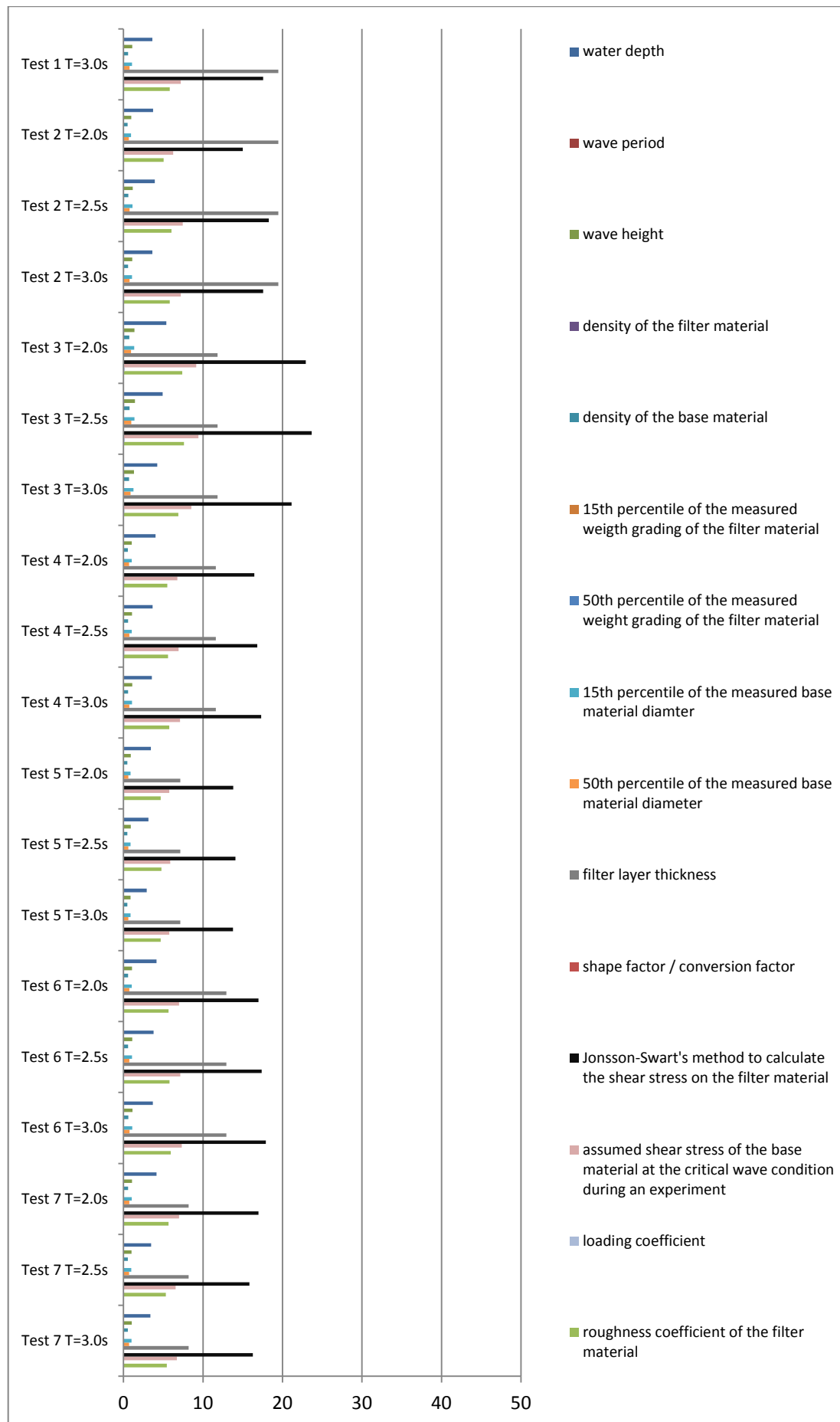


Figure D3 Influence of the error of each individual parameter on the obtained value for the load damping length.

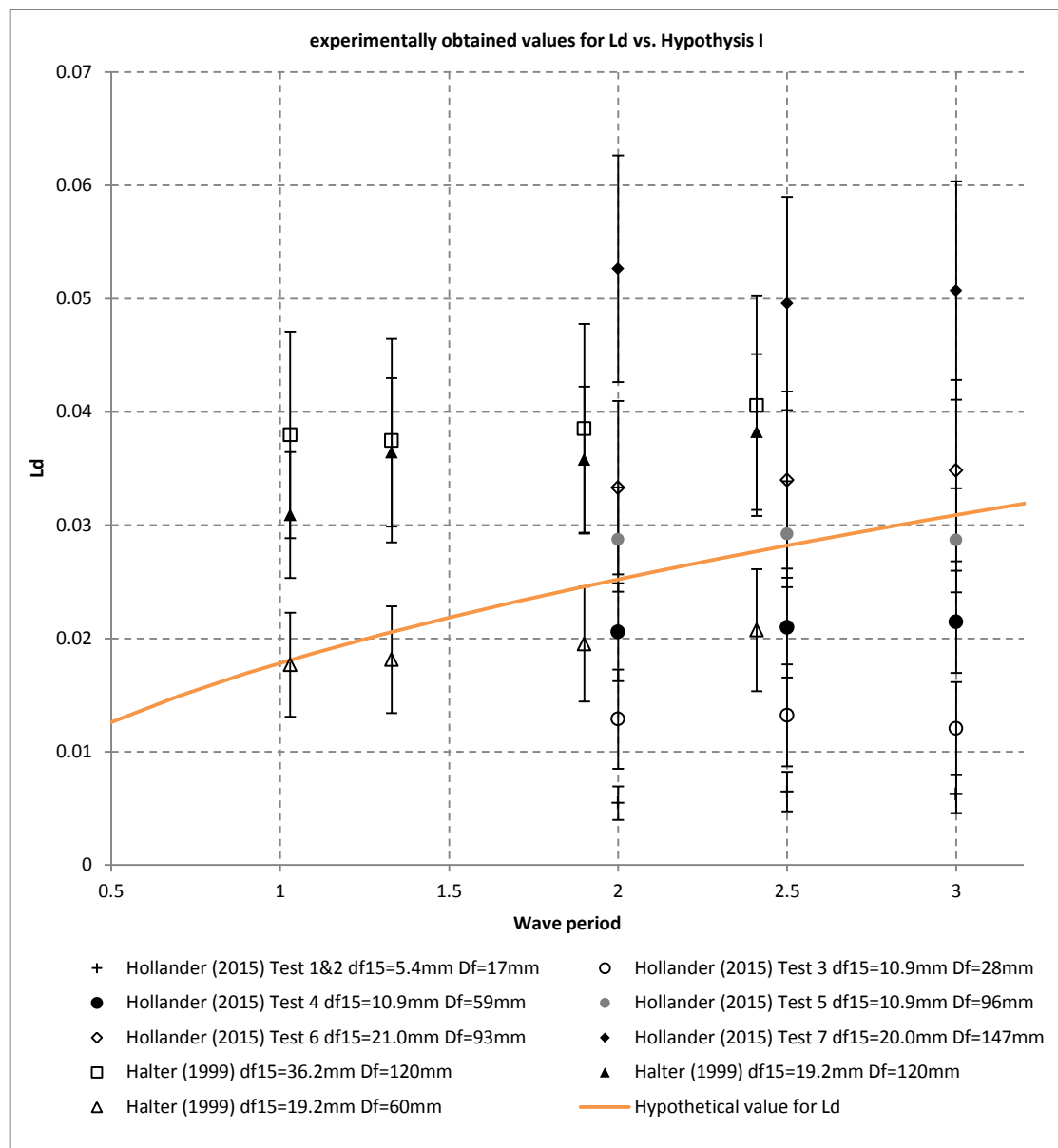
Appendix E

E Addition to analysis; graphs including uncertainties of the data

In this appendix graphs additional are shown where Halter's (1999) and Hollander's (2015) data is compared the hypotheses for the load damping length. The error of the obtained values of L_d is included in this graph. Thereby, for the comparison of the data with hypothesis II, the data is separated in multiple graphs. This gives a clear overview of the data.

E1 Graph with error bars for hypothesis 1

$$L_{d,Hypothesis\ 1} = \sqrt{\frac{c_v T_p}{\pi}}$$



E2 Graphs with error bars for hypothesis II

$$L_{d,Hypothesis II} = d_{f15} \sqrt{\frac{2T_p}{T_0}}$$

